

Curvature Learning for Generalization of Hyperbolic Neural Networks

Xiaomeng Fan¹, Yuwei Wu¹, Zhi Gao^{1*}, Mehrtash Harandi³, and Yunde Jia^{2*}

¹Beijing Laboratory of Intelligent Information Technology, School of Computer Science, Beijing Institute of Technology (BIT), Beijing, 100081, P.R. China.

²Guangdong Laboratory of Machine Perception and Intelligent Computing, Shenzhen MSU-BIT University, Shenzhen, 518172, P.R. China.

³Department of Electrical and Computer Systems Eng., Monash University, and Data61, Australia.

*Corresponding author(s). E-mail(s): zhi.gao@bit.edu.cn; jiayunde@bit.edu.cn;

Contributing authors: fanxiaomeng@bit.edu.cn; wuyuwei@bit.edu.cn; mehrtash.harandi@monash.edu;

Abstract

Hyperbolic neural networks (HNNs) have demonstrated notable efficacy in representing real-world data with hierarchical structures via exploiting the geometric properties of hyperbolic spaces characterized by negative curvatures. Curvature plays a crucial role in optimizing HNNs. Inappropriate curvatures may cause HNNs to converge to suboptimal parameters, degrading overall performance. So far, the theoretical foundation of the effect of curvatures on HNNs has not been developed. In this paper, we derive a PAC-Bayesian generalization bound of HNNs, highlighting the role of curvatures in the generalization of HNNs via their effect on the smoothness of the loss landscape. Driven by the derived bound, we propose a sharpness-aware curvature learning method to smooth the loss landscape, thereby improving the generalization of HNNs. In our method, we design a scope sharpness measure for curvatures, which is minimized through a bi-level optimization process. Then, we introduce an implicit differentiation algorithm that efficiently solves the bi-level optimization by approximating gradients of curvatures. We present the approximation error and convergence analyses of the proposed method, showing that the approximation error is upper-bounded, and the proposed method can converge by bounding gradients of HNNs. Experiments on four settings: classification, learning from long-tailed data, learning from noisy data, and few-shot learning show that our method can improve the performance of HNNs.

Keywords: Hyperbolic neural networks, Curvature learning, PAC-Bayesian generalization bound, Implicit differentiation.

1 Introduction

Hyperbolic neural networks (HNNs) work well for modeling real-world data with inherent hierarchical structures (Khrulkov et al, 2020a; Guo et al,

2022a). The efficacy of HNNs stems from their ability to capitalize on the distinct representational capabilities of hyperbolic spaces, characterized by negative curvatures (Peng et al, 2021;

Mettes et al, 2024). Hyperbolic spaces offer an effective way to capture hierarchical structures because their volume grows exponentially with the radius, consistent with the exponential increase of data numbers in the hierarchical structures with depth (Fang et al, 2021a). The curvature is significant for optimizing HNNs, and many works have empirically shown that curvature affects the performance of HNNs across various tasks, such as image classification (Gao et al, 2023a) and node classification (Fu et al, 2023). So far, the theoretical foundation of the effect of curvatures on HNNs has not been developed.

In this paper, we present a theoretical framework for exploring the effect of curvatures in hyperbolic neural networks (HNNs). We analyze the Lipschitz continuity of hyperbolic operations and derive the corresponding Lipschitz constants. Then, we establish a Lipschitz bound analysis that quantifies the approximation error between HNNs under different tangent points. We further derive a PAC-Bayesian generalization bound for HNNs, which indicates that the minima of HNNs with a smoother loss landscape generalize better than those with a sharper loss landscape.

We observe that Euclidean studies (Foret et al, 2020; Dinh et al, 2017) have reached similar conclusions, and our derivation augments them. Along the way, we further find that curvatures of hyperbolic spaces affect the smoothness of the loss landscape in the derived theorem, highlighting the significance of curvatures for generalization in HNNs. This finding drives us to investigate a curvature learning method to smooth the loss landscape, thereby improving the generalization of HNNs.

To this end, we propose a sharpness-aware curvature learning method. Specifically, we design a scope sharpness measure to capture the sharpness of a local minimum in HNNs within a given scope around the minimum. Then, the scope sharpness measure is minimized to learn optimal curvatures, providing a feasible solution to smooth the loss landscape and enhance the generalization of HNNs. Minimizing the measure is formulated as a bi-level optimization problem (*i.e.*, a nested optimization problem with inner and outer levels), where HNNs are trained in the inner level, and curvatures are optimized in the outer level. In the bi-level optimization, computing gradients of curvatures poses computational challenges due to

the need to calculate multiple Hessian matrices and unroll the inner-level optimization. We introduce an implicit differentiation algorithm that presents an approximated solution for gradients of curvatures, reducing the computational load.

The effectiveness of our method is demonstrated both theoretically and empirically. Theoretically, we prove that the approximation error in the proposed method has an upper bound, showing the rationality of approximation ways in the proposed method. We also present convergence guarantees by bounding gradients of parameters and curvatures in HNNs. Empirically, we conduct a comprehensive set of experiments to evaluate the proposed method on four tasks: classification, learning from long-tailed data, learning from noisy data, and few-shot learning. Experimental results show that the proposed method can efficiently smooth the loss landscape and thus improve the generalization of HNNs. Our contributions are summarized as follows:

- We derive the PAC-Bayesian generalization bound of HNNs, highlighting the significance of curvatures for the generalization in HNNs.
- We present foundational theoretical analyses of HNNs by characterizing the Lipschitz continuity of hyperbolic operations and quantifying the Lipschitz bound of HNNs across different tangent points.
- We propose a sharpness-aware curvature learning method that optimizes curvatures of HNNs to smooth the loss landscape, enhancing the generalization of HNNs.
- We introduce an implicit differentiation that brings an efficient bi-level optimization process by approximating gradients of curvatures.
- We present the upper bound and convergence guarantees of our method.

2 Related Work

2.1 Hyperbolic Neural Networks

Modeling via hyperbolic spaces has shown superior performances in many tasks due to their capabilities in encoding data with hierarchical structures. Hyperbolic neural networks (Ganea et al, 2018) incorporate several hyperbolic operations on the top of a neural network to obtain

hyperbolic embeddings. Guo et al (2022a) further improve the training procedure of HNNs by introducing feature clipping to prevent vanishing gradients. Efforts to learn powerful embeddings in the hyperbolic spaces have been explored for various applications, including but not limited to image retrieval (Khrulkov et al, 2020a), medical image recognition (Yu et al, 2022), action recognition (Long et al, 2020), anomaly recognition (Hong et al, 2023a), audio-visual learning (Hong et al, 2023b), image segmentation (Atigh et al, 2022), anomaly detection (Li et al, 2024), and 3D visual grounding (Wang et al, 2024b). Moreover, extensions of various neural architectures from Euclidean to hyperbolic spaces have been actively studied, such as hyperbolic convolutional (Shimizu et al, 2021), graph network (Dai et al, 2021), attention mechanism (Gulcehre et al, 2019), and variational autoencoder (Skopek et al, 2020). In addition, several works develop the well-known learning paradigms from Euclidean spaces to hyperbolic spaces, such as metric learning (Yan et al, 2021a), contrastive learning (Ge et al, 2023), self-supervised learning (Franco et al, 2023), active learning (Franco et al, 2024), clustering learning (Lin et al, 2023), and continual learning (Gao et al, 2023c). Different from them, we are the first to develop a generalization error bound of HNNs and further improve the generalization of HNNs by learning curvatures.

2.2 Curvature Learning Methods

Existing curvature learning methods aim to capture geometrical structures of data. In computer vision, curvature learning methods aim to generate curvatures to match the characteristics of image data. The methods proposed by Gao et al (2021, 2023a) automatically generate task-specific curvatures to adapt models to diverse geometric structures. A Riemannian AdamW optimizer is introduced to learn curvatures for improving training stability and computational efficiency (Bdeir and Landwehr, 2024). In data mining, curvature learning methods design graph curvatures to capture the geometric embeddings of graph data. Hyperbolic graph convolutional networks (Fu et al, 2021) treat curvatures as trainable parameters that are optimized jointly with model weights. A reinforcement learning-based strategy

proposed by Chami et al (2019) dynamically learns task-specific curvatures to better represent complex graph structures. Fu et al (2023) design class-aware graph curvatures that measure the effect of label information and neighborhood connectivity to address the hierarchy imbalance issue in node classification. κ hgcn method (Yang et al, 2023b) integrates learnable graph curvatures and curvature-based filtering mechanisms to enhance performance. Instead of focusing on the geometrical structures of data, we theoretically explore the effect of curvatures on HNNs, demonstrating that the generalization of HNNs can be improved by curvature learning.

2.3 Flat Minima and Optimization Methods

Hochreiter and Schmidhuber (1994) are the first to demonstrate that the smoothness of the loss landscape affects the generalization of neural networks. Subsequent efforts to improve generalization by smoothing the loss landscape have largely fallen into two categories. Methods of the first category opt for designing sharpness measures and minimizing them to improve the generalization. Dinh et al (2017) propose the sharpness measure by utilizing the spectrum of the Hessian. Other works (Liang et al, 2019; Petzka et al, 2021) present the scale-invariance sharpness measure, while the method proposed by Jang et al (2022) introduces a reparametrization-invariant sharpness measure.

Methods of the second category focused on finding flat minima through sharpness-aware minimization. Sharpness-aware minimization (SAM) proposed by Foret et al (2020) is the pioneering work, which seeks parameters that lie in neighborhoods having uniformly low loss value. Subsequently, some works focus on reducing the complexity of SAM by adaptively applying SAM (instead of using it at every iteration), thereby speeding up SAM (Jiang et al, 2023). Some works focus on designing improved variants for SAM. For example, the adaptive sharpness-aware minimization method (Kwon et al, 2021) adaptively adjusts maximization regions to realize scale-invariant parameters, and the surrogate gap minimization method (Zhuang et al, 2022) models a surrogate gap as an equivalent measure of sharpness to improve the generalization. Some work aim

to refine the SAM method for specific tasks, such as the sharpness-aware MAML method for few-shot learning (Abbas et al, 2022), the data augmented flatness-aware gradient projection for continual learning (Yang et al, 2023a), the SAM method for federated learning (Qu et al, 2022), and the class-conditional SAM method for long-tailed recognition (Zhou et al, 2023). In contrast to prior studies predominantly centered on Euclidean spaces, we focus on the effect of sharpness on generalization in hyperbolic spaces and derive the generalization bound of HNNs.

3 Lipschitz Continuity and Lipschitz Bound in HNNs

To construct the theoretical framework for exploring the effect of curvatures in HNNs, we analyze the Lipschitz continuity and Lipschitz bound in HNNs. Specifically, we present the details of HNNs (shown in Section 3.1), and then we analyze the Lipschitz continuity of several hyperbolic operations (shown in Section 3.2). Based on the Lipschitz continuity, we develop the Lipschitz bound for changes in tangent point (shown in Section 3.3).

3.1 Hyperbolic Neural Networks

In this subsection, we first present denotations of hyperbolic spaces and hyperbolic operations, and then introduce details of HNNs. The utilized mathematical notations are summarized in Table 1. Unlike Euclidean spaces with the fixed zero curvature, a hyperbolic spaces $\mathcal{H}^{d,c}$ is a smooth Riemannian manifold with a constant negative curvature $-c$ (Lee, 2006). We choose the d -dimensional Poincaré ball model (Cannon et al, 1997) of constant negative curvature $-c$ to work with. It is denoted as $\mathcal{H}^{d,c} = \{\mathbf{x} \in \mathbb{R}^d, c\|\mathbf{x}\|^2 < 1\}$, where $\|\cdot\|$ is the Euclidean norm. The tangent space to \mathcal{H} at a tangent point \mathbf{x} , denoted as $T_{\mathbf{x}}\mathcal{H}$, consists of all tangent vectors at that tangent point. The following hyperbolic operations will be used in our work.

Möbius Addition. For $\mathbf{x}, \mathbf{y} \in \mathcal{H}^{d,c}$, the Möbius addition of \mathbf{x} and $\mathcal{H}^{d,c}$ is

$$\mathbf{x} \oplus_c \mathbf{y} = \frac{(1 + 2c\langle \mathbf{x}, \mathbf{y} \rangle + c\|\mathbf{y}\|^2)\mathbf{x} + (1 - c\|\mathbf{x}\|^2)\mathbf{y}}{1 + 2c\langle \mathbf{x}, \mathbf{y} \rangle + c^2\|\mathbf{x}\|^2\|\mathbf{y}\|^2}. \quad (1)$$

Distance measure. For $\mathbf{x}, \mathbf{y} \in \mathcal{H}^{d,c}$, the measure of \mathbf{x} and $\mathcal{H}^{d,c}$ is

$$d^c(\mathbf{x}, \mathbf{y}) = \frac{1}{\sqrt{|c|}} \cosh^{-1} \left(1 - 2c \frac{\|\mathbf{x} - \mathbf{y}\|^2}{(1 + c\|\mathbf{x}\|^2)(1 + c\|\mathbf{y}\|^2)} \right). \quad (2)$$

Exponential map. The exponential map $\text{exp}_\mathbf{y}^c(\mathbf{x})$ projects a vector \mathbf{x} from the tangent space at the tangent point \mathbf{y} to the manifold $\mathcal{H}^{d,c}$

$$\text{exp}_\mathbf{y}^c(\mathbf{x}) = \mathbf{y} \oplus_c \left(\tanh(\sqrt{|c|} \frac{\lambda_\mathbf{y}^c \|\mathbf{x}\|}{2}) \frac{\mathbf{x}}{\sqrt{|c|} \|\mathbf{x}\|} \right), \quad (3)$$

where $\lambda_\mathbf{y}^c = 2/(1 - c\|\mathbf{y}\|^2)$ is the conformal factor. Setting $\mathbf{y} = \mathbf{0}$, the exponential map is computed as

$$\text{exp}_\mathbf{0}^c(\mathbf{s}) = \tanh(\sqrt{|c|} \|\mathbf{s}\|) \frac{\mathbf{s}}{\sqrt{|c|} \|\mathbf{s}\|}. \quad (4)$$

Logarithmic map. The Logarithmic map $\text{log}_\mathbf{y}^c(\mathbf{x})$ projects a vector \mathbf{x} from the manifold $\mathcal{H}^{d,c}$ to the tangent space $T_\mathbf{y}\mathcal{H}$,

$$\text{log}_\mathbf{y}^c(\mathbf{x}) = \frac{2}{\sqrt{|c|} \lambda_\mathbf{y}^c} \tanh^{-1}(\sqrt{|c|} \|\mathbf{x} - \mathbf{y} \oplus_c \mathbf{x}\|) \frac{-\mathbf{y} \oplus_c \mathbf{x}}{\|\mathbf{x} - \mathbf{y} \oplus_c \mathbf{x}\|}. \quad (5)$$

Hyperbolic neural networks (HNNs) (Ganea et al, 2018) combine the formalism of Möbius gyrovector spaces (Ungar, 2008, 2001) with the Riemannian geometry of hyperbolic spaces, which derive hyperbolic versions of deep learning tools: feed-forward networks and multinomial logistic regression. The feed-forward technology in HNNs aims to obtain the hyperbolic embeddings. Given the hyperbolic inputs $\mathbf{x} \in \mathcal{H}^{d,c}$, the feed-forward technology in HNNs is modeled as

$$\mathbf{x} \leftarrow \text{exp}_\mathbf{y}^c(f_a(\text{log}_\mathbf{y}^c(\mathbf{x}))) \oplus_c \mathbf{b}, \quad (6)$$

where $f_a(\cdot)$ is the feed-forward function parameterized as $\mathbf{a} \in T_\mathbf{y}\mathcal{H}$ being the linear mapping weight, and $\mathbf{b} \in \mathcal{H}^{d,c}$ is the bias. By the feed-forward technology, one can obtain the hyperbolic embeddings \mathbf{x} . In practice, the tangent point \mathbf{y} is set to $\mathbf{0}$ to simplify the computations.

To classify the hyperbolic embeddings \mathbf{x} , HNNs propose the hyperbolic Multinomial Logistic Regression (MLR) as the classifier. In HNNs, the probability that a hyperbolic embedding $\mathbf{x} \in$

Table 1 Table of notations.

Notation	Section	Definition
$\mathcal{H}^{d,c}$	3.1	d-dimensional hyperbolic spaces
\mathbb{R}^d	3.1	d-dimensional Euclidean spaces
$T_{\mathbf{x}}\mathcal{H}$	3.1	tangent space of hyperbolic spaces
c	3.1	curvature of hyperbolic spaces
\oplus_c	3.1	Möbius addition in hyperbolic spaces
$d^c(\cdot)$	3.1	distance measure in hyperbolic spaces
$\text{exp}_y^c(\mathbf{x})$	3.1	exponential map in hyperbolic spaces
$\text{log}_y^c(\mathbf{x})$	3.1	Logarithmic map in hyperbolic spaces
$\mathcal{L}(\mathbf{w}, c, \mathbf{y})$	3.1	loss on hyperbolic neural networks
$L_{\oplus_c}, L_{\oplus_x}, L_{\oplus_y}, L_{\text{Expm}_x}, L_{\text{Expm}_y}, L_{\text{logm}_y}, L_p$	3.2	Lipschitz constants of operations in hyperbolic spaces
$L_{\mathcal{L}}^{'}, L_{\mathcal{L}}, L_f$	3.3	Lipschitz constants of loss function and feed-forward function
L_{tangent}	3.3	Lipschitz constants of tangent point in HNNs
\mathcal{E}_{l_y}	3.3	Lipschitz bound of changing tangent points in HNNs
\mathcal{D}, \mathcal{S}	4	real distribution, training set
ϵ, ρ	4	perturbation of weights, perturbation radius
$\mathcal{L}_{\mathcal{S}}^{\text{sharp}}, \mathcal{E}_{l_{\text{gen}}}$	4	generalization error bound of HNNs
$\text{SN}(\cdot)$	5	scope sharpness measure
$\mathcal{F}(\cdot)$	5	outer-level objective of bi-level optimization
$\mathcal{L}(\mathbf{w}, c)$	5	loss on hyperbolic spaces after simplified notation
$\text{sn}(\cdot)$	5.1	reparametrization-invariant sharpness measure
∇	5.1	gradients
$\hat{\text{sn}}(\cdot)$	5.1	approximated reparametrization-invariant sharpness measure
$\hat{\text{sn}}(\hat{\mathbf{w}}(c))$	5.1	approximated scope sharpness measure
$\mathbf{U}_1, \mathbf{U}_2$	5.2	part of gradient with respect to curvatures c
$\mathbf{U}_1^{'}, \mathbf{U}_2^{'}$	5.2	approximation of $\mathbf{U}_1, \mathbf{U}_2$
$L_G, L_{\bar{G}}, L_H, L_{H_2}, L_{G'}, L_{G_2}, L_{G_3}, L_{G_4}, L_{H_c}$	6.1	Lipschitz constants for theoretical analysis
$\mathcal{E}_{\text{mea}}, \mathcal{E}_{\text{cur}_1}, \mathcal{E}_{\text{cur}_2}$	6.2	constants in approximation error analyses
$\mathcal{C}_{w_1}, \mathcal{C}_{w_2}, \mathcal{C}_c$	6.3	constants in convergence analyses

$\mathcal{H}^{d,c}$ classified to the k -th class is defined as

$$p(z = k | \mathbf{x}) \propto \exp \left(\frac{\lambda_{\mathbf{b}_k^{'}}^c \|\mathbf{a}_k^{'}\|}{\sqrt{c}} \sinh^{-1} \left(\frac{2\sqrt{c} \langle -\mathbf{b}_k^{'} \oplus_c \mathbf{x}, \mathbf{a}_k^{'} \rangle}{(1 - c\|\mathbf{b}_k^{'} \oplus_c \mathbf{x}\|^2) \|\mathbf{a}_k^{'}\|} \right) \right), \quad (7)$$

where $\mathbf{b}_k^{'} \in \mathcal{H}^{d,c}$, $\mathbf{a}_k^{'} \in T_{\mathbf{b}_k^{'}}\mathcal{H}$ are parameters of the classifier in HNNs, $\mathbf{a}_k^{'}$ is the normal vector, and $\mathbf{b}_k^{'}$ is the shift. Denote the parameters of HNNs as \mathbf{w} that includes $\mathbf{a}_k^{'}, \mathbf{b}_k^{'}$, and parameters for extracting hyperbolic features, *i.e.*, \mathbf{a}, \mathbf{b} . Note that some parameters of HNNs are located in hyperbolic spaces, such as \mathbf{b} and $\mathbf{b}^{'}$. Generally, to obtain parameters on the hyperbolic spaces, one utilizes $\text{exp}_y^c(\cdot)$ to project parameters from the Euclidean spaces to hyperbolic spaces. In practice,

\mathbf{y} is also set to $\mathbf{0}$ to simplify the computations, which has been empirically demonstrated to have little impact on the obtained results (Khrulkov et al, 2020a; Hu et al, 2024a).

The loss function is defined as $\mathcal{L}(\mathbf{w}, c, \mathbf{y}) \triangleq \frac{1}{n} \sum_{i=1}^n [l(\mathbf{w}, c, \mathbf{y}, \mathbf{x}_i, \iota_i)]$. The loss function takes as input the parameters of hyperbolic neural networks \mathbf{w} , curvature c , tangent point \mathbf{y} , data point \mathbf{x} , and label ι , and outputs the loss value for optimizing the parameters \mathbf{w} . The process can be summarized in three stages: (1) Utilize the hyperbolic neural network to extract the representation in hyperbolic spaces via Eq. (6); (2) Apply hyperbolic MLR in Eq. (7) to compute the probability; (3) Compute the final loss value by comparing the predicted probability with the ground truth label (*e.g.*, using the cross-entropy loss).

By setting $c = 0$ and $\mathbf{y} = \mathbf{0}$, the loss function $\mathcal{L}(\mathbf{w}, 0, \mathbf{0})$ is degenerated to loss functions in Euclidean spaces (Ganea et al, 2018).

3.2 Lipschitz Continuity of Hyperbolic Operations

To theoretically analyze the effect of curvatures in HNNs, we first analyze the Lipschitz continuity of the utilized hyperbolic operations, *i.e.*, Möbius addition $\mathbf{x} \oplus_c \mathbf{y}$, exponential map $\text{exp}_\mathbf{y}^c(\mathbf{x})$, and logarithmic map $\text{log}_\mathbf{y}^c(\mathbf{x})$. Note that for brevity and ease of reading, we present the proofs of this subsection in GitHub ¹.

3.2.1 Lipschitz Continuity of Möbius Addition

We analyze the Lipschitz continuity of the Möbius addition $\mathbf{x} \oplus_c \mathbf{y}$ with respect to curvatures c , right input \mathbf{y} , and left input \mathbf{x} in Theorems 1, 2, and 3, respectively.

Theorem 1. *Given two points on hyperbolic spaces \mathbf{x} and \mathbf{y} , the Möbius addition $\mathbf{x} \oplus_c \mathbf{y}$ is Lipschitz continuous with respect to curvatures c , *i.e.*,*

$$\|\mathbf{x} \oplus_{c_1} \mathbf{y} - \mathbf{x} \oplus_{c_2} \mathbf{y}\| \leq L_{\oplus_c} |c_1 - c_2|. \quad (8)$$

L_{\oplus_c} is computed as

$$\begin{aligned} L_{\oplus_c} &\triangleq \frac{2\|\mathbf{x}\|\|\mathbf{y}\| + 3\|\mathbf{x}\|^2\|\mathbf{y}\| + 2\|\mathbf{x}\|\|\mathbf{y}\|^2}{\mathcal{N}(c_1, \mathbf{x}, \mathbf{y})\mathcal{N}(c_2, \mathbf{x}, \mathbf{y})} \\ &+ \frac{(c_1 + c_2)\|\mathbf{x}\|^2\|\mathbf{y}\|^3 + (c_1 + c_2)\|\mathbf{x}\|^3\|\mathbf{y}\|^2}{\mathcal{N}(c_1, \mathbf{x}, \mathbf{y})\mathcal{N}(c_2, \mathbf{x}, \mathbf{y})} \\ &+ \frac{c_1 c_2 \|\mathbf{x}\|^3\|\mathbf{y}\|^4 + 3c_1 c_2 \|\mathbf{x}\|^4\|\mathbf{y}\|^3}{\mathcal{N}(c_1, \mathbf{x}, \mathbf{y})\mathcal{N}(c_2, \mathbf{x}, \mathbf{y})}. \end{aligned} \quad (9)$$

$\mathcal{N}(c_1, \mathbf{x}, \mathbf{y})$ and $\mathcal{N}(c_2, \mathbf{x}, \mathbf{y})$ are given by

$$\begin{aligned} \mathcal{N}(c_1) &= |(1 + 2c_1 \langle \mathbf{x}, \mathbf{y} \rangle + c_1^2 \|\mathbf{x}\|^2 \|\mathbf{y}\|^2)|, \\ \mathcal{N}(c_2) &= |(1 + 2c_2 \langle \mathbf{x}, \mathbf{y} \rangle + c_2^2 \|\mathbf{x}\|^2 \|\mathbf{y}\|^2)|. \end{aligned} \quad (10)$$

We also derive that

$$\|\mathbf{x} \oplus_c \mathbf{y} - (\mathbf{x} + \mathbf{y})\| \leq L_{\oplus_{c0}}, \quad (11)$$

where

$$\begin{aligned} L_{\oplus_{c0}} &\triangleq \frac{2c\|\mathbf{x}\|\|\mathbf{y}\| + 3c\|\mathbf{x}\|^2\|\mathbf{y}\| + 2c\|\mathbf{x}\|\|\mathbf{y}\|^2}{|(1 + 2c \langle \mathbf{x}, \mathbf{y} \rangle + c^2 \|\mathbf{x}\|^2 \|\mathbf{y}\|^2)|} \\ &+ \frac{c^2 \|\mathbf{x}\|^2 \|\mathbf{y}\|^3 + c^2 \|\mathbf{x}\|^3 \|\mathbf{y}\|^2}{|(1 + 2c \langle \mathbf{x}, \mathbf{y} \rangle + c^2 \|\mathbf{x}\|^2 \|\mathbf{y}\|^2)|}. \end{aligned} \quad (12)$$

¹https://github.com/XiaomengFanmcislab/ijcv_curvature_learning_for_generalization/

Moreover, $L_{\oplus_{c0}}$ satisfies that

$$\lim_{c \rightarrow 0} L_{\oplus_{c0}} = 0. \quad (13)$$

Denote the angle between \mathbf{x} and \mathbf{y} as θ . Suppose that θ satisfy $\cos(\theta) \geq \cos\tilde{\theta}$. By utilizing the hyperbolic constraint of \mathbf{x} and \mathbf{y} , L_{\oplus_x} can be further modeled as

$$L_{\oplus_c} = |c_2 - c_1| \frac{\left(\frac{6}{c^{3/2}} + \frac{2}{c} + \frac{4c_1 c_2}{c^{7/2}} + \frac{2(c_1 + c_2)}{c^{5/2}}\right)}{(1 - \cos(\tilde{\theta})^2)^2}, \quad (14)$$

and $L_{\oplus_{c0}}$ can be modeled as

$$L_{\oplus_{c0}} \triangleq \frac{\frac{8}{c^{1/2}} + 2}{(1 - \cos(\tilde{\theta})^2)^2}. \quad (15)$$

Theorem 2. *Given points on hyperbolic spaces \mathbf{x} and \mathbf{y} , the Möbius addition $\mathbf{x} \oplus_c \mathbf{y}$ is Lipschitz continuous with respect to the right input \mathbf{y} , *i.e.*,*

$$\|\mathbf{x} \oplus_c \mathbf{y}_1 - \mathbf{x} \oplus_c \mathbf{y}_2\| \leq L_{\oplus_y} \|\mathbf{y}_1 - \mathbf{y}_2\|, \quad (16)$$

L_{\oplus_y} is computed as

$$\begin{aligned} L_{\oplus_y} &\triangleq \frac{1 + c(5\|\mathbf{x}\|^2 + 5\|\mathbf{x}\|\|\mathbf{y}_1\| + \|\mathbf{x}\|\|\mathbf{y}_2\|)}{\mathcal{N}(c, \mathbf{x}, \mathbf{y}_1)\mathcal{N}(c, \mathbf{x}, \mathbf{y}_2)} + \\ &\frac{c^2\|\mathbf{x}\|^2(13\|\mathbf{x}\|\|\mathbf{y}_1\| + \|\mathbf{x}\|\|\mathbf{y}_2\| + 6\|\mathbf{y}_1\|^2 + 3\|\mathbf{y}_1\|\|\mathbf{y}_2\|)}{\mathcal{N}(c, \mathbf{x}, \mathbf{y}_1)\mathcal{N}(c, \mathbf{x}, \mathbf{y}_2)} + \\ &\frac{c^3\|\mathbf{x}\|^3(6\|\mathbf{x}\|\|\mathbf{y}_1\|^2 + 3\|\mathbf{x}\|\|\mathbf{y}_1\|\|\mathbf{y}_2\| + 2\|\mathbf{y}_1\|^3 + 2\|\mathbf{y}_1\|^2\|\mathbf{y}_2\|)}{\mathcal{N}(c, \mathbf{x}, \mathbf{y}_1)\mathcal{N}(c, \mathbf{x}, \mathbf{y}_2)}. \end{aligned} \quad (17)$$

$\mathcal{N}(c, \mathbf{x}, \mathbf{y}_1)$ and $\mathcal{N}(c, \mathbf{x}, \mathbf{y}_2)$ are given by

$$\begin{aligned} \mathcal{N}(c, \mathbf{x}, \mathbf{y}_1) &= |(1 + 2c \langle \mathbf{x}, \mathbf{y}_1 \rangle + c^2 \|\mathbf{x}\|^2 \|\mathbf{y}_1\|^2)| \\ \mathcal{N}(c, \mathbf{x}, \mathbf{y}_2) &= |(1 + 2c \langle \mathbf{x}, \mathbf{y}_2 \rangle + c^2 \|\mathbf{x}\|^2 \|\mathbf{y}_2\|^2)|. \end{aligned} \quad (18)$$

Moreover, L_{\oplus_y} satisfies that

$$\lim_{c \rightarrow 0} L_{\oplus_y} = 1. \quad (19)$$

Denote the angle between \mathbf{x} and \mathbf{y}_1 , and \mathbf{x} and \mathbf{y}_2 as θ_1 and θ_2 , respectively. Suppose that θ_1 and θ_2 satisfy $\cos(\theta_1), \cos(\theta_2) \geq \cos\tilde{\theta}$. By utilizing the hyperbolic constraint of \mathbf{x} and \mathbf{y} , L_{\oplus_y} can be further modeled as

$$L_{\oplus_y} = \frac{48}{(1 - \cos(\tilde{\theta})^2)^2}. \quad (20)$$

Theorem 3. *Given points on hyperbolic spaces \mathbf{x} and \mathbf{y} , the Möbius addition $\mathbf{x} \oplus_c \mathbf{y}$ is Lipschitz continuous with respect to \mathbf{x} , *i.e.*,*

$$\|\mathbf{x}_1 \oplus_c \mathbf{y} - \mathbf{x}_2 \oplus_c \mathbf{y}\| \leq L_{\oplus_x} \|\mathbf{x}_1 - \mathbf{x}_2\|, \quad (21)$$

where L_{\oplus_x} is computed as

$$\begin{aligned} L_{\oplus_x} &\triangleq \frac{1 + 3c\|\mathbf{y}\|^2 + 3c\|\mathbf{x}_1\|\|\mathbf{y}\| + 7c\|\mathbf{x}_2\|\|\mathbf{y}\|}{\mathcal{N}(c, \mathbf{x}_1, \mathbf{y})\mathcal{N}(c, \mathbf{x}_2, \mathbf{y})} + \\ &\frac{c^2\|\mathbf{y}\|^2(7\|\mathbf{x}_1\|\|\mathbf{x}_2\| + \|\mathbf{x}_1\|\|\mathbf{y}\| + 5\|\mathbf{x}_2\|\|\mathbf{y}\| + 6\|\mathbf{x}_2\|^2)}{\mathcal{N}(c, \mathbf{x}_1, \mathbf{y})\mathcal{N}(c, \mathbf{x}_2, \mathbf{y})} + \\ &\frac{c^3\|\mathbf{x}_2\|\|\mathbf{y}\|^3(4\|\mathbf{x}_1\|^2 + 4\|\mathbf{x}_1\|\|\mathbf{x}_2\| + 2\|\mathbf{x}_2\|\|\mathbf{y}\| + \|\mathbf{x}_1\|\|\mathbf{y}\|)}{\mathcal{N}(c, \mathbf{x}_1, \mathbf{y})\mathcal{N}(c, \mathbf{x}_2, \mathbf{y})}. \end{aligned} \quad (22)$$

$\mathcal{N}(c, \mathbf{x}_1, \mathbf{y})$ and $\mathcal{N}(c, \mathbf{x}_2, \mathbf{y})$ are given by

$$\mathcal{N}(c, \mathbf{x}_1, \mathbf{y}) = |(1 + 2c\langle \mathbf{x}_1, \mathbf{y} \rangle + c^2\|\mathbf{x}_1\|^2\|\mathbf{y}\|^2)|, \quad (23)$$

$$\mathcal{N}(c, \mathbf{x}_2, \mathbf{y}) = |(1 + 2c\langle \mathbf{x}_2, \mathbf{y} \rangle + c^2\|\mathbf{x}_2\|^2\|\mathbf{y}\|^2)|.$$

Moreover, L_{\oplus_x} satisfies that

$$\lim_{c \rightarrow 0} L_{\oplus_x} = 1. \quad (24)$$

Denote the angle between \mathbf{x}_1 and \mathbf{y} , and \mathbf{x}_2 and \mathbf{y} as θ_1 and θ_2 , respectively. Suppose that θ_1 and θ_2 satisfy $\cos(\theta_1), \cos(\theta_2) \geq \cos \theta$. By utilizing the hyperbolic constraint of \mathbf{x} and \mathbf{y} , L_{\oplus_x} can be further modeled as

$$L_{\oplus_x} \triangleq \frac{44}{(1 - \cos(\theta)^2)^2}. \quad (25)$$

3.2.2 Lipschitz Continuity of Exponential Map

In this section, we analyze the Lipschitz continuity of exponential map $\exp_{\mathbf{y}}^c(\mathbf{x})$ with respect to \mathbf{x} and \mathbf{y} in Theorems 4 and 5.

Theorem 4. The exponential map $\exp_{\mathbf{y}}^c(\mathbf{x})$ is $L_{\exp_{\mathbf{y}}} -$ Lipschitz continuous with respect to \mathbf{y} . Mathematically, for any \mathbf{y}_1 and \mathbf{y}_2 , we have that

$$\|\exp_{\mathbf{y}_1}^c(\mathbf{x}) - \exp_{\mathbf{y}_2}^c(\mathbf{x})\| \leq L_{\exp_{\mathbf{y}}} \|\mathbf{y}_1 - \mathbf{y}_2\|, \quad (26)$$

where $L_{\exp_{\mathbf{y}}}$ is computed as

$$L_{\exp_{\mathbf{y}}} \triangleq \frac{L_{\oplus_y} c \|\mathbf{x}\| (\|\mathbf{y}_2\| + \|\mathbf{y}_1\|)}{(1 - \sqrt{c})^2} + L_{\oplus_x}. \quad (27)$$

Moreover, $L_{\exp_{\mathbf{y}}}$ satisfies that

$$\lim_{c \rightarrow 0} L_{\exp_{\mathbf{y}}} = 1. \quad (28)$$

By utilizing the hyperbolic constraint of \mathbf{y} , $L_{\exp_{\mathbf{y}}}$ can be further modeled as

$$L_{\exp_{\mathbf{y}}} \triangleq \frac{2\sqrt{c}L_{\oplus_y} \|\mathbf{x}\|}{(1 - \sqrt{c})^2} + L_{\oplus_x}. \quad (29)$$

Theorem 5. The exponential map $\exp_{\mathbf{y}}^c(\mathbf{x})$ is $L_{\exp_{\mathbf{x}}} -$ Lipschitz continuous with respect to \mathbf{x} . Mathematically, for any \mathbf{x}_1 and \mathbf{x}_2 , we have that

$$\|\exp_{\mathbf{y}}^c(\mathbf{x}_1) - \exp_{\mathbf{y}}^c(\mathbf{x}_2)\| \leq L_{\exp_{\mathbf{x}}} \|\mathbf{x}_1 - \mathbf{x}_2\|, \quad (30)$$

where $L_{\exp_{\mathbf{x}}}$ is computed as

$$L_{\exp_{\mathbf{x}}} \triangleq L_{\oplus_y} \left(\left| \frac{1}{1 - c\|\mathbf{y}\|^2} \right| + \frac{2 \tanh\left(\frac{\sqrt{c}\|\mathbf{x}_2\|}{1 - c\|\mathbf{y}\|^2}\right)}{\sqrt{c}\|\mathbf{x}_2\|} \right), \quad (31)$$

and $L_{\exp_{\mathbf{x}}}$ can satisfy that

$$\lim_{c \rightarrow 0} L_{\exp_{\mathbf{x}}} = 1. \quad (32)$$

From the hyperbolic constraint of \mathbf{y} , we can further model $L_{\exp_{\mathbf{x}}}$ as

$$L_{\exp_{\mathbf{x}}} = L_{\oplus_y} \left| \frac{1}{1 - \sqrt{c}} \right| + \frac{2L_{\oplus_y}}{\sqrt{c}\|\mathbf{x}_2\|}. \quad (33)$$

3.2.3 Lipschitz Continuity of Logarithmic Map

In Theorem 6, we analyze the Lipschitz continuity of logarithmic map $\log_{\mathbf{y}}^c(\mathbf{x})$ with respect to \mathbf{y} .

Theorem 6. The logarithmic map $\log_{\mathbf{y}}^c(\mathbf{x})$ is Lipschitz continuous with the constant $L_{\log_{\mathbf{y}}}$ with respect to \mathbf{y} . Mathematically, for any \mathbf{y}_1 and \mathbf{y}_2 , we have that

$$\|\log_{\mathbf{y}_1}^c(\mathbf{x}) - \log_{\mathbf{y}_2}^c(\mathbf{x})\| \leq L_{\log_{\mathbf{y}}} \|\mathbf{y}_1 - \mathbf{y}_2\|, \quad (34)$$

where $L_{\log_{\mathbf{y}}}$ is computed as

$$L_{\log_{\mathbf{y}}} \triangleq L_{\oplus_x} (1 + c\|\mathbf{x}\| \|\mathbf{y}_1\|)^2 + \frac{\sqrt{c}}{4} \|\mathbf{y}_1 + \mathbf{y}_2\| + \sqrt{c}L_{\oplus_x}, \quad (35)$$

and $L_{\log_{\mathbf{y}}}$ satisfies that

$$\lim_{c \rightarrow 0} L_{\log_{\mathbf{y}}} = 1. \quad (36)$$

From the hyperbolic constraint of \mathbf{x} and \mathbf{y} , $L_{\log_{\mathbf{y}}}$ can be modeled as

$$L_{\log_{\mathbf{y}}} = 4L_{\oplus_x} + \frac{1}{2} + \sqrt{c}L_{\oplus_x}. \quad (37)$$

3.3 Lipschitz Bound for Changes in Tangent Points

In practice, one sets the tangent point \mathbf{y} as $\mathbf{0}$ for HNNs for the scale of simplicity. In this section, we analyze the error bound between $\mathcal{L}(\mathbf{w}, c, \mathbf{y})$ and $\mathcal{L}(\mathbf{w}, c, \mathbf{0})$. To this end, we first analyze the Lipschitz continuity of loss function $\mathcal{L}(\mathbf{w}, c, \mathbf{y})$ with respect to \mathbf{y} , shown in Theorem 7. By utilizing the developed theorem, we derive the corollary to present the Lipschitz bound for changing tangent point into $\mathbf{0}$.

Theorem 7. Suppose that the loss function $\mathcal{L}(\cdot)$ is $L_{\mathcal{L}} -$ Lipschitz continuous with respect to the predicted probability, the hyperbolic MLR in Eq. (7) is $L_p -$ Lipschitz continuous with respect to its input \mathbf{x} , and $f_{\mathbf{a}}(\cdot)$ is $L_f -$ Lipschitz continuous. For any tangent point $\mathbf{y}_1, \mathbf{y}_2 \in \mathcal{H}^{d,c}$, it holds that

$$|\mathcal{L}(\mathbf{w}, c, \mathbf{y}_1) - \mathcal{L}(\mathbf{w}, c, \mathbf{y}_2)| \leq L_{\text{tangent}} \|\mathbf{y}_1 - \mathbf{y}_2\|, \quad (38)$$

where L_{tangent} is a constant and is computed as

$$L_{\text{tangent}} \triangleq L_{\mathcal{L}} L_{\oplus_x} (L_{\exp_{\mathbf{y}}} + L_{\exp_{\mathbf{x}}} L_f L_{\log_{\mathbf{y}}} \|\mathbf{a}\|). \quad (39)$$

\mathbf{a} , a subset of \mathbf{w} , is the parameters of the function $f_{\mathbf{a}}(\cdot)$. When $c \rightarrow 0$, L_{tangent} can be further modeled as

$$\lim_{c \rightarrow 0} L_{\text{tangent}} = L_{\mathcal{L}} + L_{\mathcal{L}} L_f \|\mathbf{a}\|, \quad (40)$$

which is consistent with the property in Euclidean spaces.

Proof. We define \mathbf{x}_1 and \mathbf{x}_2 as the hyperbolic representations computed by Eq. (6), using the tangent points \mathbf{y}_1 and \mathbf{y}_2 , respectively. Mathematically, \mathbf{x}_1 and \mathbf{x}_2 are computed as

$$\begin{aligned}\mathbf{x}_1 &= \text{expm}_{\mathbf{y}_1}^c(f_{\mathbf{a}}(\text{logm}_{\mathbf{y}_1}^c(\mathbf{x}))) \oplus_c \mathbf{b}, \\ \mathbf{x}_2 &= \text{expm}_{\mathbf{y}_2}^c(f_{\mathbf{a}}(\text{logm}_{\mathbf{y}_2}^c(\mathbf{x}))) \oplus_c \mathbf{b}.\end{aligned}\quad (41)$$

Considering that the loss function is $L'_\mathcal{L}$ -Lipschitz continuous with respect to the predicted probability, and the hyperbolic MLR in Eq. (7) is L_p -Lipschitz continuous with respect to its input \mathbf{x} , we can obtain that

$$\begin{aligned}|\mathcal{L}(\mathbf{w}, c, \mathbf{y}_1) - \mathcal{L}(\mathbf{w}, c, \mathbf{y}_2)| &\leq L'_\mathcal{L} |p(z = k|\mathbf{x}_1) - p(z = k|\mathbf{x}_2)| \\ &\leq L'_\mathcal{L} L_p \|\mathbf{x}_1 - \mathbf{x}_2\|.\end{aligned}\quad (42)$$

By denoting $L_\mathcal{L} \triangleq L'_\mathcal{L} L_p$ and substituting Eq. (41) into Eq. (42), we can obtain that

$$\begin{aligned}|\mathcal{L}(\mathbf{w}, c, \mathbf{y}_1) - \mathcal{L}(\mathbf{w}, c, \mathbf{y}_2)| &\leq L_\mathcal{L} \|\mathbf{x}_1 - \mathbf{x}_2\| \\ &\leq L_\mathcal{L} \|\text{expm}_{\mathbf{y}_1}^c(f_{\mathbf{a}}(\text{logm}_{\mathbf{y}_1}^c(\mathbf{x}))) \oplus_c \mathbf{b} \\ &\quad - \text{expm}_{\mathbf{y}_2}^c(f_{\mathbf{a}}(\text{logm}_{\mathbf{y}_2}^c(\mathbf{x}))) \oplus_c \mathbf{b}\|.\end{aligned}\quad (43)$$

From the Lipschitz continuity in Theorem 3, it holds that

$$\begin{aligned}|\mathcal{L}(\mathbf{w}, c, \mathbf{y}_1) - \mathcal{L}(\mathbf{w}, c, \mathbf{y}_2)| &\leq L_\mathcal{L} \|\text{expm}_{\mathbf{y}_1}^c(f_{\mathbf{a}}(\text{logm}_{\mathbf{y}_1}^c(\mathbf{x}))) \oplus_c \mathbf{b} \\ &\quad - \text{expm}_{\mathbf{y}_2}^c(f_{\mathbf{a}}(\text{logm}_{\mathbf{y}_2}^c(\mathbf{x}))) \oplus_c \mathbf{b}\| \\ &\leq L_\mathcal{L} L_{\oplus_x} \|\text{expm}_{\mathbf{y}_1}^c(f_{\mathbf{a}}(\text{logm}_{\mathbf{y}_1}^c(\mathbf{x}))) \\ &\quad - \text{expm}_{\mathbf{y}_2}^c(f_{\mathbf{a}}(\text{logm}_{\mathbf{y}_2}^c(\mathbf{x})))\| \\ &\leq L_\mathcal{L} L_{\oplus_x} \|\text{expm}_{\mathbf{y}_1}^c(f_{\mathbf{a}}(\text{logm}_{\mathbf{y}_1}^c(\mathbf{x}))) \\ &\quad - \text{expm}_{\mathbf{y}_2}^c(f_{\mathbf{a}}(\text{logm}_{\mathbf{y}_1}^c(\mathbf{x})))\| \\ &\quad + L_\mathcal{L} L_{\oplus_x} \|\text{expm}_{\mathbf{y}_2}^c(f_{\mathbf{a}}(\text{logm}_{\mathbf{y}_1}^c(\mathbf{x}))) \\ &\quad - \text{expm}_{\mathbf{y}_2}^c(f_{\mathbf{a}}(\text{logm}_{\mathbf{y}_2}^c(\mathbf{x})))\|.\end{aligned}\quad (44)$$

From the Lipschitz continuity in Theorems 4 and 5, we can obtain that

$$\begin{aligned}\|\text{expm}_{\mathbf{y}_1}^c(f_{\mathbf{a}}(\text{logm}_{\mathbf{y}_1}^c(\mathbf{x}))) - \text{expm}_{\mathbf{y}_2}^c(f_{\mathbf{a}}(\text{logm}_{\mathbf{y}_1}^c(\mathbf{x})))\| &\leq L_{\text{expm}_y} \|\mathbf{y}_1 - \mathbf{y}_2\|,\end{aligned}\quad (45)$$

and

$$\begin{aligned}\|\text{expm}_{\mathbf{y}_2}^c(f_{\mathbf{a}}(\text{logm}_{\mathbf{y}_1}^c(\mathbf{x}))) - \text{expm}_{\mathbf{y}_2}^c(f_{\mathbf{a}}(\text{logm}_{\mathbf{y}_2}^c(\mathbf{x})))\| &\leq L_{\text{expm}_x} \|f_{\mathbf{a}}(\text{logm}_{\mathbf{y}_1}^c(\mathbf{x})) - f_{\mathbf{a}}(\text{logm}_{\mathbf{y}_2}^c(\mathbf{x}))\|.\end{aligned}\quad (46)$$

From the Lipschitz continuity assumption of $f_{\mathbf{a}}(\cdot)$ and Lipschitz continuity in Theorem 6, it holds that

$$\begin{aligned}\|f_{\mathbf{a}}(\text{logm}_{\mathbf{y}_1}^c(\mathbf{x})) - f_{\mathbf{a}}(\text{logm}_{\mathbf{y}_2}^c(\mathbf{x}))\| &\leq L_f \|\mathbf{a}\| \|\text{logm}_{\mathbf{y}_1}^c(\mathbf{x}) - \text{logm}_{\mathbf{y}_2}^c(\mathbf{x})\| \\ &\leq L_f L_{\text{logm}_y} \|\mathbf{a}\| \|\mathbf{y}_1 - \mathbf{y}_2\|.\end{aligned}\quad (47)$$

Overall, we can derive that

$$\begin{aligned}|\mathcal{L}(\mathbf{w}, c, \mathbf{y}_1) - \mathcal{L}(\mathbf{w}, c, \mathbf{y}_2)| &\leq L_\mathcal{L} L_{\oplus_x} L_{\text{expm}_y} \|\mathbf{y}_1 - \mathbf{y}_2\| \\ &\quad + L_\mathcal{L} L_{\oplus_x} L_{\text{expm}_x} L_f L_{\text{logm}_y} \|\mathbf{a}\| \|\mathbf{y}_1 - \mathbf{y}_2\|.\end{aligned}\quad (48)$$

By denoting

$$L_{\text{tangent}} \triangleq L_\mathcal{L} L_{\oplus_x} (L_{\text{expm}_y} + L_{\text{expm}_x} L_f L_{\text{logm}_y} \|\mathbf{a}\|),\quad (49)$$

we have proved that

$$|\mathcal{L}(\mathbf{w}, c, \mathbf{y}) - \mathcal{L}(\mathbf{w}, c, \mathbf{0})| \leq L_{\text{tangent}} \|\mathbf{y}_1 - \mathbf{y}_2\|. \quad (50)$$

Because $\lim_{c \rightarrow 0} L_{\oplus_x} = 1$, $\lim_{c \rightarrow 0} L_{\text{expm}_x} = 1$, $\lim_{c \rightarrow 0} L_{\text{expm}_y} = 1$, and $\lim_{c \rightarrow 0} L_{\text{logm}_y} = 1$, when $c \rightarrow 0$, Eq. (48) can be modeled as

$$\begin{aligned}\lim_{c \rightarrow 0} |\mathcal{L}(\mathbf{w}, c, \mathbf{y}_1) - \mathcal{L}(\mathbf{w}, c, \mathbf{y}_2)| &\leq (L_\mathcal{L} + L_\mathcal{L} L_f \|\mathbf{a}\|) \|\mathbf{y}_1 - \mathbf{y}_2\|.\end{aligned}\quad (51)$$

The exponential map and logarithmic map satisfy that

$$\lim_{c \rightarrow 0} \text{expm}_{\mathbf{y}}^c(\mathbf{x}) = \mathbf{x} + \mathbf{y}, \quad \lim_{c \rightarrow 0} \text{logm}_{\mathbf{y}}^c(\mathbf{x}) = \mathbf{x} - \mathbf{y}. \quad (52)$$

By utilizing this property, we can obtain the expression of $|\mathcal{L}(\mathbf{w}, c, \mathbf{y}_1) - \mathcal{L}(\mathbf{w}, c, \mathbf{y}_2)|$ in Euclidean spaces, *i.e.*,

$$\begin{aligned}\lim_{c \rightarrow 0} |\mathcal{L}(\mathbf{w}, c, \mathbf{y}_1) - \mathcal{L}(\mathbf{w}, c, \mathbf{y}_2)| &= |\mathcal{L}(f_{\mathbf{a}}(\mathbf{x} - \mathbf{y}_1) + \mathbf{y}_1 + \mathbf{b}) - \mathcal{L}(f_{\mathbf{a}}(\mathbf{x} - \mathbf{y}_2) + \mathbf{y}_2 + \mathbf{b})|.\end{aligned}\quad (53)$$

Moreover, it holds that

$$\begin{aligned}|\mathcal{L}(f_{\mathbf{a}}(\mathbf{x} - \mathbf{y}_1) + \mathbf{y}_1 + \mathbf{b}) - \mathcal{L}(f_{\mathbf{a}}(\mathbf{x} - \mathbf{y}_2) + \mathbf{y}_2 + \mathbf{b})| &\leq L_\mathcal{L} \|f_{\mathbf{a}}(\mathbf{x} - \mathbf{y}_1) - f_{\mathbf{a}}(\mathbf{x} - \mathbf{y}_2) + \mathbf{y}_1 - \mathbf{y}_2\| \\ &\leq L_\mathcal{L} (\|f_{\mathbf{a}}(\mathbf{x} - \mathbf{y}_1) - f_{\mathbf{a}}(\mathbf{x} - \mathbf{y}_2)\| + \|\mathbf{y}_1 - \mathbf{y}_2\|) \\ &\leq L_\mathcal{L} \|\mathbf{y}_1 - \mathbf{y}_2\| + L_\mathcal{L} L_f \|\mathbf{a}\| \|\mathbf{y}_1 - \mathbf{y}_2\|.\end{aligned}\quad (54)$$

In this way, we have proved that when $c \rightarrow 0$, our proof is consistent with the expression in Euclidean spaces. \square

Corollary 1. *By setting $\mathbf{y}_1 = \mathbf{y}$ and $\mathbf{y}_2 = \mathbf{0}$, it holds that*

$$|\mathcal{L}(\mathbf{w}, c, \mathbf{y}) - \mathcal{L}(\mathbf{w}, c, \mathbf{0})| \leq \mathcal{E}_{l_y}, \quad (55)$$

where \mathcal{E}_{l_y} is a constant and is computed as

$$\mathcal{E}_{l_y} = L_{\mathcal{L}} L_{\oplus_x} \|\mathbf{y}\| (L_{\text{expm}_y} + L_{\text{expm}_x} L_f L_{\text{logm}_y} \|\mathbf{a}\|). \quad (56)$$

When $\mathbf{y} \rightarrow \mathbf{0}$, it holds that

$$\lim_{\mathbf{y} \rightarrow \mathbf{0}} \mathcal{E}_{l_y} = 0, \quad (57)$$

which also conforms to common sense. By utilizing the hyperbolic property of \mathbf{y} , \mathcal{E}_{l_y} can be further modeled as

$$\mathcal{E}_{l_y} \triangleq L_{\mathcal{L}} L_{\oplus_x} \frac{1}{c} (L_{\text{expm}_y} + L_{\text{expm}_x} L_f L_{\text{logm}_y} \|\mathbf{a}\|). \quad (58)$$

From the corollary, we have proved that the approximation error of setting the tangent point \mathbf{y} as $\mathbf{0}$ is upper-bounded.

Discussion about assumptions. The assumptions in our theoretical analysis are generally mild. For example, the angular constraint ($\cos \theta \geq \cos \bar{\theta}$) essentially requires that the angle between two vectors does not approach 90 degrees. In high-dimensional spaces, two randomly sampled vectors are rarely exactly orthogonal, making this condition naturally satisfied in most cases. As for the assumptions related to the Lipschitz continuity of the network, existing theoretical analysis (Gouk et al, 2021) shows that common neural network modules, including fully connected layers, convolutional layers, ReLU, and BatchNorm, are Lipschitz continuous, with their Lipschitz constants computable or controllable via the spectral norms of the weights.

In fact, it is common for many well-established methods that rely on certain assumptions for theoretical tractability, while still achieving strong empirical performance in real-world scenarios. For example, convergence guarantees for optimization algorithms such as Adam (Kingma and Ba, 2015) typically require assumptions like Lipschitz continuity and smoothness of the loss function. Similarly, theoretical studies on Low-Rank Adaptation (LoRA) (Zeng and Lee, 2024; Hu et al, 2024b) introduce mild structural assumptions to ensure its adaptation capability. Similar to other theoretical frameworks, the assumptions in our work do not necessarily undermine the real-world applicability of our method.

In future work, we intend to extend our theoretical analysis by relaxing the current assumptions. To this end, we plan to investigate localized or parameterized Lipschitz bounds, and we will develop new approximation techniques

and bounding, thereby broadening the theoretical applicability of our results.

4 Generalization Analyses in HNNs

In order to develop the theoretical foundation of the effect of curvatures on HNNs, we derive the PAC-Bayesian generalization bound of HNNs in Theorem 8. Note that the generalization error bound in Euclidean spaces cannot be directly applied to HNNs. The reason is that the generalization error bound in Euclidean spaces assumes the parameters \mathbf{w} obeying the normal distribution (Foret et al, 2020), which does not hold for the parameters of HNNs. Moreover, the generalization error bound analysis in Euclidean spaces does not consider the hyperbolic operations in hyperbolic spaces that are essential for HNNs. This discrepancy indicates that the existing derivation does not fully account for the geometric properties of hyperbolic spaces, and thus, a tailored derivation to accommodate the characteristics of hyperbolic spaces in HNNs is necessary.

To establish the generalization error bound analysis, we first introduce two auxiliary lemmas.

Lemma 1. *The exponential map operation satisfies that $\|\mathbf{x} - \text{expm}_0^c(\mathbf{x})\| = \|\mathbf{x}\| - \tanh(\sqrt{c}\|\mathbf{x}\|) \frac{1}{\sqrt{c}}$, and $\lim_{c \rightarrow 0} \|\mathbf{x} - \text{expm}_0^c(\mathbf{x})\| = 0$.*

Proof. Recall that the exponential map is computed as

$$\text{expm}_0^c(\mathbf{x}) = \tanh(\sqrt{|c|}\|\mathbf{x}\|) \frac{\mathbf{x}}{\sqrt{|c|}\|\mathbf{x}\|}. \quad (59)$$

Therefore,

$$\begin{aligned} \|\mathbf{x} - \text{expm}_0^c(\mathbf{x})\| &= \left\| \mathbf{x} - \tanh(\sqrt{|c|}\|\mathbf{x}\|) \frac{\mathbf{x}}{\sqrt{|c|}\|\mathbf{x}\|} \right\| \\ &= \|\mathbf{x}\| \left| 1 - \frac{\tanh(\sqrt{|c|}\|\mathbf{x}\|)}{\sqrt{|c|}\|\mathbf{x}\|} \right| \\ &= \left| \|\mathbf{x}\| - \frac{\tanh(\sqrt{|c|}\|\mathbf{x}\|)}{\sqrt{|c|}} \right|. \end{aligned} \quad (60)$$

As to $\frac{\tanh(\sqrt{|c|}\|\mathbf{x}\|)}{\sqrt{|c|}}$, we observe that

$$\begin{aligned} \lim_{c \rightarrow 0} \frac{\tanh(\sqrt{|c|}\|\mathbf{x}\|)}{\sqrt{|c|}} &= \lim_{c \rightarrow 0} \frac{\text{sech}^2(\sqrt{c}\|\mathbf{x}\|) \frac{\|\mathbf{x}\|}{2\sqrt{c}}}{\frac{1}{2\sqrt{c}}} \\ &= \lim_{c \rightarrow 0} \text{sech}^2(\sqrt{c}\|\mathbf{x}\|) \|\mathbf{x}\| = \|\mathbf{x}\|. \end{aligned} \quad (61)$$

Therefore, it holds that

$$\lim_{c \rightarrow 0} \|\mathbf{x} - \text{expm}_0^c(\mathbf{x})\| = 0. \quad (62)$$

□

Lemma 2. *The logarithmic map operation satisfies that $\|\mathbf{x} - \text{logm}_0^c(\mathbf{x})\| = \|\mathbf{x}\| - \tanh^{-1}(\sqrt{c}\|\mathbf{x}\|) \frac{1}{\sqrt{c}}\|$, and $\lim_{c \rightarrow 0} \|\mathbf{x} - \text{logm}_0^c(\mathbf{x})\| = 0$.*

Proof. Recall that the exponential map is computed as

$$\text{logm}_0^c(\mathbf{x}) = \tanh^{-1}(\sqrt{|c|}\|\mathbf{x}\|) \frac{\mathbf{x}}{\sqrt{|c|}\|\mathbf{x}\|}. \quad (63)$$

Therefore, we can obtain that

$$\begin{aligned} \|\mathbf{x} - \text{logm}_0^c(\mathbf{x})\| &= \left\| \mathbf{x} - \tanh^{-1}(\sqrt{|c|}\|\mathbf{x}\|) \frac{\mathbf{x}}{\sqrt{|c|}\|\mathbf{x}\|} \right\| \\ &= \|\mathbf{x}\| \left| 1 - \frac{\tanh^{-1}(\sqrt{|c|}\|\mathbf{x}\|)}{\sqrt{|c|}\|\mathbf{x}\|} \right| \\ &= \left| \|\mathbf{x}\| - \frac{\tanh^{-1}(\sqrt{|c|}\|\mathbf{x}\|)}{\sqrt{|c|}} \right|. \end{aligned} \quad (64)$$

As to $\frac{\tanh^{-1}(\sqrt{|c|}\|\mathbf{x}\|)}{\sqrt{|c|}}$, we denote $t \triangleq \sqrt{c}$ and observe that

$$\begin{aligned} \lim_{t \rightarrow 0} \frac{\tanh^{-1}(t\|\mathbf{x}\|)}{t} &= \lim_{t \rightarrow 0} \frac{\frac{d}{dt} \tanh^{-1}(t\|\mathbf{x}\|)}{\frac{d}{dt} t} \\ &= \lim_{t \rightarrow 0} \frac{\frac{\|\mathbf{x}\|}{1-t^2\|\mathbf{x}\|^2}}{1} = \|\mathbf{x}\|, \end{aligned} \quad (65)$$

and thus

$$\frac{\tanh^{-1}(\sqrt{|c|}\|\mathbf{x}\|)}{\sqrt{|c|}} = \|\mathbf{x}\|, \quad (66)$$

Therefore,

$$\lim_{c \rightarrow 0} \|\mathbf{x} - \text{logm}_0^c(\mathbf{x})\| = 0. \quad (67)$$

□

After the auxiliary lemmas, we establish the generalization analysis in HNNs shown in Theorem 8, which quantifies the error bound between loss on any distribution and loss on training set.

Theorem 8. *Suppose that the loss function $\mathcal{L}(\cdot)$ is L'_L -Lipschitz continuous with respect to the predicted probability, the hyperbolic MLR in Eq. (7) is L_p -Lipschitz continuous with respect to its input \mathbf{x} , and $f_{\mathbf{a}}(\cdot)$ is L_f -Lipschitz continuous. For any $\rho > 0$ and any real distribution \mathcal{D} , with probability $1 - \delta$ over the choice of the training set*

$\mathcal{S} \sim \mathcal{D}$, the generalization bound on distribution \mathcal{D} is

$$\mathcal{L}_{\mathcal{D}}(\mathbf{w}, c, \mathbf{y}) \leq \mathcal{L}_{\mathcal{S}}(\mathbf{w}, c, \mathbf{y}) + \mathcal{L}_{\mathcal{S}}^{\text{sharp}} + \mathcal{E}_{l_{\text{gen}}}, \quad (68)$$

where

$$\mathcal{L}_{\mathcal{S}}^{\text{sharp}} = \max_{\|\epsilon\| \leq \rho} \mathcal{L}_{\mathcal{S}}(\mathbf{w} + \epsilon, c, \mathbf{y}) - \mathcal{L}_{\mathcal{S}}(\mathbf{w}, c, \mathbf{y}), \quad (69)$$

$\mathcal{L}_{\mathcal{D}}(\cdot)$ is the loss function on \mathcal{D} , and $\mathcal{L}_{\mathcal{S}}(\cdot)$ is the loss function on \mathcal{S} . $\mathcal{E}_{l_{\text{gen}}}'$ is given by

$$\mathcal{E}_{l_{\text{gen}}} \triangleq \mathcal{E}_{l_{\text{gen}}}' + \mathcal{E}_{l_y} + \mathcal{E}_{l_c} + \mathcal{E}_{l_y}' + \mathcal{E}_{l_c}', \quad (70)$$

where $\mathcal{E}_{l_{\text{gen}}}'$ is computed as

$$\mathcal{E}_{l_{\text{gen}}}' \triangleq \sqrt{\frac{d \log(1 + \frac{\|\mathbf{w}\|^2}{\rho^2} (1 + \sqrt{\frac{\log(n)}{d}})^2) + 4 \log \frac{n}{\delta} + 8 \log(6n + 3d)}{n - 1}}, \quad (71)$$

$$\begin{aligned} \mathcal{E}_{l_c} &= L_{\mathcal{L}} L_{\oplus_{c0}} + L_{\mathcal{L}} L_{\oplus_x} \|\mathbf{a}\| \frac{\tanh^{-1}(c^{1/4})}{\sqrt{c}} (L_f + 1), \\ \mathcal{E}_{l_c}' &= L_{\mathcal{L}} L_{\oplus_{c0}} + L_{\mathcal{L}} L_{\oplus_x} \frac{\tanh^{-1}(c^{1/4})}{\sqrt{c}} (L_f + 1) (\|\mathbf{a}\| + \rho), \\ \mathcal{E}_{l_y}' &= L_{\mathcal{L}} L_{\oplus_x} \frac{1}{c} (L_{\text{expm}_y} + L_{\text{expm}_x} L_f L_{\text{logm}_y} (\|\mathbf{a}\| + \rho)), \end{aligned} \quad (72)$$

$n = |\mathcal{S}|$, and d denotes numbers of parameters. \mathbf{a} , a subset of \mathbf{w} , is the parameters of the function $f_{\mathbf{a}}(\cdot)$. The generalization error bound of loss function with respect to HNNs satisfies that

$$\lim_{y \rightarrow 0, c \rightarrow 0} \mathcal{E}_{l_{\text{gen}}} = \mathcal{E}_{l_{\text{gen}}}'. \quad (73)$$

Proof. We aim to derive an upper bound for the loss given a distribution \mathcal{D} . The main challenge lies in the absence of important mathematical theorems, such as the KL divergence on hyperbolic spaces, which does not have an analytic expression (Cho et al., 2024). To overcome this challenge, we base our theoretical analyses on the PAC-Bayesian generalization error bound, leveraging the Lipschitz continuity and Lipschitz bound in HNNs in Section 3, as well as Lipschitz continuity of the loss function.

Follow the PAC-Bayesian generalization error bound (Foret et al., 2020), with probability $1 - \frac{1}{\sqrt{n}}$, the loss function $\mathcal{L}(\mathbf{w}, 0, \mathbf{0})$ satisfies that

$$\begin{aligned} \mathcal{L}_{\mathcal{D}}(\mathbf{w}, 0, \mathbf{0}) &\leq \max_{\|\epsilon\| \leq \rho} \mathcal{L}_{\mathcal{S}}(\mathbf{w} + \epsilon, 0, \mathbf{0}) + \\ &\quad \sqrt{\frac{d \log(1 + \frac{\|\mathbf{w}\|^2}{\rho^2} (1 + \sqrt{\frac{\log(n)}{d}})^2) + 4 \log \frac{n}{\delta} + 8 \log(6n + 3d)}{n - 1}}. \end{aligned} \quad (74)$$

We denote the constant term in Eq. (74) as $\mathcal{E}_{l_{\text{gen}}}'$,

$$\mathcal{E}'_{l_{gen}} \triangleq \sqrt{\frac{d \log(1 + \frac{\|w\|^2}{\rho^2}) (1 + \sqrt{\frac{\log(n)}{d}})^2 + 4 \log \frac{n}{\delta} + 8 \log(6n + 3d)}{n - 1}}. \quad (75)$$

We define \mathbf{x}_1 and \mathbf{x}_2 as the hyperbolic representations computed by Eq. (6), setting the curvature as c and 0, respectively. Mathematically, \mathbf{x}_1 and \mathbf{x}_2 are computed as

$$\begin{aligned} \mathbf{x}_1 &= \text{expm}_0^c(f_{\mathbf{a}}(\text{logm}_0^c(\mathbf{x}))) \oplus_c \mathbf{b} \\ \mathbf{x}_2 &= \text{expm}_0^0(f_{\mathbf{a}}(\text{logm}_0^0(\mathbf{x}))) \oplus_0 \mathbf{b} = f_{\mathbf{a}}(\mathbf{x}) + \mathbf{b}. \end{aligned} \quad (76)$$

From Eq. (42) and $L_{\mathcal{L}} = L'_{\mathcal{L}} L_p$, we can obtain that

$$\begin{aligned} |\mathcal{L}(\mathbf{w}, c, \mathbf{0}) - \mathcal{L}(\mathbf{w}, 0, \mathbf{0})| &\leq L_{\mathcal{L}} \|\mathbf{x}_1 - \mathbf{x}_2\| \\ &\leq L_{\mathcal{L}} \|\text{expm}_0^c(f_{\mathbf{a}}(\text{logm}_0^c(\mathbf{x}))) \oplus_c \mathbf{b} - (f_{\mathbf{a}}(\mathbf{x}) + \mathbf{b})\|. \end{aligned} \quad (77)$$

From Lipschitz continuity in Theorems 1 and 3, it holds that

$$\begin{aligned} |\mathcal{L}(\mathbf{w}, c, \mathbf{0}) - \mathcal{L}(\mathbf{w}, 0, \mathbf{0})| &\leq L_{\mathcal{L}} \|\text{expm}_0^c(f_{\mathbf{a}}(\text{logm}_0^c(\mathbf{x}))) \oplus_c \mathbf{b} - (f_{\mathbf{a}}(\mathbf{x}) + \mathbf{b})\| \\ &\leq L_{\mathcal{L}} L_{\oplus_x} \|\text{expm}_0^c(f_{\mathbf{a}}(\text{logm}_0^c(\mathbf{x}))) - f_{\mathbf{a}}(\mathbf{x})\| + L_{\mathcal{L}} L_{\oplus_{c0}}. \end{aligned} \quad (78)$$

We can further derive that

$$\begin{aligned} L_{\mathcal{L}} L_{\oplus_x} \|\text{expm}_0^c(f_{\mathbf{a}}(\text{logm}_0^c(\mathbf{x}))) - f_{\mathbf{a}}(\mathbf{x})\| &\leq L_{\mathcal{L}} L_{\oplus_x} (\|\text{expm}_0^c(f_{\mathbf{a}}(\text{logm}_0^c(\mathbf{x}))) - f_{\mathbf{a}}(\text{logm}_0^c(\mathbf{x}))\| \\ &\quad + \|f_{\mathbf{a}}(\text{logm}_0^c(\mathbf{x})) - f_{\mathbf{a}}(\mathbf{x})\|). \end{aligned} \quad (79)$$

From Lemma 1, left terms in Eq. (79) can be further modeled as

$$\begin{aligned} \|\text{expm}_0^c(f_{\mathbf{a}}(\text{logm}_0^c(\mathbf{x}))) - f_{\mathbf{a}}(\text{logm}_0^c(\mathbf{x}))\| &\leq \left| \|f_{\mathbf{a}}(\text{logm}_0^c(\mathbf{x}))\| - \tanh(\sqrt{c}\|f_{\mathbf{a}}(\text{logm}_0^c(\mathbf{x}))\|) \frac{1}{\sqrt{c}} \right|. \end{aligned} \quad (80)$$

Because

$$\|f_{\mathbf{a}}(\text{logm}_0^c(\mathbf{x}))\| > \tanh(\sqrt{c}\|f_{\mathbf{a}}(\text{logm}_0^c(\mathbf{x}))\|) \frac{1}{\sqrt{c}}, \quad (81)$$

and $f(x) - \tanh^{-1}(\sqrt{c}x)/\sqrt{c}$ is an increasing function, it holds that

$$\begin{aligned} \left| \|f_{\mathbf{a}}(\text{logm}_0^c(\mathbf{x}))\| - \tanh(\sqrt{c}\|f_{\mathbf{a}}(\text{logm}_0^c(\mathbf{x}))\|) \frac{1}{\sqrt{c}} \right| &\leq \tilde{N} - \frac{\tanh(\sqrt{c}\tilde{N})}{\sqrt{c}}, \end{aligned} \quad (82)$$

where \tilde{N} is denoted as the upper bound of $f_{\mathbf{a}}(\text{logm}_0^c(\mathbf{x}))$, i.e., $\|f_{\mathbf{a}}(\text{logm}_0^c(\mathbf{x}))\| \leq \tilde{N}$.

From the Lipschitz continuity assumption of $f_{\mathbf{a}}(\cdot)$ and Lemma 2, the right term in Eq. (79) can be further modeled as

$$\begin{aligned} \|f_{\mathbf{a}}(\text{logm}_0^c(\mathbf{x})) - f_{\mathbf{a}}(\mathbf{x})\| &\leq L_f \|\mathbf{a}\| \|\text{logm}_0^c(\mathbf{x}) - \mathbf{x}\| \\ &\leq L_f \|\mathbf{a}\| \left| \|\mathbf{x}\| - \tanh^{-1}(\sqrt{c}\|\mathbf{x}\|) \frac{1}{\sqrt{c}} \right|. \end{aligned} \quad (83)$$

Besides, because

$$\tanh^{-1}(\sqrt{c}\|\mathbf{x}\|) \frac{1}{\sqrt{c}} > \|\mathbf{x}\|, \quad (84)$$

Eq. (83) is converted into

$$\begin{aligned} \|f_{\mathbf{a}}(\text{logm}_0^c(\mathbf{x})) - f_{\mathbf{a}}(\mathbf{x})\| &\leq L_f \|\mathbf{a}\| \left(\tanh^{-1}(\sqrt{c}\|\mathbf{x}\|) \frac{1}{\sqrt{c}} - \|\mathbf{x}\| \right). \end{aligned} \quad (85)$$

In this way, Eq. (79) can be transformed as

$$\begin{aligned} L_{\mathcal{L}} L_{\oplus_x} \|\text{expm}_0^c(f_{\mathbf{a}}(\text{logm}_0^c(\mathbf{x}))) - f_{\mathbf{a}}(\mathbf{x})\| &\leq L_{\mathcal{L}} L_{\oplus_x} \left(\tilde{N} - \frac{\tanh(\sqrt{c}\tilde{N})}{\sqrt{c}} \right. \\ &\quad \left. + L_f \|\mathbf{a}\| \left(\tanh^{-1}(\sqrt{c}\|\mathbf{x}\|) \frac{1}{\sqrt{c}} - \|\mathbf{x}\| \right) \right). \end{aligned} \quad (86)$$

In conclusion, the loss function $\mathcal{L}(\cdot)$ satisfies that

$$\begin{aligned} |\mathcal{L}(\mathbf{w}, c, \mathbf{0}) - \mathcal{L}(\mathbf{w}, 0, \mathbf{0})| &\leq L_{\mathcal{L}} L_{\oplus_{c0}} \\ &\quad + L_{\mathcal{L}} L_{\oplus_x} \left(\tilde{N} - \frac{\tanh(\sqrt{c}\tilde{N})}{\sqrt{c}} \right. \\ &\quad \left. + L_f \|\mathbf{a}\| \left(\tanh^{-1}(\sqrt{c}\|\mathbf{x}\|) \frac{1}{\sqrt{c}} - \|\mathbf{x}\| \right) \right). \end{aligned} \quad (87)$$

By denoting

$$\begin{aligned} \mathcal{E}_{l_c} &\triangleq L_{\mathcal{L}} L_{\oplus_{c0}} + L_{\mathcal{L}} L_{\oplus_x} \left(\tilde{N} - \frac{\tanh(\sqrt{c}\tilde{N})}{\sqrt{c}} \right. \\ &\quad \left. + L_f \|\mathbf{a}\| \left(\tanh^{-1}(\sqrt{c}\|\mathbf{x}\|) \frac{1}{\sqrt{c}} - \|\mathbf{x}\| \right) \right), \end{aligned} \quad (88)$$

it can be proved that

$$|\mathcal{L}(\mathbf{w}, c, \mathbf{0}) - \mathcal{L}(\mathbf{w}, 0, \mathbf{0})| \leq \mathcal{E}_{l_c}. \quad (89)$$

From the established theorems, we have that

$$\begin{cases} \lim_{c \rightarrow 0} \tilde{N} - \frac{\tanh(\sqrt{c}\tilde{N})}{\sqrt{c}} = 0 \\ \lim_{c \rightarrow 0} \tanh^{-1}(\sqrt{c}\|\mathbf{x}\|) \frac{1}{\sqrt{c}} - \|\mathbf{x}\| = 0 \\ \lim_{c \rightarrow 0} L'_{\oplus_{c0}} = 0 \end{cases} \quad (90)$$

Therefore, \mathcal{E}_{l_c} satisfies that

$$\lim_{c \rightarrow 0} \mathcal{E}_{l_c} = 0. \quad (91)$$

By constraining the upper bound of $\|\mathbf{x}\|$, i.e., $\|\mathbf{x}\| \leq \frac{1}{c^{1/4}}$, \mathcal{E}_{l_c} can be modeled as

$$\begin{aligned} \mathcal{E}_{l_c} &\leq L_{\mathcal{L}} L_{\oplus_x} (\|f_{\mathbf{a}}(\text{logm}_0^c(\mathbf{x}))\| \\ &\quad + L_f \|\mathbf{a}\| \tanh^{-1}(\sqrt{c}\|\mathbf{x}\|) \frac{1}{\sqrt{c}}) + L_{\mathcal{L}} L_{\oplus_{c0}}, \end{aligned} \quad (92)$$

where

$$\begin{aligned}\|f_{\mathbf{a}}(\text{logm}_{\mathbf{0}}^c(\mathbf{x}))\| &\leq \|\mathbf{a}\| \|\text{logm}_{\mathbf{0}}^c(\mathbf{x})\| \\ &\leq \frac{\|\mathbf{a}\| \tanh^{-1}(\sqrt{c} \|\mathbf{x}\|)}{\sqrt{c}}.\end{aligned}\quad (93)$$

Therefore, the error bound can be further modeled as

$$\mathcal{E}_{l_c} = L_{\mathcal{L}} L_{\oplus_{c0}} + L_{\mathcal{L}} L_{\oplus_x} \|\mathbf{a}\| \frac{\tanh^{-1}(c^{1/4})}{\sqrt{c}} (L_f + 1). \quad (94)$$

From the above analysis, we have

$$|\mathcal{L}(\mathbf{w}, c, \mathbf{0}) - \mathcal{L}(\mathbf{w}, c, \mathbf{y})| \leq \mathcal{E}_{l_c}. \quad (95)$$

By substituting $\mathcal{L}_{\mathcal{D}}$ and $\mathcal{L}_{\mathcal{S}}$ into Eq. (89), we have that

$$\begin{aligned}\mathcal{L}_{\mathcal{D}}(\mathbf{w}, c, \mathbf{0}) - \mathcal{L}_{\mathcal{D}}(\mathbf{w}, 0, \mathbf{0}) &\leq \mathcal{E}_{l_c}, \\ \mathcal{L}_{\mathcal{S}}(\mathbf{w}, c, \mathbf{0}) - \mathcal{L}_{\mathcal{S}}(\mathbf{w}, 0, \mathbf{0}) &\leq \mathcal{E}_{l_c}.\end{aligned}\quad (96)$$

Moreover, the loss function $\mathcal{L}_{\mathcal{S}}(\cdot)$ satisfies that

$$\mathcal{L}_{\mathcal{S}}(\mathbf{w} + \boldsymbol{\epsilon}, 0, \mathbf{0}) \leq \mathcal{L}_{\mathcal{S}}(\mathbf{w} + \boldsymbol{\epsilon}, c, \mathbf{0}) + \mathcal{E}'_{l_c}. \quad (97)$$

Here, \mathcal{E}'_{l_c} is computed as

$$\begin{aligned}\mathcal{E}'_{l_c} &\triangleq L_{\mathcal{L}} L_{\oplus_{c0}} + L_{\mathcal{L}} L_{\oplus_x} \left(\tilde{N} - \frac{\tanh(\sqrt{c}\tilde{N})}{\sqrt{c}} \right. \\ &\quad \left. + L_f(\|\mathbf{a}\| + \|\boldsymbol{\epsilon}\|) \left(\frac{\tanh^{-1}(\sqrt{c}\|\mathbf{x}\|)}{\sqrt{c}} - \|\mathbf{x}\| \right) \right) \\ &= L_{\mathcal{L}} L_{\oplus_{c0}} + L_{\mathcal{L}} L_{\oplus_x} \frac{\tanh^{-1}(c^{1/4})}{\sqrt{c}} (L_f + 1)(\|\mathbf{a}\| + \|\boldsymbol{\epsilon}\|),\end{aligned}\quad (98)$$

where \mathcal{E}'_{l_c} also satisfies that

$$\lim_{c \rightarrow 0} \mathcal{E}'_{l_c} = 0. \quad (99)$$

From Corollary 1, we have proved that

$$\mathcal{L}_{\mathcal{D}}(\mathbf{w}, c, \mathbf{y}) - \mathcal{L}_{\mathcal{D}}(\mathbf{w}, c, \mathbf{0}) \leq \mathcal{E}_{l_y}, \quad (100)$$

and thus we can prove that

$$\begin{aligned}\mathcal{L}_{\mathcal{D}}(\mathbf{w}, c, \mathbf{y}) &\leq \mathcal{L}_{\mathcal{D}}(\mathbf{w}, c, \mathbf{0}) + \mathcal{E}_{l_y} \\ &\leq \mathcal{L}_{\mathcal{D}}(\mathbf{w}, 0, \mathbf{0}) + \mathcal{E}_{l_c} + \mathcal{E}_{l_y}.\end{aligned}\quad (101)$$

As to $\mathcal{L}_{\mathcal{S}}(\cdot)$, we also have that

$$\mathcal{L}_{\mathcal{S}}(\mathbf{w}, c, \mathbf{0}) \leq \mathcal{L}_{\mathcal{S}}(\mathbf{w}, c, \mathbf{y}) + \mathcal{E}_{l_y}, \quad (102)$$

and thus

$$\mathcal{L}_{\mathcal{S}}(\mathbf{w} + \boldsymbol{\epsilon}, c, \mathbf{0}) \leq \mathcal{L}_{\mathcal{S}}(\mathbf{w} + \boldsymbol{\epsilon}, c, \mathbf{y}) + \mathcal{E}'_{l_y}. \quad (103)$$

Here, \mathcal{E}'_{l_y} is given by

$$\begin{aligned}\mathcal{E}'_{l_y} &\triangleq L_{\mathcal{L}} L_{\oplus_x} (L_{\text{expm}}_y \|\mathbf{y}\| \\ &\quad + L_{\text{expm}}_x L_f L_{\text{logm}}_y \|\mathbf{y}\| (\|\mathbf{a}\| + \|\boldsymbol{\epsilon}\|)) \\ &= L_{\mathcal{L}} L_{\oplus_x} \frac{1}{c} (L_{\text{expm}}_y + L_{\text{expm}}_x L_f L_{\text{logm}}_y (\|\mathbf{a}\| + \|\boldsymbol{\epsilon}\|)),\end{aligned}\quad (104)$$

where \mathcal{E}'_{l_y} also satisfies that

$$\lim_{\mathbf{y} \rightarrow \mathbf{0}} \mathcal{E}'_{l_y} = 0. \quad (105)$$

By combining Eq. (97) and Eq. (103), we derive that

$$\begin{aligned}\mathcal{L}_{\mathcal{S}}(\mathbf{w} + \boldsymbol{\epsilon}, 0, \mathbf{0}) &\leq \mathcal{L}_{\mathcal{S}}(\mathbf{w} + \boldsymbol{\epsilon}, c, \mathbf{0}) + \mathcal{E}'_{l_c} \\ &\leq \mathcal{L}_{\mathcal{S}}(\mathbf{w} + \boldsymbol{\epsilon}, c, \mathbf{y}) + \mathcal{E}'_{l_y} + \mathcal{E}'_{l_c},\end{aligned}\quad (106)$$

and thus

$$\max_{\|\boldsymbol{\epsilon}\| \leq \rho} \mathcal{L}_{\mathcal{S}}(\mathbf{w} + \boldsymbol{\epsilon}, 0, \mathbf{0}) \leq \max_{\|\boldsymbol{\epsilon}\| \leq \rho} \mathcal{L}_{\mathcal{S}}(\mathbf{w} + \boldsymbol{\epsilon}, c, \mathbf{y}) + \mathcal{E}'_{l_y} + \mathcal{E}'_{l_c}. \quad (107)$$

From $\|\boldsymbol{\epsilon}\| \leq \rho$, $\mathcal{E}'_{l_y}, \mathcal{E}'_{l_c}$ can be further modeled as

$$\begin{aligned}\mathcal{E}'_{l_c} &= L_{\mathcal{L}} L_{\oplus_{c0}} + L_{\mathcal{L}} L_{\oplus_x} \frac{\tanh^{-1}(c^{1/4})}{\sqrt{c}} (L_f + 1)(\|\mathbf{a}\| + \rho), \\ \mathcal{E}'_{l_y} &= L_{\mathcal{L}} L_{\oplus_x} \frac{1}{c} (L_{\text{expm}}_y + L_{\text{expm}}_x L_f L_{\text{logm}}_y (\|\mathbf{a}\| + \rho)).\end{aligned}\quad (108)$$

In this way, by utilizing Eq. (74), we establish the connection between $\mathcal{L}_{\mathcal{D}}(\mathbf{w}, c, \mathbf{y})$ and $\max_{\|\boldsymbol{\epsilon}\| \leq \rho} \mathcal{L}_{\mathcal{S}}(\mathbf{w} + \boldsymbol{\epsilon}, c, \mathbf{y})$, i.e.,

$$\begin{aligned}\mathcal{L}_{\mathcal{D}}(\mathbf{w}, c, \mathbf{y}) &\leq \mathcal{L}_{\mathcal{D}}(\mathbf{w}, 0, \mathbf{0}) + \mathcal{E}_{l_y} + \mathcal{E}_{l_c} \\ &\leq \max_{\|\boldsymbol{\epsilon}\| \leq \rho} \mathcal{L}_{\mathcal{S}}(\mathbf{w} + \boldsymbol{\epsilon}, 0, \mathbf{0}) + \mathcal{E}'_{l_{gen}} + \mathcal{E}_{l_y} + \mathcal{E}_{l_c} \\ &\leq \max_{\|\boldsymbol{\epsilon}\| \leq \rho} \mathcal{L}_{\mathcal{S}}(\mathbf{w} + \boldsymbol{\epsilon}, c, \mathbf{y}) + \mathcal{E}'_{l_{gen}} + \mathcal{E}_{l_y} + \mathcal{E}_{l_c} + \mathcal{E}'_{l_y} + \mathcal{E}'_{l_c}.\end{aligned}\quad (109)$$

Besides, by denoting

$$\mathcal{L}_{\mathcal{S}}^{\text{sharp}} \triangleq \max_{\|\boldsymbol{\epsilon}\| \leq \rho} \mathcal{L}_{\mathcal{S}}(\mathbf{w} + \boldsymbol{\epsilon}, c, \mathbf{y}) - \mathcal{L}_{\mathcal{S}}(\mathbf{w}, c, \mathbf{y}), \quad (110)$$

and

$$\mathcal{E}_{l_{gen}} \triangleq \mathcal{E}'_{l_{gen}} + \mathcal{E}_{l_y} + \mathcal{E}_{l_c} + \mathcal{E}'_{l_y} + \mathcal{E}'_{l_c}, \quad (111)$$

we have proved the theorem.

From Corollary 1 and the above analysis, we have obtained that

$$\lim_{\mathbf{y} \rightarrow \mathbf{0}} \mathcal{E}_{l_y} = 0, \lim_{c \rightarrow 0} \mathcal{E}_{l_c} = 0, \lim_{\mathbf{y} \rightarrow \mathbf{0}} \mathcal{E}'_{l_y} = 0, \lim_{c \rightarrow 0} \mathcal{E}'_{l_c} = 0, \quad (112)$$

and thus

$$\lim_{\mathbf{y} \rightarrow \mathbf{0}, c \rightarrow 0} \mathcal{E}_{l_{gen}} = \mathcal{E}'_{l_{gen}}. \quad (113)$$

□

In the implementation, we set the tangent point \mathbf{y} as $\mathbf{0}$ that is a special case of \mathbf{y} , and thus Theorem 8 also satisfies when $\mathbf{y} = \mathbf{0}$. To minimize $\mathcal{L}_{\mathcal{D}}$, we only need to minimize the first two terms in Eq. (68), since $\mathcal{E}'_{l_{gen}}$ is a constant. The first term $\mathcal{L}_{\mathcal{S}}(\mathbf{w}, c, \mathbf{y})$ is the loss value of HNNs

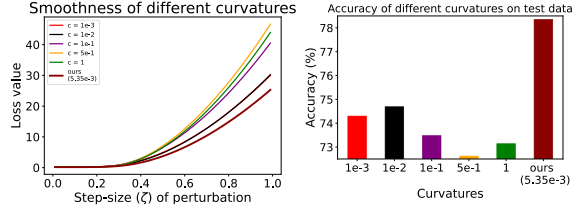
on the training set. The second term $\mathcal{L}_S^{\text{sharp}}$ captures the sharpness of \mathcal{L}_S at \mathbf{w} by measuring how quickly the training loss can be increased by moving from \mathbf{w} to a nearby parameter value on hyperbolic spaces, where $\{\mathbf{w} + \epsilon : \|\epsilon\| \leq \rho\}$ is the neighborhood of \mathbf{w} on hyperbolic spaces. In this case, we demonstrate that the smoothness (*i.e.*, $\mathcal{L}_S^{\text{sharp}}$) of the loss landscape affects the generalization of HNNs. Specifically, models converging to smoother regions (*i.e.*, with smaller values of $\mathcal{L}_S^{\text{sharp}}$) exhibit better generalization, while those converging to sharper regions (*i.e.*, with larger values of $\mathcal{L}_S^{\text{sharp}}$) generalize worse.

Notably, the sharpness term $\mathcal{L}_S^{\text{sharp}}$ is strongly related to the curvatures c . Setting inappropriate curvatures to train HNNs may cause the loss landscape around \mathbf{w} to become sharp, limiting the generalization of HNNs. In contrast, appropriate curvatures help smooth the loss landscape around \mathbf{w} , and improve the generalization of HNNs.

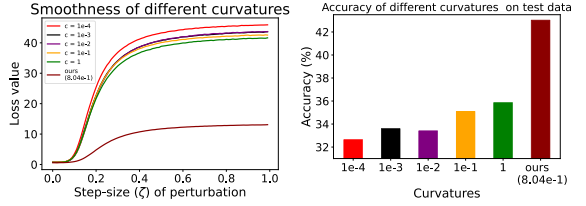
We further conduct experiments to confirm this point. Specifically, we set multiple different curvatures to train HNNs. After obtaining the trained HNNs, we perturbed parameters of the model as $\tilde{\mathbf{w}} = \mathbf{w} + \frac{\zeta \|\mathbf{w}\| \mathbf{o}}{\|\mathbf{o}\|}$. Here \mathbf{o} is the direction of perturbation that is the same for all models, and $\zeta \in (0, 1)$ is the step-size of perturbation. The perturbed HNNs are utilized to compute the loss on the training set to analyze the smoothness of HNNs and compute the accuracy on the test set. As shown in Fig. 1, HNNs trained with different curvatures exhibit different sharpness and generalization performances. HNNs trained with $c = 5e-1$ and $c = 1e-4$ converge to the sharpest minima and achieve the worst performance on the test set. On the contrary, HNNs with $c = 1e-2$ and $c = 1$ converge to the smoothest minima and achieve the best performance on the test set among HNNs trained with fixed curvatures. These phenomena confirm that curvatures are significant for the generalization of HNNs by affecting the smoothness of the loss landscape.

5 Method

The proposed sharpness-aware curvature learning method trains curvatures to improve the generalization of HNNs by smoothing the loss landscape. Concretely, we first design a scope sharpness measure $\text{SN}(\cdot)$ to measure the sharpness of the local



(a) Analysis on the task of classification



(b) Analysis on the task of long-tailed classification

Fig. 1 Generalization analysis

minimum trained with learnable curvatures within a given scope. Then, we minimize $\text{SN}(\cdot)$ to train curvatures for smoothing the loss landscape.

The proposed $\text{SN}(\cdot)$ is not directly affected by the curvature c ; rather, $\text{SN}(\cdot)$ is indirectly affected by the curvature c by influencing \mathbf{w} . Details are in Section 4.1. As a result, the gradient of $\text{SN}(\cdot)$ with respect to c is $\frac{\partial \text{SN}}{\partial c} = \mathbf{0}$.

To propagate the sharpness information from $\text{SN}(\cdot)$ to c , we view the curvatures as hyper-parameters. Given that optimizing hyper-parameters typically resorts to bi-level optimization (Franceschi et al, 2018), the minimization process is formulated as a bi-level optimization process,

$$\begin{aligned} \min_c \mathcal{F}(\mathbf{w}^*(c), c, \mathbf{y}) &:= \mathcal{L}_V(\mathbf{w}^*(c), c, \mathbf{y}) + \text{SN}(\mathbf{w}^*(c)) \\ \text{s.t. } \mathbf{w}^*(c) &= \arg \min_{\mathbf{w}} \mathcal{L}_S(\mathbf{w}, c, \mathbf{y}). \end{aligned} \quad (114)$$

In implementation, we set $\mathbf{y} = 0$ consistently. For simplicity and readability, we omit \mathbf{y} in $\mathcal{L}(\mathbf{w}, \mathbf{y}, c)$ and simplify the denotation of loss function as $\mathcal{L}(\mathbf{w}, c)$ here and in the following part. Then, the bi-level optimization process is re-denoted as

$$\begin{aligned} \min_c \mathcal{F}(\mathbf{w}^*(c), c) &:= \mathcal{L}_V(\mathbf{w}^*(c), c) + \text{SN}(\mathbf{w}^*(c)) \\ \text{s.t. } \mathbf{w}^*(c) &= \arg \min_{\mathbf{w}} \mathcal{L}_S(\mathbf{w}, c). \end{aligned} \quad (115)$$

This optimization problem can be divided into two sub-problems, *i.e.*, the inner-level and outer-level problems. In the inner-level optimization, HNNs are trained with fixed curvatures, while curvatures are learned in the outer-level optimization.

Then, the gradients of $\text{SN}(\cdot)$ with respect to c using the chain rule,

$$\frac{\partial \text{SN}(\mathbf{w}^*(c))}{\partial c} = \frac{\partial \text{SN}(\mathbf{w}^*(c))}{\partial \mathbf{w}^*(c)} \frac{\partial \mathbf{w}^*(c)}{\partial c}. \quad (116)$$

To efficiently compute gradients of curvature in the bi-level optimization, we introduce an implicit differentiation algorithm.

5.1 Scope Sharpness Measure

In this subsection, we first define the proposed scope sharpness measure $\text{SN}(\mathbf{w}^*(c))$, which measures the sharpness across the neighborhood of the local minimum \mathbf{w}^* trained with the curvature c . Then, we approximate $\text{SN}(\mathbf{w}^*(c))$ to reduce the time and space complexities by utilizing the Neumann series, polynomial expansion, and Taylor expansion.

Mathematically, the proposed scope sharpness measure $\text{SN}(\mathbf{w}^*)$ is defined as

$$\text{SN}(\mathbf{w}^*(c)) = \max_{\|\epsilon\| \leq \rho} \text{sn}(\mathbf{w}^*(c) + \epsilon), \quad (117)$$

where $\text{sn}(\mathbf{w}^*(c))$ is the reparametrization-invariant sharpness measure (Jang et al, 2022) to capture the sharpness of the local minima. $\text{sn}(\mathbf{w}^*(c))$ is computed as

$$\begin{aligned} \text{sn}(\mathbf{w}^*(c)) &= \nabla_{\mathbf{w}} \mathcal{L}_{\mathcal{S}}(\mathbf{w}^*(c), c)^\top \left(\nabla_{\mathbf{w}} \mathcal{L}_{\mathcal{S}}(\mathbf{w}^*(c), c) \right. \\ &\quad \left. \times \nabla_{\mathbf{w}} \mathcal{L}_{\mathcal{S}}(\mathbf{w}^*(c), c)^\top \right)^{-1} \nabla_{\mathbf{w}} \mathcal{L}_{\mathcal{S}}(\mathbf{w}^*(c), c)^2 \end{aligned} \quad (118)$$

where ∇ represents gradients, and $\nabla_{\mathbf{w}} \mathcal{L}_{\mathcal{S}}(\mathbf{w}, c) = \frac{\partial \mathcal{L}_{\mathcal{S}}(\mathbf{w}, c)}{\partial \mathbf{w}}$. We note that $\text{sn}(\cdot)$ in Eq. (118) contains the inverse of the Fisher matrix $\left(\nabla_{\mathbf{w}} \mathcal{L}_{\mathcal{S}}(\mathbf{w}^*(c), c) \nabla_{\mathbf{w}} \mathcal{L}_{\mathcal{S}}(\mathbf{w}^*(c), c)^\top \right)$. Assuming that the number of parameters \mathbf{w} as d , the time complexity of the Fisher matrix is $\mathcal{O}(d^3)$, and the space complexity is $\mathcal{O}(d^2)$. It is intractable to handle such a notoriously time and memory-consuming operation for HNNs. In order to address this issue, following existing work (Lorraine et al, 2020), we utilize the first K terms of

² \times denotes standard multiplication of matrices, vectors or scalars, which is added at the line break for clarity and is omitted elsewhere.

Neumann series to approximate this term,

$$\begin{aligned} \left(\nabla_{\mathbf{w}} \mathcal{L}_{\mathcal{S}}(\mathbf{w}^*(c), c) \nabla_{\mathbf{w}} \mathcal{L}_{\mathcal{S}}(\mathbf{w}^*(c), c)^\top \right)^{-1} &\approx \\ \sum_{i=0}^K \left(\mathbf{I} - \nabla_{\mathbf{w}} \mathcal{L}_{\mathcal{S}}(\mathbf{w}^*(c), c) \nabla_{\mathbf{w}} \mathcal{L}_{\mathcal{S}}(\mathbf{w}^*(c), c)^\top \right)^i. \end{aligned} \quad (119)$$

By substituting Eq. (119) into Eq. (118), $\text{sn}(\mathbf{w}^*(c))$ can be approximated as

$$\begin{aligned} \text{sn}(\mathbf{w}^*(c)) &\approx \hat{\text{sn}}(\mathbf{w}^*(c)) \\ &\triangleq \sum_{i=0}^K \nabla_{\mathbf{w}} \mathcal{L}_{\mathcal{S}}(\mathbf{w}^*(c), c)^\top \left(\mathbf{I} - \nabla_{\mathbf{w}} \mathcal{L}_{\mathcal{S}}(\mathbf{w}^*(c), c) \right. \\ &\quad \left. \times \nabla_{\mathbf{w}} \mathcal{L}_{\mathcal{S}}(\mathbf{w}^*(c), c)^\top \right)^i \nabla_{\mathbf{w}} \mathcal{L}_{\mathcal{S}}(\mathbf{w}^*(c), c). \end{aligned} \quad (120)$$

Eq. (120) can be further simplified, as shown in Proposition 1.

Proposition 1. $\hat{\text{sn}}(\mathbf{w}^*(c))$ in Eq. (120) has an equivalent expression, which is computed as

$$\hat{\text{sn}}(\mathbf{w}^*(c)) = 1 - \left(1 - \left\| \nabla_{\mathbf{w}} \mathcal{L}_{\mathcal{S}}(\mathbf{w}^*(c), c) \right\|^2 \right)^K. \quad (121)$$

Proof. In this proof, we expand the polynomial in Eq. (120) to avoid the computation of $\nabla_{\mathbf{w}} \mathcal{L}_{\mathcal{S}}(\mathbf{w}^*(c), c) \nabla_{\mathbf{w}} \mathcal{L}_{\mathcal{S}}(\mathbf{w}^*(c), c)^\top$ whose time and space complexities are non-trivial.

For simplicity, we omit $*$ and (c) from $\mathbf{w}^*(c)$ in the proof. Intuitively, we substitute $i = 0, 1, 2, \dots$ into the original $\hat{\text{sn}}(\mathbf{w})$, and observe that

$$i = 0 :$$

$$\begin{aligned} (\nabla_{\mathbf{w}} \mathcal{L}_{\mathcal{S}}(\mathbf{w}, c))^\top \left[\mathbf{I} - (\nabla_{\mathbf{w}} \mathcal{L}_{\mathcal{S}}(\mathbf{w}, c))(\nabla_{\mathbf{w}} \mathcal{L}_{\mathcal{S}}(\mathbf{w}, c))^\top \right]^0 \\ \times (\nabla_{\mathbf{w}} \mathcal{L}_{\mathcal{S}}(\mathbf{w}, c)) = (\nabla_{\mathbf{w}} \mathcal{L}_{\mathcal{S}}(\mathbf{w}, c))^\top \nabla_{\mathbf{w}} \mathcal{L}_{\mathcal{S}}(\mathbf{w}, c). \end{aligned} \quad (122)$$

Beside, when $i = k$, we have that

$$\begin{aligned} \left[\mathbf{I} - (\nabla_{\mathbf{w}} \mathcal{L}_{\mathcal{S}}(\mathbf{w}, c))(\nabla_{\mathbf{w}} \mathcal{L}_{\mathcal{S}}(\mathbf{w}, c))^\top \right]^K &= \binom{K}{0} + \dots + \\ \binom{K}{K-2} (-1)^{K-2} \left[(\nabla_{\mathbf{w}} \mathcal{L}_{\mathcal{S}}(\mathbf{w}, c))(\nabla_{\mathbf{w}} \mathcal{L}_{\mathcal{S}}(\mathbf{w}, c))^\top \right]^{K-2} + \\ \binom{K}{K-1} (-1)^{K-1} \left[(\nabla_{\mathbf{w}} \mathcal{L}_{\mathcal{S}}(\mathbf{w}, c))(\nabla_{\mathbf{w}} \mathcal{L}_{\mathcal{S}}(\mathbf{w}, c))^\top \right]^{K-1} + \\ \binom{K}{K} (-1)^K \left[(\nabla_{\mathbf{w}} \mathcal{L}_{\mathcal{S}}(\mathbf{w}, c))(\nabla_{\mathbf{w}} \mathcal{L}_{\mathcal{S}}(\mathbf{w}, c))^\top \right]^K. \end{aligned} \quad (123)$$

Let Eq. (123) multiple the vector $\nabla_{\mathbf{w}} \mathcal{L}_{\mathcal{S}}(\mathbf{w}, c)$ on the left and multiple the vector $(\nabla_{\mathbf{w}} \mathcal{L}_{\mathcal{S}}(\mathbf{w}, c))^\top$. By denoting $(\nabla_{\mathbf{w}} \mathcal{L}_{\mathcal{S}}(\mathbf{w}, c))^\top (\nabla_{\mathbf{w}} \mathcal{L}_{\mathcal{S}}(\mathbf{w}, c))$ as \mathcal{A} ,

we have

$$\begin{aligned}
& (\nabla_{\mathbf{w}} \mathcal{L}_{\mathcal{S}}(\mathbf{w}, c))^{\top} [\mathbf{I} - (\nabla_{\mathbf{w}} \mathcal{L}_{\mathcal{S}}(\mathbf{w}, c))] \\
& \times (\nabla_{\mathbf{w}} \mathcal{L}_{\mathcal{S}}(\mathbf{w}, c))^{\top}]^K (\nabla_{\mathbf{w}} \mathcal{L}_{\mathcal{S}}(\mathbf{w}, c)) \\
& = \mathcal{A} \left[\binom{K}{0} + \dots + \binom{K}{K-2} (-1)^{K-2} \mathcal{A}^{K-2} \right. \\
& \left. + \binom{K}{K-1} (-1)^{K-1} \mathcal{A}^{K-1} + \binom{K}{K} (-1)^K \mathcal{A}^K \right] \\
& = \mathcal{A} (1 - \mathcal{A})^K
\end{aligned} \tag{124}$$

Then $\text{sn}(\mathbf{w}^*(c))$ is approximated as

$$\begin{aligned}
\text{sn}(\mathbf{w}^*(c)) & \approx \hat{\text{sn}}(\mathbf{w}^*(c)) \\
& \triangleq 1 - \left(1 - \|\nabla_{\mathbf{w}} \mathcal{L}_{\mathcal{S}}(\mathbf{w}^*(c), c)\|^2 \right)^{K+1}.
\end{aligned} \tag{125}$$

□

Notably, the time and space complexities of $\hat{\text{sn}}(\mathbf{w}^*(c))$ are only $\mathcal{O}(d)$, which significantly reduce the required complexity and make it feasible for large-scale HNNs. We substitute Eq. (121) into Eq. (117), and compute the scope sharpness measure as

$$\begin{aligned}
\text{SN}(\mathbf{w}^*(c)) & \approx \max_{\|\boldsymbol{\epsilon}\| \leq \rho} \hat{\text{sn}}(\mathbf{w}^*(c) + \boldsymbol{\epsilon}) \\
& = \max_{\|\boldsymbol{\epsilon}\| \leq \rho} 1 - \left(1 - \|\nabla_{\mathbf{w}} \mathcal{L}_{\mathcal{S}}(\mathbf{w}^*(c) + \boldsymbol{\epsilon}, c)\|^2 \right)^{K+1}.
\end{aligned} \tag{126}$$

The maximization problem in Eq. (126) is still tedious; hence, we propose an approximation for Eq. (126). By the first-order Taylor expansion, Eq. (126) can be approximated as

$$\begin{aligned}
\text{SN}(\mathbf{w}^*(c)) & \approx \max_{\|\boldsymbol{\epsilon}\| \leq \rho} \hat{\text{sn}}(\mathbf{w}^*(c)) + \boldsymbol{\epsilon}^{\top} \frac{\partial \hat{\text{sn}}(\mathbf{w}^*(c))}{\partial \mathbf{w}^*} \\
& = \max_{\|\boldsymbol{\epsilon}\| \leq \rho} \boldsymbol{\epsilon}^{\top} \frac{\partial \hat{\text{sn}}(\mathbf{w}^*(c))}{\partial \mathbf{w}^*}.
\end{aligned} \tag{127}$$

Eq. (127) is a classical dual norm problem, which can be solved as

$$\hat{\boldsymbol{\epsilon}} = \rho \frac{\partial \hat{\text{sn}}(\mathbf{w}^*(c))}{\partial \mathbf{w}^*(c)} / \left\| \frac{\partial \hat{\text{sn}}(\mathbf{w}^*(c))}{\partial \mathbf{w}^*(c)} \right\|. \tag{128}$$

By substituting Eq. (128) into Eq. (126), the scope sharpness measure is finally approximated as

$$\begin{aligned}
\text{SN}(\mathbf{w}^*(c)) & \approx \hat{\text{sn}}(\hat{\mathbf{w}}(c)) \\
& = 1 - \left(1 - \|\nabla_{\mathbf{w}} \mathcal{L}_{\mathcal{S}}(\hat{\mathbf{w}}(c), c)\|^2 \right)^{K+1},
\end{aligned} \tag{129}$$

where $\hat{\mathbf{w}}(c) = \mathbf{w}^*(c) + \hat{\boldsymbol{\epsilon}}$. By minimizing the sharpness measure to train curvatures, the obtained curvatures can smooth the loss landscape of the neighborhood of local minima and further improve the generalization.

5.2 Implicit Differentiation for Curvature Optimization

Based on the approximated scope sharpness measure in Eq. (129), the bi-level optimization objective in Eq. (115) can be rewritten as

$$\begin{aligned}
\min_c \mathcal{F}(\mathbf{w}^*(c), c) & := \mathcal{L}_{\mathcal{V}}(\mathbf{w}^*(c), c) + \hat{\text{sn}}(\hat{\mathbf{w}}(c)) \\
\text{s.t. } \mathbf{w}^*(c) & = \arg \min_{\mathbf{w}} \mathcal{L}_{\mathcal{S}}(\mathbf{w}, c).
\end{aligned} \tag{130}$$

In this subsection, we analyze the challenges of solving the bi-level optimization problem in Eq. (130). Then, we propose an implicit differentiation method to solve the bi-level optimization problem efficiently.

In the inner-level optimization of Eq. (130), we aim to obtain the optimal parameters \mathbf{w}^* by minimizing the objective $\mathcal{L}_{\mathcal{S}}(\cdot)$ with fixed curvatures. Following SAM (Foret et al, 2020), \mathbf{w} is updated as

$$\begin{aligned}
\mathbf{w} & \leftarrow \mathbf{w} - \eta \nabla_{\mathbf{w}} \mathcal{L}_{\mathcal{S}}(\mathbf{w}', c), \\
\text{where } \mathbf{w}' & = \mathbf{w} + \hat{\rho} \nabla_{\mathbf{w}} \mathcal{L}_{\mathcal{S}}(\mathbf{w}, c) / \left\| \nabla_{\mathbf{w}} \mathcal{L}_{\mathcal{S}}(\mathbf{w}, c) \right\|.
\end{aligned} \tag{131}$$

Here, η is the step-size, and $\hat{\rho}$ is the perturbation radius.

We update curvatures by minimizing the objective $\mathcal{F}(\cdot)$ of Eq. (130), in the outer-level optimization problem. By using the gradient descent method, c is updated as

$$c \leftarrow c - \eta_c \frac{d\mathcal{F}(\mathbf{w}^*(c), c)}{dc}, \tag{132}$$

where η_c is the step-size for optimizing curvatures. By the chain rule, the gradient of c is calculated as

$$\begin{aligned}
\frac{d\mathcal{F}(\mathbf{w}^*(c), c)}{dc} & = \nabla_c \mathcal{F}(\mathbf{w}^*(c), c) \\
& + \nabla_{\mathbf{w}} \mathcal{F}(\mathbf{w}^*(c), c) \nabla_c \mathbf{w}^*(c),
\end{aligned} \tag{133}$$

where $\nabla_c \mathbf{w}^*(c) = \frac{\partial \mathbf{w}^*(c)}{\partial c}$. $\nabla_c \mathcal{F}(\mathbf{w}^*(c), c)$ can be computed easily via automatic differentiation technique. Then we focus on $\nabla_{\mathbf{w}} \mathcal{F}(\mathbf{w}^*(c), c)$ and $\nabla_c \mathbf{w}^*(c)$ in Eq. (133). By the chain rule, $\nabla_{\mathbf{w}} \mathcal{F}(\mathbf{w}^*(c), c)$ is expanded as

$$\begin{aligned}
\nabla_{\mathbf{w}} \mathcal{F}(\mathbf{w}^*(c), c) & = \nabla_{\mathbf{w}} \mathcal{L}_{\mathcal{V}}(\mathbf{w}^*, c) \\
& + 2K \left(1 - \|\nabla_{\mathbf{w}} \mathcal{L}_{\mathcal{S}}(\hat{\mathbf{w}}, c)\|^2 \right)^{K-1} \nabla_{\mathbf{w}} \mathcal{L}_{\mathcal{S}}(\hat{\mathbf{w}}, c) \nabla_{\mathbf{w}}^2 \mathcal{L}_{\mathcal{S}}(\hat{\mathbf{w}}, c),
\end{aligned} \tag{134}$$

where $\nabla_{\mathbf{w}}^2 \mathcal{L}_{\mathcal{S}}(\hat{\mathbf{w}}, c) = \frac{\partial^2 \mathcal{L}_{\mathcal{S}}(\hat{\mathbf{w}}, c)}{\partial \hat{\mathbf{w}}^2}$ denotes the Hessian matrices.

Suppose that $\mathbf{w}^*(c)$ is obtained by inner-level optimization for T steps, $\nabla_c \mathbf{w}^*(c)$ can be

expanded as

$$\begin{aligned}\nabla_c \mathbf{w}^*(c) = & - \sum_{j \leq T} \left(\prod_{k < j} \mathbf{I} - \nabla_{\mathbf{w}}^2 \mathcal{L}_{\mathcal{S}}(\mathbf{w}^{(T-k)}, c) \right) \\ & \times \nabla_{\mathbf{w}c}^2 \mathcal{L}_{\mathcal{S}}(\mathbf{w}^{(T-j)}, c),\end{aligned}\quad (135)$$

where $\nabla_{\mathbf{w}c}^2 \mathcal{L}_{\mathcal{S}}(\mathbf{w}, c) = \frac{\partial^2 \mathcal{L}_{\mathcal{S}}(\mathbf{w}, c)}{\partial \mathbf{w} \partial c}$. Computing Eq. (135) needs to unroll the inner-level optimization and compute the product of complex Hessian matrices $\nabla_{\mathbf{w}}^2 \mathcal{L}_{\mathcal{S}}(\mathbf{w}^{(T-k)}, c)$, which requires massive time and memory consumption.

Motivated by the work of (Lorraine et al, 2020), we introduce an implicit differentiation method (Lorraine et al, 2020) to compute $\nabla_c \mathbf{w}^*(c)$ efficiently,

$$\nabla_c \mathbf{w}^*(c) = - \left(\nabla_{\mathbf{w}}^2 \mathcal{L}_{\mathcal{S}}(\mathbf{w}^*, c) \right)^{-1} \nabla_{\mathbf{w}c}^2 \mathcal{L}_{\mathcal{S}}(\mathbf{w}^*, c). \quad (136)$$

By substituting Eq. (136) and Eq. (134) into Eq. (133), the second term in Eq. (133) is computed as the sum of two terms, *i.e.*,

$$\nabla_{\mathbf{w}} \mathcal{F}(\mathbf{w}^*(c), c) \nabla_c \mathbf{w}^*(c) = \mathbf{U}_1 + \mathbf{U}_2, \quad (137)$$

where

$$\mathbf{U}_1 \triangleq -\nabla_{\mathbf{w}} \mathcal{L}_{\mathcal{V}}(\mathbf{w}^*, c) \left(\nabla_{\mathbf{w}}^2 \mathcal{L}_{\mathcal{S}}(\mathbf{w}^*, c) \right)^{-1} \nabla_{\mathbf{w}c}^2 \mathcal{L}_{\mathcal{S}}(\mathbf{w}^*, c), \quad (138)$$

and

$$\begin{aligned}\mathbf{U}_2 \triangleq & -2K \left(1 - \|\nabla_{\mathbf{w}} \mathcal{L}_{\mathcal{S}}(\hat{\mathbf{w}}, c)\| \right)^{K-1} \nabla_{\mathbf{w}} \mathcal{L}_{\mathcal{S}}(\hat{\mathbf{w}}, c) \\ & \times \nabla_{\mathbf{w}}^2 \mathcal{L}_{\mathcal{S}}(\hat{\mathbf{w}}, c) \left(\nabla_{\mathbf{w}}^2 \mathcal{L}_{\mathcal{S}}(\mathbf{w}^*, c) \right)^{-1} \nabla_{\mathbf{w}c}^2 \mathcal{L}_{\mathcal{S}}(\mathbf{w}^*, c).\end{aligned}\quad (139)$$

Computing \mathbf{U}_1 and \mathbf{U}_2 remains challenging, since they are required to compute the intractable inverse of Hessian matrices in HNNs. Here we present approximation for \mathbf{U}_1 and \mathbf{U}_2 .

Approximation of \mathbf{U}_1 . Computing \mathbf{U}_1 in Eq. (138) contains the inverse of the Hessian matrix, which is non-trivial to compute for deep neural networks. Here, we utilize the first J terms of the Neumann series to approximate the inverse of the Hessian matrix. Then \mathbf{U}_1 can be approximated as

$$\begin{aligned}\mathbf{U}_1 \approx \mathbf{U}_1' \triangleq & -\nabla_{\mathbf{w}} \mathcal{L}_{\mathcal{V}}(\mathbf{w}^*, c) \\ & \times \sum_{j=0}^J \left(\mathbf{I} - \nabla_{\mathbf{w}}^2 \mathcal{L}_{\mathcal{S}}(\mathbf{w}^*, c) \right)^j \nabla_{\mathbf{w}c}^2 \mathcal{L}_{\mathcal{S}}(\mathbf{w}^*, c).\end{aligned}\quad (140)$$

To compute Eq. (140), we first initialize two intermediate variables \mathbf{v}^0 and \mathbf{p}^0 both as $\nabla_{\mathbf{w}} \mathcal{L}_{\mathcal{V}}(\mathbf{w}^*)$.

For every iteration, we update the intermediate variable as

$$\mathbf{v}^{i+1} = \mathbf{v}^i \left(\mathbf{I} - \nabla_{\mathbf{w}}^2 \mathcal{L}_{\mathcal{S}}(\mathbf{w}^*, c) \right), \quad \mathbf{p}^{i+1} = \mathbf{p}^i + \mathbf{v}^{i+1}. \quad (141)$$

After J iterations, \mathbf{U}_1' is given by

$$\mathbf{U}_1' = -\mathbf{p}^J \nabla_{\mathbf{w}c}^2 \mathcal{L}_{\mathcal{S}}(\mathbf{w}^*, c). \quad (142)$$

Obviously, the intermediate variable keeps the vector during iterations, thus computing \mathbf{U}_1' only needs Hessian-vector product and Jacobian-vector product (Baydin et al, 2018), eliminating the need of time-consuming and memory-consuming Hessian and Jacobian.

Approximation of \mathbf{U}_2 . We utilize $\nabla_{\mathbf{w}}^2 \mathcal{L}_{\mathcal{S}}(\hat{\mathbf{w}}, c)$ to approximate $\nabla_{\mathbf{w}}^2 \mathcal{L}_{\mathcal{S}}(\mathbf{w}^*, c)$ in Eq. (139), and \mathbf{U}_2 is approximated as

$$\begin{aligned}\mathbf{U}_2 \approx \mathbf{U}_2' \triangleq & -2K \left(1 - \|\nabla_{\mathbf{w}} \mathcal{L}_{\mathcal{S}}(\hat{\mathbf{w}}, c)\| \right)^{K-1} \\ & \times \nabla_{\mathbf{w}} \mathcal{L}_{\mathcal{S}}(\hat{\mathbf{w}}, c) \nabla_{\mathbf{w}c}^2 \mathcal{L}_{\mathcal{S}}(\mathbf{w}^*, c).\end{aligned}\quad (143)$$

By substituting Eq. (140), Eq. (143), and Eq. (137) into Eq. (133), the gradient of the curvature c is computed as

$$\begin{aligned}\frac{d\mathcal{F}(\mathbf{w}^*(c), c)}{dc} = & \nabla_c \mathcal{F}(\mathbf{w}^*(c), c) + \mathbf{U}_1 + \mathbf{U}_2 \\ \approx & \nabla_c \mathcal{F}(\mathbf{w}^*(c), c) - \nabla_{\mathbf{w}} \mathcal{L}_{\mathcal{V}}(\mathbf{w}^*, c) \\ & \times \sum_{j=0}^J \left(\mathbf{I} - \nabla_{\mathbf{w}}^2 \mathcal{L}_{\mathcal{S}}(\mathbf{w}^*, c) \right)^j \nabla_{\mathbf{w}c}^2 \mathcal{L}_{\mathcal{S}}(\mathbf{w}^*, c) \\ & - 2K \left(1 - \|\nabla_{\mathbf{w}} \mathcal{L}_{\mathcal{S}}(\hat{\mathbf{w}}, c)\| \right)^{K-1} \nabla_{\mathbf{w}} \mathcal{L}_{\mathcal{S}}(\hat{\mathbf{w}}, c) \nabla_{\mathbf{w}c}^2 \mathcal{L}_{\mathcal{S}}(\mathbf{w}^*, c).\end{aligned}\quad (144)$$

Compared with the gradient of c in Eq. (133), the estimated gradient in Eq. (144) significantly reduces time complexity. The overall algorithm is summarized in Algorithm 1.

6 Theoretical Guarantees of Our Method

In this section, we present theoretical guarantees of the proposed method. Specifically, in Section 6.2, we conduct approximation error analyses to present error bounds for the approximation ways used in our method, supporting the validity of the introduced approximation algorithms. In Section 6.3, we further establish the convergence analyses to demonstrate that the weights and curvatures in HNNs can converge. Then, in Section 6.4, we conduct efficiency analyses for proving the efficiency of the approximation algorithms.

6.1 Assumptions

To quantify the following approximation errors and analyze the convergence performance, we introduce the following assumptions.

Assumption 1. (*Lipschitz continuity*). Assume that \mathcal{L}_S , \mathcal{L}_V , $\nabla_{\mathbf{w}}\mathcal{L}_S(\mathbf{w}, c)$, $\nabla_{\mathbf{w}}\mathcal{L}_V(\mathbf{w}, c)$, $\nabla_{\mathbf{w}}^2\mathcal{L}_S(\mathbf{w}, c)$, $\nabla_{\mathbf{w}c}^2\mathcal{L}_S(\mathbf{w}, c)$, and $\nabla\mathcal{F}(c)$ are Lipschitz continuous w.r.t. \mathbf{w} with constants $L_G, L_{\bar{G}}, H, L_{H_2}, L_{G'}, L_{G_2}, L_{H_c}$. Assume that $\nabla_{\mathbf{w}}\mathcal{L}_S(\mathbf{w}, c)$ is Lipschitz continuous w.r.t. c with constant L_{G_3} . Assume that $\frac{\partial \hat{s}\hat{n}}{\partial \mathbf{w}}$ is Lipschitz continuous with constant L_{G_4} .

Remark. The assumptions are commonly used in the convergence analysis of SGD-based methods (Kingma and Ba, 2015; Reddi et al., 2018; Zhuang et al., 2022) and bi-level optimization methods (Rajeswaran et al., 2019; Ji et al., 2022).

Algorithm 1 Training process of the proposed method.

Input: Initial parameters \mathbf{w} and curvature c , maximum iterations for inner level T and outer level \mathcal{T} , perturbation radius $\hat{\rho}$, inner-level step-size η , and outer-level step-size η_c .

```

1:  $I_{\text{outer}} = 0$ .
2: while  $I_{\text{outer}} < \mathcal{T}$  do
3:    $I_{\text{inner}} = 0$ 
4:   while  $I_{\text{inner}} \leq T$  do
5:     Update parameters  $\mathbf{w}$  via Eq. (131).
6:   end while
7:   Compute loss function  $\mathcal{F}(\mathbf{w}^*(c), c)$  in Eq. (130).
8:   Compute the direct gradient  $\nabla_c\mathcal{F}(\mathbf{w}^*(c), c)$ .
9:    $\mathbf{v}^0 = \mathbf{p}^0 = \nabla_{\mathbf{w}}\mathcal{L}_V(\mathbf{w}^*(c), c)$ .
10:   $i = 0$ 
11:  while  $i \leq J$  do
12:    Update intermediate vector  $\mathbf{v}_i$  and  $\mathbf{p}_i$  via
        Eq. (141).
13:  end while
14:  Compute gradients of curvatures via Eq. (144).
15:  Update curvatures via Eq. (132).
16: end while
17: Return the updated curvature  $c$  and updated
    parameters  $\mathbf{w}$ .
```

6.2 Approximation Error Analyses in Our Method

We utilize $\hat{s}\hat{n}(\hat{\mathbf{w}}(c))$ to efficiently compute $\text{SN}(\mathbf{w}^*(c))$. Moreover, we utilize \mathbf{U}'_1 and \mathbf{U}'_2 to approximate \mathbf{U}_1 and \mathbf{U}_2 respectively, aiming to

simplify the gradient of c . In this subsection, we present theoretical analyses of approximation error of scope sharpness measure and approximation error of gradients of curvatures. These analyses indicate that the approximation errors are upper-bounded, showing the rationality of approximation ways in the proposed method.

6.2.1 Approximation Error of Scope Sharpness Measure

In Theorem 9, we present the approximation error of scope sharpness measure, i.e., the upper bound of $|\text{SN}(\mathbf{w}^*(c)) - \hat{s}\hat{n}(\hat{\mathbf{w}}(c))|$.

Theorem 9. Suppose the above assumptions hold, $\hat{s}\hat{n}(\hat{\mathbf{w}}(c))$ satisfies

$$|\text{SN}(\mathbf{w}^*(c)) - \hat{s}\hat{n}(\hat{\mathbf{w}}(c))| \leq \mathcal{E}_{\text{mea}}, \quad (145)$$

where \mathcal{E}_{mea} is a constant and computed as

$$\mathcal{E}_{\text{mea}} \triangleq 1 + \rho^2 L_{G_4}. \quad (146)$$

Proof. Recall that $\hat{s}\hat{n}(\hat{\mathbf{w}}(c))$ and $\text{SN}(\mathbf{w}^*(c))$ are computed as

$$\begin{aligned} \hat{s}\hat{n}(\hat{\mathbf{w}}(c)) &= 1 - \left(1 - \left\|\nabla_{\mathbf{w}}\mathcal{L}_S(\hat{\mathbf{w}}(c), c)\right\|^2\right)^{K+1}, \\ \text{SN}(\mathbf{w}^*(c)) &= \max_{\|\epsilon\| \leq \rho} \text{sn}(\mathbf{w}^*(c) + \epsilon). \end{aligned} \quad (147)$$

We adopt two approximation ways to approximate $\text{SN}(\mathbf{w}^*(c))$ as $\hat{s}\hat{n}(\hat{\mathbf{w}}(c))$. (1) We utilize $\hat{s}\hat{n}(\mathbf{w}) \triangleq 1 - \left(1 - \left\|\nabla_{\mathbf{w}}\mathcal{L}_S(\mathbf{w}, c)\right\|^2\right)^{K+1}$ to approximate $\text{sn}(\mathbf{w}) \triangleq \sum_{i=0}^{\infty} \nabla_{\mathbf{w}}\mathcal{L}_S(\mathbf{w}, c)^{\top} (\mathbf{I} - \nabla_{\mathbf{w}}\mathcal{L}_S(\mathbf{w}, c)\nabla_{\mathbf{w}}\mathcal{L}_S(\mathbf{w}, c)^{\top})^i \nabla_{\mathbf{w}}\mathcal{L}_S(\mathbf{w}, c)$. (2) We utilize $\hat{s}\hat{n}(\mathbf{w}^*(c)) + \epsilon^{\top} \frac{\partial \hat{s}\hat{n}(\mathbf{w}^*(c))}{\partial \mathbf{w}^*}$ to approximate $\hat{s}\hat{n}(\mathbf{w}^*(c) + \epsilon)$.

We first present the error bound for the first approximation. From the construction of $\text{sn}(\mathbf{w})$ and $\hat{s}\hat{n}(\mathbf{w})$, we have

$$\begin{aligned} |\text{sn}(\mathbf{w}) - \hat{s}\hat{n}(\mathbf{w})| &= \left| \sum_{i=K+1}^{\infty} (\nabla_{\mathbf{w}}\mathcal{L}_S(\mathbf{w}, c))^{\top} \right. \\ &\quad \times \left. (\mathbf{I} - \nabla_{\mathbf{w}}\mathcal{L}_S(\mathbf{w}, c)\nabla_{\mathbf{w}}\mathcal{L}_S(\mathbf{w}, c)^{\top})^i (\nabla_{\mathbf{w}}\mathcal{L}_S(\mathbf{w}, c)) \right| \\ &= \sum_{i=K+1}^{\infty} \left\| \nabla_{\mathbf{w}}\mathcal{L}_S(\mathbf{w}, c) \right\|^2 \left(1 - \left\| \nabla_{\mathbf{w}}\mathcal{L}_S(\mathbf{w}, c) \right\|^2\right)^i \leq 1. \end{aligned} \quad (148)$$

The last inequality holds because

$$\left\| \nabla_{\mathbf{w}}\mathcal{L}_S(\mathbf{w}, c) \right\|^2 < 1, \quad (149)$$

and

$$\begin{aligned} & \sum_{i=K+1}^{\infty} \left| \|\nabla_{\mathbf{w}} \mathcal{L}_{\mathcal{S}}(\mathbf{w}, c)\|^2 (1 - \|\nabla_{\mathbf{w}} \mathcal{L}_{\mathcal{S}}(\mathbf{w}, c)\|^2)^i \right| \\ &= (1 - \|\nabla_{\mathbf{w}} \mathcal{L}_{\mathcal{S}}(\mathbf{w}, c)\|^2)^{K+1} \leq 1 \end{aligned} \quad (150)$$

As to the second approximation, we mainly adopt the Taylor expansion for approximation. The upper bound of error is given by

$$\begin{aligned} & \left| \hat{\mathbf{s}}(\mathbf{w}^*(c) + \boldsymbol{\epsilon}) - \hat{\mathbf{s}}(\mathbf{w}^*(c)) - \boldsymbol{\epsilon}^\top \frac{\partial \hat{\mathbf{s}}(\mathbf{w}^*(c))}{\partial \mathbf{w}^*} \right| \\ & \leq \frac{1}{2} \left| \boldsymbol{\epsilon}^\top \frac{\partial^2 \hat{\mathbf{s}}(\mathbf{w}^*)}{\partial \mathbf{w}^* \partial \mathbf{w}^{*\top}} \boldsymbol{\epsilon} \right| \leq \frac{1}{2} \|\boldsymbol{\epsilon}\|^2 \left\| \frac{\partial^2 \hat{\mathbf{s}}(\mathbf{w}^*)}{\partial \mathbf{w}^* \partial \mathbf{w}^{*\top}} \right\| \leq \rho^2 L_{G_4}. \end{aligned} \quad (151)$$

By denoting \mathcal{E}_{mea} as $1 + \rho^2 L_{G_4}$, we prove the theorem. \square

6.2.2 Approximation Error of Gradients of Curvatures

We denote the exact gradients of c as $\nabla c \triangleq \frac{d\mathcal{F}(\mathbf{w}^*(c), c)}{dc}$, while we denote the approximated gradients of c in Eq. (144) as $\hat{\nabla}c$. The approximation error has an upper bound, as shown in Theorem 10. We first present Lemmas 3 and 4 to analyze the approximation error of \mathbf{U}_1 and \mathbf{U}_2 , respectively.

Approximation error for \mathbf{U}_1 . We adopt two approximation ways for computing \mathbf{U}_1 .

(1) \mathbf{U}_1 deriving with implicit differentiation algorithm requires $\nabla_{\mathbf{w}} \mathcal{L}_{\mathcal{S}}(\mathbf{w}^*, c) = 0$. While it is non-trivial to optimize \mathbf{w} to let the gradient of \mathbf{w}^* equals to 0, *i.e.*, $\nabla_{\mathbf{w}} \mathcal{L}_{\mathcal{S}}(\mathbf{w}^*, c) \neq 0$ in practice. Suppose that $\nabla_{\mathbf{w}} \mathcal{L}_{\mathcal{S}}(\mathbf{w}^{**}, c) = 0$. The exact term \mathbf{U}_1^* needs to be computed using \mathbf{w}^{**} , *i.e.*,

$$\mathbf{U}_1^* \triangleq \nabla_{\mathbf{w}} \mathcal{L}_{\mathcal{V}}(\mathbf{w}^{**}(c), c) [\nabla_{\mathbf{w}}^2 \mathcal{L}_{\mathcal{S}}(\mathbf{w}^{**}, c)]^{-1} \nabla_{\mathbf{w}^c}^2 \mathcal{L}_{\mathcal{S}}(\mathbf{w}^{**}, c) \quad (152)$$

(2) We utilize the first J terms Neumann series to approximate the inverse of the Hessian matrix in Eq. (140).

The error of the first approximation way, *i.e.*, the upper bound of $\|\mathbf{U}_1^* - \mathbf{U}_1'\|$, is presented in Lemma 3.

Lemma 3. *Assume that $\|\mathbf{w}^{**} - \mathbf{w}^*\| \leq \delta$. \mathbf{U}_1' satisfies*

$$\|\mathbf{U}_1^* - \mathbf{U}_1'\| \leq \mathcal{E}_{cur_1}, \quad (153)$$

where \mathcal{E}_{cur_1} is given by

$$\mathcal{E}_{cur_1} = \mathcal{E}'_{cur_1} \delta + \mathcal{E}''_{cur_1}. \quad (154)$$

Here, \mathcal{E}'_{cur_1} and \mathcal{E}''_{cur_1} are constants that only depend on the Lipschitz constants, which are computed as

$$\begin{aligned} \mathcal{E}'_{cur_1} & \triangleq \frac{L_{\bar{G}} L_{G'} L_{G_3} + L_{G_3} L_{H_2} L_H + L_{\bar{G}} L_{G_2} L_H}{L_{H_s}^2} \\ \mathcal{E}''_{cur_1} & \triangleq \frac{L_{\bar{G}} L_{G_3} (L_H - L_{H_s} + L_{H_s} (1 + L_H)^J)}{L_H L_{H_s}}. \end{aligned} \quad (155)$$

Proof. To quantify the error bound of $\|\mathbf{U}_1^* - \mathbf{U}_1'\|$, we utilize the Lipschitz continuity assumptions of $\mathcal{L}_{\mathcal{V}}$, $\nabla_{\mathbf{w}} \mathcal{L}_{\mathcal{S}}(\mathbf{w}, c)$, $\nabla \mathcal{L}_{\mathcal{V}}(\mathbf{w})$, $\nabla_{\mathbf{w}}^2 \mathcal{L}_{\mathcal{S}}(\mathbf{w}, c)$, $\nabla_{\mathbf{w}^c}^2 \mathcal{L}_{\mathcal{S}}(\mathbf{w}, c)$, and $\nabla_{\mathbf{w}} \mathcal{L}_{\mathcal{S}}(\mathbf{w}, c)$.

Recall that \mathbf{U}_1^* and \mathbf{U}_1' are computed as

$$\begin{aligned} \mathbf{U}_1^* &= -\nabla_{\mathbf{w}} \mathcal{L}_{\mathcal{V}}(\mathbf{w}^{**}, c) [\nabla_{\mathbf{w}}^2 \mathcal{L}_{\mathcal{S}}(\mathbf{w}^{**}, c)]^{-1} \nabla_{\mathbf{w}^c}^2 \mathcal{L}_{\mathcal{S}}(\mathbf{w}^{**}, c) \\ \mathbf{U}_1' &= -\nabla_{\mathbf{w}} \mathcal{L}_{\mathcal{V}}(\mathbf{w}^*, c) \sum_{j=0}^J [\mathbf{I} - \nabla_{\mathbf{w}}^2 \mathcal{L}_{\mathcal{S}}(\mathbf{w}^*, c)]^j \nabla_{\mathbf{w}^c}^2 \mathcal{L}_{\mathcal{S}}(\mathbf{w}^*, c). \end{aligned} \quad (156)$$

Thus we have

$$\begin{aligned} & \|\mathbf{U}_1^* - \mathbf{U}_1'\| = \\ & \|\nabla_{\mathbf{w}} \mathcal{L}_{\mathcal{V}}(\mathbf{w}^{**}, c) [\nabla_{\mathbf{w}}^2 \mathcal{L}_{\mathcal{S}}(\mathbf{w}^{**}, c)]^{-1} \nabla_{\mathbf{w}^c}^2 \mathcal{L}_{\mathcal{S}}(\mathbf{w}^{**}, c) - \\ & \nabla_{\mathbf{w}} \mathcal{L}_{\mathcal{V}}(\mathbf{w}^*, c) [\nabla_{\mathbf{w}}^2 \mathcal{L}_{\mathcal{S}}(\mathbf{w}^*, c)]^{-1} \nabla_{\mathbf{w}^c}^2 \mathcal{L}_{\mathcal{S}}(\mathbf{w}^*, c) + \\ & \nabla_{\mathbf{w}} \mathcal{L}_{\mathcal{V}}(\mathbf{w}^*, c) [\nabla_{\mathbf{w}}^2 \mathcal{L}_{\mathcal{S}}(\mathbf{w}^*, c)]^{-1} \nabla_{\mathbf{w}^c}^2 \mathcal{L}_{\mathcal{S}}(\mathbf{w}^*, c) - \\ & \nabla_{\mathbf{w}} \mathcal{L}_{\mathcal{V}}(\mathbf{w}^*, c) \sum_{j=0}^J [\mathbf{I} - \nabla_{\mathbf{w}}^2 \mathcal{L}_{\mathcal{S}}(\mathbf{w}^*, c)]^j \nabla_{\mathbf{w}^c}^2 \mathcal{L}_{\mathcal{S}}(\mathbf{w}^*, c)\| \\ & \leq \|\nabla_{\mathbf{w}} \mathcal{L}_{\mathcal{V}}(\mathbf{w}^{**}, c) [\nabla_{\mathbf{w}}^2 \mathcal{L}_{\mathcal{S}}(\mathbf{w}^{**}, c)]^{-1} \nabla_{\mathbf{w}^c}^2 \mathcal{L}_{\mathcal{S}}(\mathbf{w}^{**}, c)\| \\ & - \|\nabla_{\mathbf{w}} \mathcal{L}_{\mathcal{V}}(\mathbf{w}^*, c) [\nabla_{\mathbf{w}}^2 \mathcal{L}_{\mathcal{S}}(\mathbf{w}^*, c)]^{-1} \nabla_{\mathbf{w}^c}^2 \mathcal{L}_{\mathcal{S}}(\mathbf{w}^*, c)\| \\ & + \|\nabla_{\mathbf{w}} \mathcal{L}_{\mathcal{V}}(\mathbf{w}^*, c) [\nabla_{\mathbf{w}}^2 \mathcal{L}_{\mathcal{S}}(\mathbf{w}^*, c)]^{-1} \nabla_{\mathbf{w}^c}^2 \mathcal{L}_{\mathcal{S}}(\mathbf{w}^*, c) - \\ & \nabla_{\mathbf{w}} \mathcal{L}_{\mathcal{V}}(\mathbf{w}^*, c) \sum_{j=0}^J [\mathbf{I} - \nabla_{\mathbf{w}}^2 \mathcal{L}_{\mathcal{S}}(\mathbf{w}^*, c)]^j \nabla_{\mathbf{w}^c}^2 \mathcal{L}_{\mathcal{S}}(\mathbf{w}^*, c)\|. \end{aligned} \quad (157)$$

We first focus on the first term to the right of c . inequality and have

$$\begin{aligned} & \|\nabla_{\mathbf{w}} \mathcal{L}_{\mathcal{V}}(\mathbf{w}^{**}, c) [\nabla_{\mathbf{w}}^2 \mathcal{L}_{\mathcal{S}}(\mathbf{w}^{**}, c)]^{-1} \nabla_{\mathbf{w}^c}^2 \mathcal{L}_{\mathcal{S}}(\mathbf{w}^{**}, c) - \\ & \nabla_{\mathbf{w}} \mathcal{L}_{\mathcal{V}}(\mathbf{w}^*, c) [\nabla_{\mathbf{w}}^2 \mathcal{L}_{\mathcal{S}}(\mathbf{w}^*, c)]^{-1} \nabla_{\mathbf{w}^c}^2 \mathcal{L}_{\mathcal{S}}(\mathbf{w}^*, c)\| \\ & \leq \|\nabla_{\mathbf{w}} \mathcal{L}_{\mathcal{V}}(\mathbf{w}^{**}, c) [\nabla_{\mathbf{w}}^2 \mathcal{L}_{\mathcal{S}}(\mathbf{w}^{**}, c)]^{-1} \nabla_{\mathbf{w}^c}^2 \mathcal{L}_{\mathcal{S}}(\mathbf{w}^{**}, c) - \\ & \nabla_{\mathbf{w}} \mathcal{L}_{\mathcal{V}}(\mathbf{w}^*, c) [\nabla_{\mathbf{w}}^2 \mathcal{L}_{\mathcal{S}}(\mathbf{w}^*, c)]^{-1} \nabla_{\mathbf{w}^c}^2 \mathcal{L}_{\mathcal{S}}(\mathbf{w}^{**}, c)\| \\ & + \|\nabla_{\mathbf{w}} \mathcal{L}_{\mathcal{V}}(\mathbf{w}^*, c) [\nabla_{\mathbf{w}}^2 \mathcal{L}_{\mathcal{S}}(\mathbf{w}^*, c)]^{-1} \nabla_{\mathbf{w}^c}^2 \mathcal{L}_{\mathcal{S}}(\mathbf{w}^{**}, c) - \\ & \nabla_{\mathbf{w}} \mathcal{L}_{\mathcal{V}}(\mathbf{w}^*, c) [\nabla_{\mathbf{w}}^2 \mathcal{L}_{\mathcal{S}}(\mathbf{w}^*, c)]^{-1} \nabla_{\mathbf{w}^c}^2 \mathcal{L}_{\mathcal{S}}(\mathbf{w}^*, c)\|. \end{aligned} \quad (158)$$

Here, the first term to the right of inequality satisfies that

$$\begin{aligned} & \|\nabla_{\mathbf{w}} \mathcal{L}_{\mathcal{V}}(\mathbf{w}^{**}, c)[\nabla_{\mathbf{w}}^2 \mathcal{L}_{\mathcal{S}}(\mathbf{w}^{**}, c)]^{-1} \nabla_{\mathbf{w}c}^2 \mathcal{L}_{\mathcal{S}}(\mathbf{w}^{**}, c) - \\ & \nabla_{\mathbf{w}} \mathcal{L}_{\mathcal{V}}(\mathbf{w}^*, c)[\nabla_{\mathbf{w}}^2 \mathcal{L}_{\mathcal{S}}(\mathbf{w}^*, c)]^{-1} \nabla_{\mathbf{w}c}^2 \mathcal{L}_{\mathcal{S}}(\mathbf{w}^{**}, c)\| \\ & \leq \|\nabla_{\mathbf{w}} \mathcal{L}_{\mathcal{V}}(\mathbf{w}^{**}, c)[\nabla_{\mathbf{w}}^2 \mathcal{L}_{\mathcal{S}}(\mathbf{w}^{**}, c)]^{-1} \\ & - \nabla_{\mathbf{w}} \mathcal{L}_{\mathcal{V}}(\mathbf{w}^*, c)[\nabla_{\mathbf{w}}^2 \mathcal{L}_{\mathcal{S}}(\mathbf{w}^*, c)]^{-1}\| \|\nabla_{\mathbf{w}c}^2 \mathcal{L}_{\mathcal{S}}(\mathbf{w}^{**}, c)\|, \end{aligned} \quad (159)$$

where

$$\begin{aligned} & \|\nabla_{\mathbf{w}} \mathcal{L}_{\mathcal{V}}(\mathbf{w}^{**}, c)[\nabla_{\mathbf{w}}^2 \mathcal{L}_{\mathcal{S}}(\mathbf{w}^{**}, c)]^{-1} - \\ & \nabla_{\mathbf{w}} \mathcal{L}_{\mathcal{V}}(\mathbf{w}^*, c)[\nabla_{\mathbf{w}}^2 \mathcal{L}_{\mathcal{S}}(\mathbf{w}^*, c)]^{-1}\| \leq \\ & \|\nabla_{\mathbf{w}} \mathcal{L}_{\mathcal{V}}(\mathbf{w}^{**}, c)\| \|[\nabla_{\mathbf{w}}^2 \mathcal{L}_{\mathcal{S}}(\mathbf{w}^{**}, c)]^{-1} - [\nabla_{\mathbf{w}}^2 \mathcal{L}_{\mathcal{S}}(\mathbf{w}^*, c)]^{-1}\| \\ & + \|\nabla_{\mathbf{w}} \mathcal{L}_{\mathcal{V}}(\mathbf{w}^{**}, c) - \nabla_{\mathbf{w}} \mathcal{L}_{\mathcal{V}}(\mathbf{w}^*, c)\| \|[\nabla_{\mathbf{w}}^2 \mathcal{L}_{\mathcal{S}}(\mathbf{w}^*, c)]^{-1}\|. \end{aligned} \quad (160)$$

From assumptions, we have that

$$\|[\nabla_{\mathbf{w}}^2 \mathcal{L}_{\mathcal{S}}(\mathbf{w}^*, c)]^{-1}\| \leq \frac{1}{L_{H_s}}. \quad (161)$$

Then as to the error bound of $\|[\nabla_{\mathbf{w}}^2 \mathcal{L}_{\mathcal{S}}(\mathbf{w}^{**}, c)]^{-1} - [\nabla_{\mathbf{w}}^2 \mathcal{L}_{\mathcal{S}}(\mathbf{w}^*, c)]^{-1}\|$, we have

$$\begin{aligned} & \|[\nabla_{\mathbf{w}}^2 \mathcal{L}_{\mathcal{S}}(\mathbf{w}^{**}, c)]^{-1} - [\nabla_{\mathbf{w}}^2 \mathcal{L}_{\mathcal{S}}(\mathbf{w}^*, c)]^{-1}\| \\ & \leq \|[\nabla_{\mathbf{w}}^2 \mathcal{L}_{\mathcal{S}}(\mathbf{w}^{**}, c)]^{-1}\| \|[\nabla_{\mathbf{w}}^2 \mathcal{L}_{\mathcal{S}}(\mathbf{w}^*, c)]^{-1}\| \\ & \times \|\nabla_{\mathbf{w}}^2 \mathcal{L}_{\mathcal{S}}(\mathbf{w}^{**}, c) - \nabla_{\mathbf{w}}^2 \mathcal{L}_{\mathcal{S}}(\mathbf{w}^*, c)\| \leq \frac{L_{G'} \delta}{L_{H_s}^2} \end{aligned} \quad (162)$$

Moreover, we have that

$$\begin{aligned} & \|\nabla_{\mathbf{w}} \mathcal{L}_{\mathcal{V}}(\mathbf{w}^{**}, c) - \nabla_{\mathbf{w}} \mathcal{L}_{\mathcal{V}}(\mathbf{w}^*, c)\| \\ & \times \|[\nabla_{\mathbf{w}}^2 \mathcal{L}_{\mathcal{S}}(\mathbf{w}^*, c)]^{-1}\| \leq \frac{L_{H_2} \delta}{L_{H_s}}, \end{aligned} \quad (163)$$

$$\begin{aligned} & \|\nabla_{\mathbf{w}} \mathcal{L}_{\mathcal{V}}(\mathbf{w}^{**}, c)[\nabla_{\mathbf{w}}^2 \mathcal{L}_{\mathcal{S}}(\mathbf{w}^{**}, c)]^{-1} \\ & - \nabla_{\mathbf{w}} \mathcal{L}_{\mathcal{V}}(\mathbf{w}^*, c)[\nabla_{\mathbf{w}}^2 \mathcal{L}_{\mathcal{S}}(\mathbf{w}^*, c)]^{-1}\| \\ & \leq \frac{L_{\bar{G}} L_{G'} \delta}{L_{H_s}^2} + \frac{L_{H_2} \delta}{L_{H_s}}, \end{aligned} \quad (164)$$

and

$$\begin{aligned} & \|\nabla_{\mathbf{w}} \mathcal{L}_{\mathcal{V}}(\mathbf{w}^{**}, c)[\nabla_{\mathbf{w}}^2 \mathcal{L}_{\mathcal{S}}(\mathbf{w}^{**}, c)]^{-1} \nabla_{\mathbf{w}c}^2 \mathcal{L}_{\mathcal{S}}(\mathbf{w}^{**}, c) - \\ & \nabla_{\mathbf{w}} \mathcal{L}_{\mathcal{V}}(\mathbf{w}^*, c)[\nabla_{\mathbf{w}}^2 \mathcal{L}_{\mathcal{S}}(\mathbf{w}^*, c)]^{-1} \nabla_{\mathbf{w}c}^2 \mathcal{L}_{\mathcal{S}}(\mathbf{w}^{**}, c)\| \\ & \leq \frac{L_{\bar{G}} L_{G'} L_{G_3} \delta}{L_{H_s}^2} + \frac{L_{G_3} L_{H_2} \delta}{L_{H_s}}. \end{aligned} \quad (165)$$

Now we consider the last terms in Eq. (158),

$$\begin{aligned} & \|\nabla_{\mathbf{w}} \mathcal{L}_{\mathcal{V}}(\mathbf{w}^*, c)[\nabla_{\mathbf{w}}^2 \mathcal{L}_{\mathcal{S}}(\mathbf{w}^*, c)]^{-1} \nabla_{\mathbf{w}c}^2 \mathcal{L}_{\mathcal{S}}(\mathbf{w}^{**}, c) - \\ & \nabla_{\mathbf{w}} \mathcal{L}_{\mathcal{V}}(\mathbf{w}^*, c)[\nabla_{\mathbf{w}}^2 \mathcal{L}_{\mathcal{S}}(\mathbf{w}^*, c)]^{-1} \nabla_{\mathbf{w}c}^2 \mathcal{L}_{\mathcal{S}}(\mathbf{w}^*, c)\| \leq \\ & \|\nabla_{\mathbf{w}} \mathcal{L}_{\mathcal{V}}(\mathbf{w}^*, c)\| \|[\nabla_{\mathbf{w}}^2 \mathcal{L}_{\mathcal{S}}(\mathbf{w}^*, c)]^{-1}\| \\ & \times \|\nabla_{\mathbf{w}c}^2 \mathcal{L}_{\mathcal{S}}(\mathbf{w}^{**}, c) - \nabla_{\mathbf{w}c}^2 \mathcal{L}_{\mathcal{S}}(\mathbf{w}^*, c)\| \leq \frac{L_{\bar{G}} L_{G_2} \delta}{L_{H_s}}. \end{aligned} \quad (166)$$

In this way, the error bound of the first term to the right of inequality in Eq. (157) is

$$\begin{aligned} & \|\nabla_{\mathbf{w}} \mathcal{L}_{\mathcal{V}}(\mathbf{w}^{**}, c)[\nabla_{\mathbf{w}}^2 \mathcal{L}_{\mathcal{S}}(\mathbf{w}^{**}, c)]^{-1} \nabla_{\mathbf{w}c}^2 \mathcal{L}_{\mathcal{S}}(\mathbf{w}^{**}, c) - \\ & \nabla_{\mathbf{w}} \mathcal{L}_{\mathcal{V}}(\mathbf{w}^*, c)[\nabla_{\mathbf{w}}^2 \mathcal{L}_{\mathcal{S}}(\mathbf{w}^*, c)]^{-1} \nabla_{\mathbf{w}c}^2 \mathcal{L}_{\mathcal{S}}(\mathbf{w}^*, c)\| \\ & \leq \frac{L_{\bar{G}} L_{G'} L_{G_3} \delta}{L_{H_s}^2} + \frac{L_{G_3} L_{H_2} \delta}{L_{H_s}} + \frac{L_{\bar{G}} L_{G_2} \delta}{L_{H_s}}. \end{aligned} \quad (167)$$

Next, we consider the second term to the right of inequality in Eq. (157), i.e.,

$$\begin{aligned} & \|\nabla_{\mathbf{w}} \mathcal{L}_{\mathcal{V}}(\mathbf{w}^*, c)[\nabla_{\mathbf{w}}^2 \mathcal{L}_{\mathcal{S}}(\mathbf{w}^*, c)]^{-1} \nabla_{\mathbf{w}c}^2 \mathcal{L}_{\mathcal{S}}(\mathbf{w}^*, c) - \\ & \nabla_{\mathbf{w}} \mathcal{L}_{\mathcal{V}}(\mathbf{w}^*, c) \sum_{j=0}^J [\mathbf{I} - \nabla_{\mathbf{w}}^2 \mathcal{L}_{\mathcal{S}}(\mathbf{w}^*, c)]^j \nabla_{\mathbf{w}c}^2 \mathcal{L}_{\mathcal{S}}(\mathbf{w}^*, c)\| \\ & \leq \|\nabla_{\mathbf{w}} \mathcal{L}_{\mathcal{V}}(\mathbf{w}^*, c)\| \|[\nabla_{\mathbf{w}}^2 \mathcal{L}_{\mathcal{S}}(\mathbf{w}^*, c)]^{-1}\| \\ & - \sum_{j=0}^J [\mathbf{I} - \nabla_{\mathbf{w}}^2 \mathcal{L}_{\mathcal{S}}(\mathbf{w}^*, c)]^j \| \|\nabla_{\mathbf{w}c}^2 \mathcal{L}_{\mathcal{S}}(\mathbf{w}^*, c)\|, \end{aligned} \quad (168)$$

and then it satisfies that

$$\begin{aligned} & \|\nabla_{\mathbf{w}} \mathcal{L}_{\mathcal{V}}(\mathbf{w}^*, c)[\nabla_{\mathbf{w}}^2 \mathcal{L}_{\mathcal{S}}(\mathbf{w}^*, c)]^{-1} \nabla_{\mathbf{w}c}^2 \mathcal{L}_{\mathcal{S}}(\mathbf{w}^*, c) - \\ & \nabla_{\mathbf{w}} \mathcal{L}_{\mathcal{V}}(\mathbf{w}^*, c) \sum_{j=0}^J [\mathbf{I} - \nabla_{\mathbf{w}}^2 \mathcal{L}_{\mathcal{S}}(\mathbf{w}^*, c)]^j \nabla_{\mathbf{w}c}^2 \mathcal{L}_{\mathcal{S}}(\mathbf{w}^*, c)\| \\ & \leq L_{\bar{G}} L_{G_3} \|[\nabla_{\mathbf{w}}^2 \mathcal{L}_{\mathcal{S}}(\mathbf{w}^*, c)]^{-1} - \sum_{j=0}^J [\mathbf{I} - \nabla_{\mathbf{w}}^2 \mathcal{L}_{\mathcal{S}}(\mathbf{w}^*, c)]^j\| \\ & \leq L_{\bar{G}} L_{G_3} \left(\frac{1}{L_{H_s}} + \frac{(1+L_H)^J - 1}{L_H} \right) \\ & = \frac{L_{\bar{G}} L_{G_3} (L_H - L_{H_s} + L_{H_s} (1+L_H)^J)}{L_H L_{H_s}}. \end{aligned} \quad (169)$$

In this way, the error bound between \mathbf{U}_1^* and \mathbf{U}_1' is given by

$$\begin{aligned} & \|\mathbf{U}_1^* - \mathbf{U}_1'\| \\ & \leq \frac{L_{\bar{G}} L_{G'} L_{G_3} + L_{G_3} L_{H_2} H + L_{\bar{G}} L_{G_2} L_H}{L_{H_s}^2} \delta \\ & + \frac{L_{\bar{G}} L_{G_3} (L_H - L_{H_s} + L_{H_s} (1+L_H)^J)}{L_H L_{H_s}}. \end{aligned} \quad (170)$$

By denoting

$$\begin{aligned} \mathcal{E}_{cur_1}' & \triangleq \frac{L_{\bar{G}} L_{G'} L_{G_3} + L_{G_3} L_{H_2} H + L_{\bar{G}} L_{G_2} L_H}{L_{H_s}^2} \\ \mathcal{E}_{cur_1}'' & \triangleq \frac{L_{\bar{G}} L_{G_3} (L_H - L_{H_s} + L_{H_s} (1+L_H)^J)}{L_H L_{H_s}}, \end{aligned} \quad (171)$$

we have proved Lemma 3. \square

Approximation error of \mathbf{U}_2 . We adopt an approximation way to simplify the computation of \mathbf{U}_2 , which has been presented in Eq. (143). The generalization error for \mathbf{U}_2 is presented in the following lemma.

Lemma 4. *Supposing that the assumptions holds, the approximated \mathbf{U}_2 satisfies that*

$$\|\mathbf{U}_2 - \mathbf{U}'_2\| \leq \mathcal{E}_{cur_2}, \quad (172)$$

where \mathcal{E}_{cur_2} is a constant that only depends on the Lipschitz constants, which is computed as

$$\mathcal{E}_{cur_2} \triangleq \frac{2\rho K L_G L_{G'} L_{G_3}}{L_{H_s}}. \quad (173)$$

Proof. In the following proof, we mainly leverage the Lipschitz continuity assumptions of \mathcal{L}_S , $\nabla_w^2 \mathcal{L}_S(\mathbf{w}, c)$, and $\nabla_w \mathcal{L}_S(\mathbf{w}, c)$, and the upper bound of the norm of ϵ .

Review that \mathbf{U}_2 is computed as

$$\begin{aligned} \mathbf{U}_2 = & -2K(1 - \|\nabla_w \mathcal{L}_S(\hat{\mathbf{w}}, c)\|)^{K-1} \nabla_w \mathcal{L}_S(\hat{\mathbf{w}}, c) \\ & \times \nabla_w^2 \mathcal{L}_S(\hat{\mathbf{w}}, c) [\nabla_w^2 \mathcal{L}_S(\mathbf{w}^*, c)]^{-1} \nabla_{w_c}^2 \mathcal{L}_S(\mathbf{w}^*, c), \end{aligned} \quad (174)$$

while \mathbf{U}'_2 is computed as

$$\begin{aligned} \mathbf{U}'_2 = & -2K(1 - \|\nabla_w \mathcal{L}_S(\hat{\mathbf{w}}, c)\|)^{K-1} \\ & \times \nabla_w \mathcal{L}_S(\hat{\mathbf{w}}, c) \nabla_{w_c}^2 \mathcal{L}_S(\mathbf{w}^*, c). \end{aligned} \quad (175)$$

The approximation error is computed as

$$\begin{aligned} \|\mathbf{U}_2 - \mathbf{U}'_2\| = & (2K(1 - \|\nabla_w \mathcal{L}_S(\hat{\mathbf{w}}, c)\|)^{K-1}) \times \\ & \left\| \nabla_w \mathcal{L}_S(\hat{\mathbf{w}}, c) \nabla_w^2 \mathcal{L}_S(\hat{\mathbf{w}}, c) [\nabla_w^2 \mathcal{L}_S(\mathbf{w}^*, c)]^{-1} \nabla_{w_c}^2 \mathcal{L}_S(\mathbf{w}^*, c) \right. \\ & \left. - \nabla_w \mathcal{L}_S(\hat{\mathbf{w}}, c) \nabla_w^2 \mathcal{L}_S(\mathbf{w}^*, c) [\nabla_w^2 \mathcal{L}_S(\mathbf{w}^*, c)]^{-1} \nabla_{w_c}^2 \mathcal{L}_S(\mathbf{w}^*, c) \right\|. \end{aligned} \quad (176)$$

Then the approximation error satisfies that

$$\begin{aligned} \|\mathbf{U}_2 - \mathbf{U}'_2\| \leq & (2K(1 - \|\nabla_w \mathcal{L}_S(\hat{\mathbf{w}}, c)\|)^{K-1}) \\ & \times \|\nabla_w^2 \mathcal{L}_S(\hat{\mathbf{w}}, c) - \nabla_w^2 \mathcal{L}_S(\mathbf{w}^*, c)\| \|[\nabla_w^2 \mathcal{L}_S(\mathbf{w}^*, c)]^{-1}\| \\ & \times \|\nabla_{w_c}^2 \mathcal{L}_S(\mathbf{w}^*, c)\| \|\nabla_w \mathcal{L}_S(\hat{\mathbf{w}}, c)\| \\ \leq & 2K \frac{L_G L_{G'} L_{G_3}}{L_{H_s}} \|\hat{\mathbf{w}} - \mathbf{w}^*\| \leq \frac{2\rho K L_G L_{G'} L_{G_3}}{L_{H_s}}. \end{aligned} \quad (177)$$

By denoting

$$\mathcal{E}_{cur_2} \triangleq \frac{2\rho K L_G L_{G'} L_{G_3}}{L_{H_s}}, \quad (178)$$

we have proved Lemma 4. \square

After proving Lemma 3 and Lemma 4, we can obtain the upper bound of the approximation error in $\hat{\nabla}c$, as shown in Theorem 10.

Theorem 10. *Suppose assumptions hold, the approximated gradients of curvatures $\hat{\nabla}c$ satisfy*

$$\begin{aligned} \|\nabla c - \hat{\nabla}c\| \leq & \|\mathbf{U}_1 - \mathbf{U}'_1\| + \|\mathbf{U}_2 - \mathbf{U}'_2\| \\ \leq & \mathcal{E}_{cur_1} + \mathcal{E}_{cur_2}, \end{aligned} \quad (179)$$

where \mathcal{E}_{cur_1} and \mathcal{E}_{cur_2} are constants and have been defined in Lemma 3 and Lemma 4, respectively.

By the aforementioned analyses, we demonstrate the approximation error in gradients of curvatures is upper-bounded, thus approximation ways in our method are rational.

6.3 Convergence Analyses

We establish the convergence analyses of the parameters \mathbf{w} and the curvatures c , which are presented in Theorem 11 and Theorem 12, respectively. Theoretical analyses show that parameters \mathbf{w} and the curvatures c can converge, thereby demonstrating the effectiveness of our method.

In Theorem 11, we bound the gradient of parameters \mathbf{w} to analyze the convergence.

Theorem 11. *Set the iteration number of training parameters of HNNs as T , and choose step-size of parameters \mathbf{w} as $\eta^{(t)} = \frac{\eta^{(0)}}{\sqrt{t}}$ and perturbation radius $\hat{\rho}^{(t)}$ satisfies $\frac{\hat{\rho}^{(0)}}{\sqrt{t}}$, parameters \mathbf{w} satisfy*

$$\min_{t \in [1, \dots, T]} \|\nabla_w \mathcal{L}_S(\mathbf{w}^{(t)}, c)\|^2 \leq \frac{\mathcal{C}_{w_1}}{\ln T} + \frac{\mathcal{C}_{w_2}(1 + \ln T)}{\ln T}, \quad (180)$$

where \mathcal{C}_{w_1} and \mathcal{C}_{w_2} are constants and computed as

$$\begin{aligned} \mathcal{C}_{w_1} = & \frac{\beta_{\max}}{\eta^{(0)}} \left(\mathcal{L}_S(\mathbf{w}^{(0)}, c) - \mathcal{L}_S(\mathbf{w}^{(T+1)}, c) \right) \\ \mathcal{C}_{w_2} = & \frac{\beta_{\max}}{\eta^{(0)}} \left(\frac{1}{\beta_{\min}} L_H L_G \eta^{(0)} \hat{\rho}^{(0)} + \frac{1}{2} L_H L_G^2 \eta^{(0)2} \right). \end{aligned} \quad (181)$$

Proof. Recall that the parameters of HNNs are updated as

$$\begin{aligned} \mathbf{w} \leftarrow & \mathbf{w} - \eta \nabla_w \mathcal{L}_S(\mathbf{w}', c), \\ \text{where } \mathbf{w}' = & \mathbf{w} + \hat{\rho} \nabla_w \mathcal{L}_S(\mathbf{w}, c) / \|\nabla_w \mathcal{L}_S(\mathbf{w}, c)\|. \end{aligned} \quad (182)$$

To bound the gradients of parameters \mathbf{w} , we utilize the Lipschitz continuity assumptions of \mathcal{L}_S , \mathcal{L}_V and $\nabla_w \mathcal{L}_S(\mathbf{w}, c)$, and establish the connection between the update vector $\nabla_w \mathcal{L}_S(\mathbf{w}', c)$ and gradients $\nabla_w \mathcal{L}_S(\mathbf{w}, c)$ by decomposing the update

vector. It follows that

$$\begin{aligned}
\mathcal{L}_S(\mathbf{w}^{(t+1)}, c) &\leq \mathcal{L}_S(\mathbf{w}^{(t)}, c) + \frac{L_H}{2} \|\mathbf{w}^{(t+1)} - \mathbf{w}^{(t)}\|^2 \\
&+ (\nabla_{\mathbf{w}} \mathcal{L}_S(\mathbf{w}^{(t)}, c))^{\top} (\mathbf{w}^{(t+1)} - \mathbf{w}^{(t)}) \\
&= \mathcal{L}_S(\mathbf{w}^{(t)}, c) + \frac{L_H}{2} \|\eta^{(t)} \nabla_{\mathbf{w}} \mathcal{L}_S(\mathbf{w}', c)\|^2 \\
&- (\nabla_{\mathbf{w}} \mathcal{L}_S(\mathbf{w}^{(t)}, c))^{\top} \eta^{(t)} \nabla_{\mathbf{w}} \mathcal{L}_S(\mathbf{w}', c).
\end{aligned} \tag{183}$$

Then, we have

$$\begin{aligned}
\mathcal{L}_S(\mathbf{w}^{(t+1)}, c) - \mathcal{L}_S(\mathbf{w}^{(t)}, c) &\leq \frac{L_H}{2} \eta^{(t)2} \|\nabla_{\mathbf{w}} \mathcal{L}_S(\mathbf{w}', c)\|^2 \\
&- \eta^{(t)} (\nabla_{\mathbf{w}} \mathcal{L}_S(\mathbf{w}^{(t)}, c))^{\top} \nabla_{\mathbf{w}} \mathcal{L}_S(\mathbf{w}', c).
\end{aligned} \tag{184}$$

We decompose vectors $\nabla_{\mathbf{w}} \mathcal{L}_S(\mathbf{w}', c)$ into parallel direction $\nabla f_{\parallel}^{(t)}$ of vector $\nabla_{\mathbf{w}} \mathcal{L}_S(\mathbf{w}, c)$ and orthogonal direction $\nabla f_{\perp}^{(t)}$, i.e.,

$$\nabla f_{\parallel}^{(t)} = \beta_t \nabla_{\mathbf{w}} \mathcal{L}_S(\mathbf{w}, c), \quad \nabla f_{\perp}^{(t)} = \nabla_{\mathbf{w}} \mathcal{L}_S(\mathbf{w}, c) - \nabla f_{\parallel}^{(t)}. \tag{185}$$

We have that

$$\begin{aligned}
&\left\langle \nabla_{\mathbf{w}} \mathcal{L}_S(\mathbf{w}^{(t)}, c), \nabla_{\mathbf{w}} \mathcal{L}_S(\mathbf{w}', c) \right\rangle \\
&= \left\langle \nabla_{\mathbf{w}} \mathcal{L}_S(\mathbf{w}^{(t)}, c), \frac{1}{\beta_t} (\nabla_{\mathbf{w}} \mathcal{L}_S(\mathbf{w}, c) - f_{\perp}^{(t)}) \right\rangle \\
&= \frac{1}{\beta_t} \|\nabla_{\mathbf{w}} \mathcal{L}_S(\mathbf{w}^{(t)}, c)\|^2 - \frac{1}{\beta_t} \|\nabla_{\mathbf{w}} \mathcal{L}_S(\mathbf{w}^{(t)}, c)\|^2 \\
&\times (|\tan(\theta_t)| + O(\theta_t^2)),
\end{aligned} \tag{186}$$

where $\sin(\theta_t)$ is the angle between $\nabla_{\mathbf{w}} \mathcal{L}_S(\mathbf{w}^{(t)}, c)$ and $\nabla_{\mathbf{w}} \mathcal{L}_S(\mathbf{w}'^{(t)}, c)$. Moreover, from assumptions, we have

$$\begin{aligned}
|\tan \theta_t| &\leq \frac{\|\nabla_{\mathbf{w}} \mathcal{L}_S(\mathbf{w}^{(t)}, c) - \nabla_{\mathbf{w}} \mathcal{L}_S(\mathbf{w}'^{(t)}, c)\|}{\|\nabla_{\mathbf{w}} \mathcal{L}_S(\mathbf{w}^{(t)}, c)\|} \\
&\leq \frac{\hat{\rho}^t L_H \|\frac{\nabla_{\mathbf{w}} \mathcal{L}_S(\mathbf{w}^{(t)}, c)}{\|\nabla_{\mathbf{w}} \mathcal{L}_S(\mathbf{w}^{(t)}, c)\|}\|}{\|\nabla_{\mathbf{w}} \mathcal{L}_S(\mathbf{w}^{(t)}, c)\|} = \frac{\hat{\rho}^t L_H}{\|\nabla_{\mathbf{w}} \mathcal{L}_S(\mathbf{w}^{(t)}, c)\|}.
\end{aligned} \tag{187}$$

Moreover, we have that

$$\begin{aligned}
&\mathcal{L}_S(\mathbf{w}^{(t+1)}, c) - \mathcal{L}_S(\mathbf{w}^{(t)}, c) \\
&\leq -\eta^{(t)} \left\langle \nabla_{\mathbf{w}} \mathcal{L}_S(\mathbf{w}^{(t)}, c), \nabla_{\mathbf{w}} \mathcal{L}_S(\mathbf{w}'^{(t)}, c) \right\rangle \\
&+ \frac{1}{2} L_H \eta^{(t)2} \|\nabla_{\mathbf{w}} \mathcal{L}_S(\mathbf{w}'^{(t)}, c)\|^2.
\end{aligned} \tag{188}$$

Hence, we can obtain that

$$\begin{aligned}
&\mathcal{L}_S(\mathbf{w}^{(t+1)}, c) - \mathcal{L}_S(\mathbf{w}^{(t)}, c) \\
&\leq \frac{\eta^{(t)}}{\beta_t} \|\nabla_{\mathbf{w}} \mathcal{L}_S(\mathbf{w}^{(t)}, c)\|^2 |\tan(\theta_t)| \\
&- \frac{\eta^{(t)}}{\beta_t} \|\nabla_{\mathbf{w}} \mathcal{L}_S(\mathbf{w}^{(t)}, c)\|^2 + \frac{1}{2} L_H \eta^{(t)2} \|\nabla_{\mathbf{w}} \mathcal{L}_S(\mathbf{w}'^{(t)}, c)\|^2 \\
&\leq \frac{\eta^{(t)}}{\beta_t} L_H \hat{\rho}^{(t)} \|\nabla_{\mathbf{w}} \mathcal{L}_S(\mathbf{w}^{(t)}, c)\| \\
&- \frac{\eta^{(t)}}{\beta_t} \|\nabla_{\mathbf{w}} \mathcal{L}_S(\mathbf{w}^{(t)}, c)\|^2 + \frac{1}{2} L_H \eta^{(t)2} \|\nabla_{\mathbf{w}} \mathcal{L}_S(\mathbf{w}'^{(t)}, c)\|^2.
\end{aligned} \tag{189}$$

We further assume that

$$0 < \beta_{\min} \leq \beta_t \leq \beta_{\max}, \tag{190}$$

and thus have

$$\begin{aligned}
&\mathcal{L}_S(\mathbf{w}^{(t+1)}, c) - \mathcal{L}_S(\mathbf{w}^{(t)}, c) \\
&\leq -\frac{\eta^{(t)}}{\beta_{\max}} \|\nabla_{\mathbf{w}} \mathcal{L}_S(\mathbf{w}^{(t)}, c)\|^2 \\
&+ \frac{1}{\beta_{\min}} L_H \hat{\rho}^{(t)} \eta^{(t)} L_G + \frac{1}{2} L_H \eta^{(t)2} L_G^2.
\end{aligned} \tag{191}$$

By rearranging the term in Eq. (191), we have

$$\begin{aligned}
&\frac{\eta^{(t)}}{\beta_{\max}} \|\nabla_{\mathbf{w}} \mathcal{L}_S(\mathbf{w}^{(t)}, c)\|^2 \\
&\leq \mathcal{L}_S(\mathbf{w}^{(t)}, c) - \mathcal{L}_S(\mathbf{w}^{(t+1)}, c) \\
&+ \frac{1}{\beta_{\min}} L_H \hat{\rho}^{(t)} \eta^{(t)} L_G \sum_{t=1}^T \hat{\rho}^{(t)} \eta^{(t)} + \frac{1}{2} L_H L_G^2 \sum_{t=1}^T \eta^{(t)2}.
\end{aligned} \tag{192}$$

Telescoping from $t=1$ to T , we have

$$\begin{aligned}
&\frac{1}{\beta_{\max}} \sum_{t=1}^T \eta^{(t)} \|\nabla_{\mathbf{w}} \mathcal{L}_S(\mathbf{w}^{(t)}, c)\|^2 \\
&\leq \mathcal{L}_S(\mathbf{w}^{(1)}, c) - \mathcal{L}_S(\mathbf{w}^{(T+1)}, c) \\
&+ \frac{1}{\beta_{\min}} L_H \hat{\rho}^{(t)} \eta^{(t)} L_G \sum_{t=1}^T \hat{\rho}^{(t)} \eta^{(t)} + \frac{1}{2} L_H L_G^2 \sum_{t=1}^T \eta^{(t)2}.
\end{aligned} \tag{193}$$

Let $\eta^{(t)} = \frac{\eta^{(0)}}{\sqrt{t}}$ and $\hat{\rho}^{(t)} = \frac{\hat{\rho}^{(0)}}{\sqrt{t}}$, we have that

$$\begin{aligned}
&\frac{\eta^{(0)}}{\beta_{\max}} \sum_{t=1}^T \frac{1}{\sqrt{t}} \|\nabla_{\mathbf{w}} \mathcal{L}_S(\mathbf{w}^{(t)}, c)\|^2 \\
&\leq \mathcal{L}_S(\mathbf{w}^{(0)}, c) - \mathcal{L}_S(\mathbf{w}^{(T+1)}, c) \\
&+ \frac{1}{\beta_{\min}} L_H L_G \eta^{(0)} \hat{\rho}^{(0)} (1 + \ln T) + \frac{1}{2} L_H L_G^2 \eta^{(0)2} (1 + \ln T).
\end{aligned} \tag{194}$$

Because we have

$$\begin{aligned}
&\sum_{t=1}^T \frac{1}{\sqrt{t}} \|\nabla_{\mathbf{w}} \mathcal{L}_S(\mathbf{w}^{(t)}, c)\|^2 \\
&\geq \sum_{t=1}^T \frac{1}{\sqrt{t}} \min_{t \in [1, \dots, T]} \|\nabla_{\mathbf{w}} \mathcal{L}_S(\mathbf{w}^{(t)}, c)\|^2 \\
&\geq \ln T \min_{t \in [1, \dots, T]} \|\nabla_{\mathbf{w}} \mathcal{L}_S(\mathbf{w}^{(t)}, c)\|^2,
\end{aligned} \tag{195}$$

it holds that

$$\begin{aligned} & \min_{t \in [1, \dots, T]} \|\nabla_{\mathbf{w}} \mathcal{L}_{\mathcal{S}}(\mathbf{w}^{(t)}, c)\|^2 \leq \\ & + \frac{\beta_{\max}}{\eta^{(0)}} \frac{1}{\ln T} \left(\mathcal{L}_{\mathcal{S}}(\mathbf{w}^{(0)}, c) - \mathcal{L}_{\mathcal{S}}(\mathbf{w}^{(T+1)}, c) \right) \\ & + \frac{\beta_{\max} (1 + \ln T)}{\eta^{(0)} \ln T} \left(\frac{1}{\beta_{\min}} L_H L_G \eta^{(0)} \hat{\rho}^{(0)} + \frac{1}{2} L_H L_G^2 \eta^{(0)2} \right). \end{aligned} \quad (196)$$

By denoting

$$\begin{aligned} \mathcal{C}_{w_1} &= \frac{\beta_{\max}}{\eta^{(0)}} \left(\mathcal{L}_{\mathcal{S}}(\mathbf{w}^{(0)}, c) - \mathcal{L}_{\mathcal{S}}(\mathbf{w}^{(T+1)}, c) \right) \\ \mathcal{C}_{w_2} &= \frac{\beta_{\max}}{\eta^{(0)}} \left(\frac{1}{\beta_{\min}} L_H L_G \eta^{(0)} \hat{\rho}^{(0)} + \frac{1}{2} L_H L_G^2 \eta^{(0)2} \right), \end{aligned} \quad (197)$$

we obtain the theorem. \square

In Theorem 12, we present the convergence performance of the curvatures c by providing the upper bound of $\frac{1}{\mathcal{T}} \sum_{t=1}^{\mathcal{T}} \|\nabla c^{(t)}\|^2$.

Theorem 12. Set the iteration number of training curvatures as \mathcal{T} , and choose the step-size as $\frac{1}{8L_{H_c}} \leq \eta_c^{(t)} \leq \frac{1}{4L_{H_c}}$, the obtained curvature c satisfies

$$\frac{1}{\mathcal{T}} \sum_{t=1}^{\mathcal{T}} \|\nabla c^{(t)}\|^2 \leq \frac{64}{3} L_{H_c} \frac{\mathcal{F}(c^{(1)}) - \mathcal{F}(c^{(\mathcal{T}+1)})}{\mathcal{T}} + \mathcal{C}_c, \quad (198)$$

where \mathcal{C}_c is a constant and computed as $\mathcal{C}_c \triangleq 9\mathcal{E}_{cur_1}^2 + 9\mathcal{E}_{cur_2}^2$.

Proof. To analyze the bound of gradients of curvatures, we utilize the Lipschitz continuity assumptions, and then leverage the connection between the update vector $\hat{\nabla}c^{(\tau)}$ and the gradients of curvatures $\nabla c^{(\tau)}$ by Theorem 10. From the assumption, we have that

$$\begin{aligned} \mathcal{F}(c^{(\tau+1)}) &\leq \mathcal{F}(c^{(\tau)}) - \eta_c^{(t)} \langle \nabla c^{(\tau)}, \hat{\nabla}c^{(\tau)} \rangle \\ &+ \frac{1}{2} L_{H_c} \eta_c^{(t)2} \|c^{(\tau+1)} - c^{(\tau)}\|^2 \\ &= \mathcal{F}(c^{(\tau)}) + \frac{1}{2} L_{H_c} \eta_c^{(t)2} \|\hat{\nabla}c^{(\tau)}\|^2 \\ &- \eta_c^{(t)} \langle \nabla c^{(\tau)}, \hat{\nabla}c^{(\tau)} - \nabla c^{(\tau)} + \nabla c^{(\tau)} \rangle, \end{aligned} \quad (199)$$

and we further have that

$$\begin{aligned} \mathcal{F}(c^{(\tau+1)}) &\leq \mathcal{F}(c^{(\tau)}) + \frac{1}{2} L_{H_c} \eta_c^{(t)2} \|\hat{\nabla}c^{(\tau)}\|^2 \\ &- \eta_c^{(t)} \langle \nabla c^{(\tau)}, \hat{\nabla}c^{(\tau)} - \nabla c^{(\tau)} \rangle - \eta_c^{(t)2} \|\nabla c^{(\tau)}\|^2 \\ &\leq \mathcal{F}(c^{(\tau)}) - \left(\frac{1}{2} \eta_c^{(t)} - \eta_c^{(t)2} L_{H_c} \right) \|\nabla c^{(\tau)}\|^2 \\ &+ \left(\frac{1}{2} \eta_c^{(t)} + \eta_c^{(t)2} L_{H_c} \right) \|\nabla c^{(\tau)} - \hat{\nabla}c^{(\tau)}\|^2. \end{aligned} \quad (200)$$

From Theorem 10, we have that

$$\|\nabla c^{(\tau)} - \hat{\nabla}c^{(\tau)}\|^2 \leq 3\mathcal{E}_{cur_1}^2 + 3\mathcal{E}_{cur_2}^2. \quad (201)$$

Thus Eq. (200) can be rewritten as

$$\begin{aligned} & \left(\frac{1}{2} \eta_c^{(t)} - \eta_c^{(t)2} L_{H_c} \right) \|\nabla c^{(\tau)}\|^2 \leq \mathcal{F}(c^{(\tau)}) - \mathcal{F}(c^{(\tau+1)}) \\ & + \left(\frac{1}{2} \eta_c^{(t)} + \eta_c^{(t)2} L_{H_c} \right) (3\mathcal{E}_{cur_1}^2 + 3\mathcal{E}_{cur_2}^2). \end{aligned} \quad (202)$$

Telescoping from $t=1$ to \mathcal{T} and according to assumptions, we have

$$\begin{aligned} & \left(\frac{1}{2} \eta_c - \eta_c^2 L_{H_c} \right) \frac{1}{\mathcal{T}} \sum_{t=1}^{\mathcal{T}} \|\nabla c^{(\tau)}\|^2 \leq \frac{\mathcal{F}(c^{(1)}) - \mathcal{F}(c^{(\mathcal{T}+1)})}{\mathcal{T}} \\ & + \left(\frac{1}{2} \eta_c^2 + \eta_c^2 L_{H_c} \right) (3\mathcal{E}_{cur_1}^2 + 3\mathcal{E}_{cur_2}^2). \end{aligned} \quad (203)$$

By setting $\frac{1}{8L_{H_c}} \leq \eta_c \leq \frac{1}{4L_{H_c}}$, we have

$$\begin{aligned} \frac{1}{\mathcal{T}} \sum_{t=1}^{\mathcal{T}} \|\nabla c^{(\tau)}\|^2 &\leq \frac{64}{3} L_{H_c} \frac{\mathcal{F}(c^{(1)}) - \mathcal{F}(c^{(\mathcal{T}+1)})}{\mathcal{T}} \\ &+ 9(\mathcal{E}_{cur_1}^2 + \mathcal{E}_{cur_2}^2). \end{aligned} \quad (204)$$

By denoting $\mathcal{C}_c \triangleq 9\mathcal{E}_{cur_1}^2 + 9\mathcal{E}_{cur_2}^2$, we have proved the theorem. \square

Based on Theorem 11 and Theorem 12, we analyze the convergence performance of the parameters of HNNs \mathbf{w} and curvatures c , which again demonstrate the rationality of our algorithm.

6.4 Efficiency Analyses

6.4.1 Analysis of Scope Sharpness Measure

We adopt two approximation ways to approximate $\text{SN}(\mathbf{w})$ as $\hat{\text{sn}}(\hat{\mathbf{w}}(c))$. (1) We utilize $\hat{\text{sn}}(\mathbf{w}^*(c))$ to approximate $\text{sn}(\mathbf{w}^*(c))$. (2) We utilize $\hat{\text{sn}}(\mathbf{w}^*(c)) + \epsilon^{\top} \frac{\partial \hat{\text{sn}}(\mathbf{w}^*(c))}{\partial \mathbf{w}^*}$ to approximate $\hat{\text{sn}}(\mathbf{w}^*(c) + \epsilon)$. Here, we present the efficiency analysis for the first approximation way. Suppose that the number of the parameter \mathbf{w} as d , then the complexity of computing $\text{sn}(\cdot)$ equals to

$$\mathcal{O}(\text{sn}(\cdot)) = \mathcal{O}(d^3 + d^2 + 2d). \quad (205)$$

In contrast, the complexity of $\hat{\text{sn}}(\cdot)$ is

$$\mathcal{O}(\hat{\text{sn}}(\cdot)) = \mathcal{O}(d). \quad (206)$$

Obviously, the approximated $\hat{\text{sn}}(\cdot)$ significantly reduce the computation complexity of $\text{sn}(\cdot)$.

As to the second approximation way, it is non-trivial to analyze efficiency since the complexity and computation time for the maximization problem are impossible to analyze. Intuitively,

the approximation way can efficiently solve the maximization problem, only needing a one-step update.

6.4.2 Analysis of Implicit Differentiation

We also provide a comparison of the computation complexity of different algorithms to compute gradient with respect to c . Some works show that the complexity of computing gradients or Jacobian-vector products of a differentiable function is no more than five times the complexity of computing the function itself, and the complexity of computing Hessian-vector products is no more than five times the complexity of computing gradients, see (Griewank, 1993; Griewank and Walther, 2008) for details.

Recall that the gradient of c is computed by

$$\begin{aligned} \frac{d\mathcal{F}(\mathbf{w}^*(c), c)}{dc} &= \nabla_c \mathcal{F}(\mathbf{w}^*(c), c) \\ &+ \nabla_{\mathbf{w}} \mathcal{F}(\mathbf{w}^*(c), c) \nabla_c \mathbf{w}^*(c), \end{aligned} \quad (207)$$

where $\nabla_{\mathbf{w}} \mathcal{F}(\mathbf{w}^*(c), c)$ is expanded as

$$\begin{aligned} \nabla_{\mathbf{w}} \mathcal{F}(\mathbf{w}^*(c), c) &= \nabla_{\mathbf{w}} \mathcal{L}_{\mathcal{V}}(\mathbf{w}^*, c) + \\ &2K \left(1 - \|\nabla_{\mathbf{w}} \mathcal{L}_{\mathcal{S}}(\hat{\mathbf{w}}, c)\| \right)^{K-1} \nabla_{\mathbf{w}} \mathcal{L}_{\mathcal{S}}(\hat{\mathbf{w}}, c) \nabla_{\mathbf{w}}^2 \mathcal{L}_{\mathcal{S}}(\hat{\mathbf{w}}, c), \end{aligned} \quad (208)$$

and $\nabla_c \mathbf{w}^*(c)$ can be expanded as

$$\begin{aligned} \nabla_c \mathbf{w}^*(c) &= - \sum_{j \leq T} \left(\prod_{k < j} \mathbf{I} - \nabla_{\mathbf{w}}^2 \mathcal{L}_{\mathcal{S}}(\mathbf{w}^{(T-k)}, c) \right) \\ &\times \nabla_{\mathbf{w}c}^2 \mathcal{L}_{\mathcal{S}}(\mathbf{w}^{(T-j)}, c). \end{aligned} \quad (209)$$

By utilizing the above-mentioned principles, the complexity of computing $\nabla_{\mathbf{w}} \mathcal{F}(\mathbf{w}^*(c), c)$ satisfies that

$$\mathcal{O}(\nabla_{\mathbf{w}} \mathcal{F}(\mathbf{w}^*(c), c)) \leq 35\mathcal{O}(\mathcal{L}(\cdot)) + \mathcal{O}(2d). \quad (210)$$

The complexity of computing $\frac{\partial \mathbf{w}^*(c)}{\partial c}$ satisfies that

$$\begin{aligned} \mathcal{O}(\nabla_c \mathbf{w}^*(c)) &\leq \\ &\mathcal{O} \left(\frac{T(T+1)}{2} (25\mathcal{O}(\mathcal{L}(\cdot)) + d) + 25T\mathcal{O}(\mathcal{L}(\cdot)) \right). \end{aligned} \quad (211)$$

By utilizing the above-mentioned principles, the complexity of the gradient in Eq. (207) satisfies that

$$\begin{aligned} \mathcal{O} \left(\frac{d\mathcal{F}(\mathbf{w}^*(c), c)}{dc} \right) &\leq \frac{T(T+1)+6}{2} \mathcal{O}(d) \\ &+ \left(\frac{25T(T+1)}{2} + 25T + 40 \right) \mathcal{O}(\mathcal{L}(\cdot)). \end{aligned} \quad (212)$$

We denote the gradient of c computed by implicit differentiation as $\frac{d\mathcal{F}_i(\mathbf{w}^*(c), c)}{dc}$. Recall that it is computed as

$$\begin{aligned} \frac{d\mathcal{F}_i(\mathbf{w}^*(c), c)}{dc} &= \nabla_c \mathcal{F}(\mathbf{w}^*(c), c) \\ &- \nabla_{\mathbf{w}} \mathcal{F}(\mathbf{w}^*(c), c) \left(\nabla^2 \mathcal{L}_{\mathcal{S}}(\mathbf{w}^*) \right)^{-1} \nabla_{\mathbf{w}c}^2 \mathcal{L}_{\mathcal{S}}(\mathbf{w}^*, c). \end{aligned} \quad (213)$$

Its complexity satisfies that

$$\begin{aligned} \mathcal{O} \left(\frac{d\mathcal{F}_i(\mathbf{w}^*(c), c)}{dc} \right) &\leq 65\mathcal{O}(\mathcal{L}(\cdot)) + \mathcal{O}(d^3) + 2\mathcal{O}(d^2) + 3\mathcal{O}(d). \end{aligned} \quad (214)$$

Obviously, computing $\frac{d\mathcal{F}_i(\mathbf{w}^*(c), c)}{dc}$ requires $\mathcal{O}(d^2)$ and $\mathcal{O}(d^3)$, which are intractable for deep neural works.

We further adopt \mathbf{U}'_1 and \mathbf{U}'_2 to approximate \mathbf{U}_1 and \mathbf{U}_2 . Specifically, \mathbf{U}'_1 and \mathbf{U}'_2 are computed by

$$\begin{aligned} \mathbf{U}'_1 &= -\nabla_{\mathbf{w}} \mathcal{L}_{\mathcal{V}}(\mathbf{w}^*, c) \\ &\times \sum_{j=0}^J \left(\mathbf{I} - \nabla_{\mathbf{w}}^2 \mathcal{L}_{\mathcal{S}}(\mathbf{w}^*, c) \right)^j \nabla_{\mathbf{w}c}^2 \mathcal{L}_{\mathcal{S}}(\mathbf{w}^*, c) \\ \mathbf{U}'_2 &= -2K \left(1 - \left\| \nabla_{\mathbf{w}} \mathcal{L}_{\mathcal{S}}(\hat{\mathbf{w}}, c) \right\| \right)^{K-1} \\ &\times \nabla_{\mathbf{w}} \mathcal{L}_{\mathcal{S}}(\hat{\mathbf{w}}, c) \nabla_{\mathbf{w}c}^2 \mathcal{L}_{\mathcal{S}}(\mathbf{w}^*, c). \end{aligned} \quad (215)$$

The complexity of \mathbf{U}'_1 satisfies that

$$\mathcal{O}(\mathbf{U}'_1) \leq (25J + 30)\mathcal{O}(\mathcal{L}(\cdot)) + J\mathcal{O}(d), \quad (216)$$

while the complexity of \mathbf{U}'_2 satisfies that

$$\mathcal{O}(\mathbf{U}'_2) \leq 30\mathcal{O}(\mathcal{L}(\cdot)) + \mathcal{O}(d). \quad (217)$$

We denote the gradient of c approximated with the proposed method as $\frac{d\mathcal{F}_o(\mathbf{w}^*(c), c)}{dc}$. The complexity of $\frac{d\mathcal{F}_o(\mathbf{w}^*(c), c)}{dc}$ satisfies that

$$\begin{aligned} \mathcal{O} \left(\frac{d\mathcal{F}_o(\mathbf{w}^*(c), c)}{dc} \right) &\leq \\ &(25J + 60)\mathcal{O}(\mathcal{L}(\cdot)) + (J + 1)\mathcal{O}(d). \end{aligned} \quad (218)$$

Here, J usually is set as 2. By substituting $J = 2$ into Eq. (218), the complexity of our method is

$$\mathcal{O} \left(\frac{d\mathcal{F}_o(\mathbf{w}^*(c), c)}{dc} \right) \leq 110\mathcal{O}(\mathcal{L}(\cdot)) + 3\mathcal{O}(d). \quad (219)$$

Remark. In summary, the complexity of $\frac{d\mathcal{F}(\mathbf{w}^*(c), c)}{dc}$ is

$$\begin{aligned} \mathcal{O} \left(\frac{d\mathcal{F}(\mathbf{w}^*(c), c)}{dc} \right) &\leq \frac{T(T+1)+6}{2} \mathcal{O}(d) \\ &+ \left(\frac{25T(T+1)}{2} + 25T + 40 \right) \mathcal{O}(\mathcal{L}(\cdot)), \end{aligned} \quad (220)$$

the complexity of $\frac{d\mathcal{F}(\mathbf{w}^*(c), c)}{dc}$ is

$$\begin{aligned} & \mathcal{O}\left(\frac{d\mathcal{F}_i(\mathbf{w}^*(c), c)}{dc}\right) \\ & \leq 65\mathcal{O}(\mathcal{L}(\cdot)) + \mathcal{O}(d^3) + 2\mathcal{O}(d^2) + 3\mathcal{O}(d), \end{aligned} \quad (221)$$

while the complexity of the approximated gradient $\frac{d\mathcal{F}_o(\mathbf{w}^*(c), c)}{dc}$ in our method is

$$\mathcal{O}\left(\frac{d\mathcal{F}_o(\mathbf{w}^*(c), c)}{dc}\right) \leq 110\mathcal{O}(\mathcal{L}(\cdot)) + 3\mathcal{O}(d). \quad (222)$$

Compared with $\frac{d\mathcal{F}(\mathbf{w}^*(c), c)}{dc}$, the proposed gradient $\frac{d\mathcal{F}_o(\mathbf{w}^*(c), c)}{dc}$ avoids to unroll the inner-level optimization process. The complexity of the proposed gradient is independent of the inner-level update step T , thereby reducing the complexity. Compared with $\frac{d\mathcal{F}_i(\mathbf{w}^*(c), c)}{dc}$, $\frac{d\mathcal{F}_o(\mathbf{w}^*(c), c)}{dc}$ avoids the complexity of $\mathcal{O}(d^3)$ by avoiding the inverse of the Hessian matrix, thereby further reducing the complexity.

7 Experiments

7.1 Settings

We conduct experiments on four settings: classification, learning from long-tailed data, learning from noisy data, and few-shot learning to evaluate the performance of our method. In this subsection, we present the task descriptions and implementation details of these four experimental settings, including the dataset descriptions, baseline introduction, and hyper-parameters.

Classification. Following C-HNNs (Guo et al, 2022a) that is a popular hyperbolic learning method, we conduct experiments on three commonly used datasets: CIFAR10 (Krizhevsky, 2009), CIFAR100 (Krizhevsky, 2009), and ImageNet (Deng et al, 2009). For the CIFAR10 and CIFAR100, we utilize ResNet18 (He et al, 2016), WideResNet28-2 (Zagoruyko and Komodakis, 2016), and PyramidNet110 (Han et al, 2017) as backbones to evaluate the performance of the proposed method. As to ImageNet, we utilize ResNet18 as the backbone. We follow training setups of C-HNNs (Guo et al, 2022a) to conduct experiments. For experiments on CIFAR10 and CIFAR100 datasets, we set the initial learning rate as 0.1, use the cosine learning rate scheduler, and set the batch size as 128. As to the perturbation radius $\hat{\rho}$, we set $\hat{\rho} = 0.005$ for CIFAR100, and set $\hat{\rho} = 0.01$ for CIFAR10. For ImageNet, we set the

initial learning rate as 0.1 and decay it by 10 every 30 epochs. The batch size is 256. We set $\hat{\rho} = 10^{-4}$ for ImageNet.

Learning from long-tailed Data. We conduct classification on the long-tailed data to evaluate the generalization of our method. The long-tailed data refers to the fact that a few classes in the training set contain a major number of samples, while the remaining classes have only a small number of samples (Ma et al, 2024). The number of samples in each category in the test set is consistent. It is challenging to learn using the long-tailed data since the data distribution of the training set is different from that of the test set (Yang et al, 2022).

We conduct experiments on three major long-tailed datasets: CIFAR10-LT, CIFAR100-LT, and ImageNet-LT. Following the setting of (Cao et al, 2019), we construct the CIFAR10-LT and CIFAR100-LT datasets by sampling from the original datasets with different imbalance ratios $IR = \frac{N_{\max}}{N_{\min}}$, where N_{\max} and N_{\min} are the corresponding number of the most and least frequent classes. We set the imbalance ratio as $\{200, 100, 50\}$ for evaluation. We utilize the same way to construct the ImageNet-LT dataset, with the imbalance ratio being 256. We adopt ResNet32 (He et al, 2016) as the backbone for CIFAR10-LT and CIFAR100-LT, and adopt ResNeXt-50 (Xie et al, 2017) as the backbone for ImageNet-LT.

We apply our method to the cross-entropy (CE) method, rebalanced classifier methods: DRW (Cao et al, 2019), LDAM-DRW (Cao et al, 2019), GCL (Li et al, 2022a), and contrastive learning methods: GL-Mixture (Du et al, 2023). To the best of our knowledge, the ability of hyperbolic spaces has not been explored in the long-tailed setting. To develop the proposed method to these five baseline methods, we first project the feature to hyperbolic spaces and utilize the hyperbolic MLR to classify the images. Then, we utilize the SAM method to train HNNs and apply the proposed method to learn curvatures to improve the generalization of HNNs.

As to CIFAR10-LT and CIFAR100-LT datasets, we set the batch size as 64 for five baselines. The other hyper-parameters of different baselines are various, which are shown in Table 2. We utilize the cosine learning rate schedule to decay the learning rate for these five baselines. In terms of the experiment on the ImageNet-LT, we

Table 2 Hyper-parameters for CIFAR10-LT and CIFAR100-LT datasets.

Baseline	CE	DRW	LDAM	GCL	GL-Mixture
Learning rate	0.1/0.1	0.1/0.1	0.1/0.1	0.1/0.1	0.01/0.01
Perturbation radius $\hat{\rho}$	0.1/0.2	0.5/0.8	0.8/0.8	0.5/0.5	0.05/0.05

Table 3 Test Accuracy (%) on the classification task.

	Method	ENNs	HNNs	C-HNNs	Ours+HNNs	Ours+C-HNNs
CIFAR10	ResNet18	95.32 \pm 0.13	93.83 \pm 0.09	95.20 \pm 0.30	96.03 \pm 0.07	96.50 \pm 0.04
	WideResNet28-2	94.81 \pm 0.42	88.82 \pm 0.51	94.76 \pm 0.44	95.96 \pm 0.21	96.11 \pm 0.13
	PyramidNet110	96.19 \pm 0.11	95.89 \pm 0.21	96.03 \pm 0.14	97.26 \pm 0.05	97.48 \pm 0.06
CIFAR100	ResNet18	78.32 \pm 0.32	69.97 \pm 0.20	78.43 \pm 0.15	79.51 \pm 0.03	80.61 \pm 0.02
	WideResNet28-2	75.45 \pm 0.25	72.26 \pm 0.41	75.88 \pm 0.38	76.88 \pm 0.05	78.35 \pm 0.03
	PyramidNet110	82.74 \pm 0.12	80.29 \pm 0.26	82.16 \pm 0.08	84.39 \pm 0.06	85.62 \pm 0.02
ImageNet	ResNet18	69.82	65.74	68.45	68.23	70.53

The best results are shown in bold. The experiments on CIFAR10 and CIFAR100 datasets are repeated for 5 times, and we report both average accuracy and standard deviation.

set the batch size as 256, set the initial learning rate as 0.01, decay it by 10 every 30 epochs, and set the perturbation radius $\hat{\rho}$ as 1e-4.

Learning from noisy data. We conduct classification on noisy data to evaluate the robustness and generalization of our method, where the noisy data refers to some labels in the datasets corrupted from ground-truth labels. We conduct experiments on the Clothing1M dataset (Xiao et al, 2015) that is a large-scale clothing dataset obtained by crawling images from several online shopping websites. The Clothing1M dataset comprises 14 classes and contains over a million noisy labeled samples, along with a small set of approximately 50,000 clean samples used for constructing validation and testing datasets. In our study, we adopt the ELMC method (Taraday and Baskin, 2023) and GENKL (Huang and Chong, 2023) as baselines, and we employ HNNs as the backbone for evaluating the proposed method. Following prior works, we use HNNs with ResNet50 (He et al, 2016) as the backbone and pre-train the backbone on ImageNet. The HNNs are trained for 5 epochs. Hyper-parameters are consistent with the baseline method ELMC and GENKL. In terms of the ELMC baseline, we set the learning rate as 0.1, the batch size as 512, and the $\hat{\rho}$ as 0.8. In terms of the GENKL baseline, we set the learning

rate as 0.001, the batch size as 32, and the $\hat{\rho}$ as 0.02.

Few-shot learning. The few-shot learning problem aims to recognize samples from unseen classes, given very few labeled examples. Studies such as (Khrulkov et al, 2020a; Hong et al, 2023b; Li et al, 2023) have shown that modeling data on hyperbolic spaces leads to better performance. Inspired by it, we project the features onto hyperbolic spaces and build a hyperbolic classifier via hyperbolic distances following the work of (Khrulkov et al, 2020a). Following the setting of MAML (Finn et al, 2017), we learn the hyperbolic classifier for few-shot learning. We conduct experiments on two popular datasets: mini-ImageNet (Vinyals et al, 2016) and tiered-ImageNet (Ren et al, 2018). In terms of the few-shot learning task, as to the mini-Imagenet, we set the learning rate as 0.1, the batch size as 32, and the $\hat{\rho}$ as 0.01; as to the tiered-Imagenet, we set the learning rate as 0.05, the batch size as 32, and the $\hat{\rho}$ as 0.01.

Hierarchical structures of datasets. The utilized datasets (including CIFAR, mini-ImageNet, tiered-ImageNet, ImageNet, Clothing1M) all exhibit inherent hierarchical structures that can be well captured by the hyperbolic spaces. Existing works have shown that the CIFAR,

mini-ImageNet, tiered-ImageNet, and ImageNet datasets have hierarchical structures, and the four datasets are commonly used to evaluate hyperbolic algorithms (Khrulkov et al, 2020b; Fang et al, 2021b; Gao et al, 2023b; Yan et al, 2021b; Guo et al, 2022b; Ermolov et al, 2022). For example, the work (Nickel and Kiela, 2017) suggests that the semantics of images in ImageNet have a hierarchical structure, with details illustrated in a prominent visual analysis conducted by Bostock (2018). CIFAR100 also has a two-level hierarchical structure, with 20 root nodes and 100 leaf nodes, with details described in the work (Krizhevsky et al, 2009). Although Clothing1M dataset has not been utilized to evaluate the performance of hyperbolic algorithms, this dataset also presents the hierarchical structure with four root nodes (including Tops, Bottoms, Footwear, and Accessories) and fourteen leaf nodes.

To further confirm the above points, we compute δ -Hyperbolicity (Khrulkov et al, 2020b; Adcock et al, 2013; Zhang et al, 2021b) to measure whether the used datasets have hierarchical structures. A δ -Hyperbolicity value closer to 0 indicates a stronger hyperbolic structure of a dataset. The values of δ -Hyperbolicity are **0.24**, **0.21**, **0.25**, **0.22**, **0.23**, and **0.24** on the mini-ImageNet, tiered-ImageNet, CIFAR10, CIFAR100, ImageNet, and Clothing1M datasets, respectively. These results reveal that the utilized datasets are appropriate for evaluating the performance of hyperbolic algorithms.

7.2 Main Results

In this subsection, we present the main results, compared methods, and experimental analyses of four settings. Overall, our method surpassed all compared baseline methods and achieves state-of-the-art performance in some settings, demonstrating the effectiveness and superiority of our method.

Classification. We compare our method with methods on hyperbolic spaces: HNNs (Ganea et al, 2018), HWe compare our method with methods on hyperbolic spaces: HNNs (Guo et al, 2022a), and the methods on the Euclidean spaces. Results on CIFAR10, CIFAR100, and ImageNet datasets are shown in Table 3. Our method, when applied to HNNs ('Ours + HNNs'), outperforms the standard HNNs, and when applied to C-HNNs

('Ours + C-HNNs'), it surpasses the standard C-HNNs. 'Ours + C-HNNs' achieves improvements of about 2.67%, 7.29%, 1.59% over HNNs, and about 1.3%, 1.35%, 1.45% over C-HNNs on the ResNet18, WideResNet28-2, PyramidNet110 backbones, respectively. on the CIFAR100 dataset, 'Ours + C-HNNs' achieves about 10.64%, 6.12%, 5.32% improvement over HNNs and about 2.17%, 1.47%, 1.23% improvement over C-HNNs on the ResNet18, WideResNet28-2, PyramidNet110 backbones, respectively; on the ImageNet dataset, our method also surpasses the other methods, where it achieves about 5% improvement over HNNs and about 2% improvement over C-HNNs. These results show that our method improves the performance and generalization of HNNs and C-HNNs. This demonstrates that our method enhances both the performance and generalization of HNNs and C-HNNs.

Learning from long-tailed data. We compare our method with five baselines using Euclidean neural networks, HNNs, and C-HNNs on the CIFAR10-LT and CIFAR100-LT datasets. To the best of our knowledge, these five baselines have not been developed to the hyperbolic spaces. For comparison, we reproduce these five baseline methods on the hyperbolic spaces with HNNs and C-HNNs. Results are shown in Table 4. The performance of our method applied to HNNs ('Ours + HNNs') and C-HNNs ('Ours + C-HNNs') surpasses that of the standard HNNs and C-HNNs, respectively. These results further demonstrate that our method enhances both the performance and generalization of HNNs and C-HNNs when the distributions of training set and test set differ. Notably, our method significantly improves the performance with IR set as 200. This improvement is attributed to the fact that baseline methods converge to the very sharp regions with IR set as 200, while our method can significantly reduce the sharpness of the loss curve and improve generalization. Further evidence is presented in section 7.3.1.

We also compare our method, based on the GL-Mixture method (Du et al, 2023), with other long-tailed methods from three categories: rebalanced classifier methods, contrastive learning methods, and SAM-based methods. Results on CIFAR10-LT, CIFAR100-LT, and ImageNet-LT are shown in Table 5 and Table 6, respectively. Our method achieves superior performance compared to existing methods. Notably, when IR =

Table 4 Top-1 Accuracy (%) on CIFAR10-LT and CIFAR100-LT datasets.

Imbalance Ratio	CIFAR10-LT			CIFAR100-LT		
	200	100	50	200	100	50
CE	65.68	70.70	74.81	34.84	38.43	43.90
CE+HNNs	64.50	68.09	74.3	33.60	37.44	42.66
CE+C-HNNs	65.25	69.96	76.53	34.44	38.34	42.97
CE+HNNs+Ours	65.03	71.07	77.90	35.19	39.02	43.79
CE+C-HNNs+Ours	66.26	72.3	78.99	35.99	39.67	44.66
DRW (Cao et al, 2019)	67.85	75.47	79.67	37.21	40.66	46.41
DRW+HNNs	68.12	73.03	79.17	35.01	38.37	44.65
DRW+C-HNNs	68.12	75.52	81.1	37.16	41.29	46.33
DRW+HNNs+Ours	69.07	78.99	81.83	39.15	43.11	48.56
DRW+C-HNNs+Ours	69.97	80.48	82.64	40.62	44.77	49.5
LDAM (Cao et al, 2019)	73.52	77.03	81.03	38.91	42.04	47.62
LDAM+HNNs	72.29	76.96	80.54	34.27	38.94	46.35
LDAM+C-HNNs	72.81	76.96	81.54	35.1	39.94	46.99
LDAM+HNNs+Ours	76.66	79.92	83.99	41.75	45.78	50.33
LDAM+C-HNNs+Ours	78.89	82.01	85.05	43.03	47.13	51.02
GCL (Li et al, 2022a)	79.03	82.68	85.46	44.88	48.71	53.55
GCL+HNNs	78.76	82.67	84.88	41.76	46.25	50.77
GCL+C-HNNs	80.19	82.71	85.19	43.53	45.27	52.61
GCL+HNNs+Ours	80.16	83.93	86.30	44.84	49.50	53.04
GCL+C-HNNs+Ours	80.82	84.25	86.42	45.65	49.84	53.96
GL-Mixture (Du et al, 2023)	81.86	88.5	91.04	44.79	57.97	63.78
GL-Mixture+HNNs	82.72	85.97	89.26	49.31	56.52	60.81
GL-Mixture+C-HNNs	70.71	86.01	89.2	33.43	49.93	58.53
GL-Mixture+HNNs+Ours	85.07	88.96	91.72	52.33	59.43	64.11
GL-Mixture+C-HNNs+Ours	81.86	87.64	90.75	45.18	57.80	62.8

The best results of each baseline and its variations are shown in bold.

200, our method exceeds the current best method by 2.3% on CIFAR10-LT and 6.4% on CIFAR100-LT. On ImageNet-LT, our method also achieves state-of-the-art performance, demonstrating the superiority of our method.

Learning from noisy data. We compare our method with the baseline methods on the Euclidean spaces: ELMC (Taraday and Baskin, 2023) and GENKL (Huang and Chong, 2023). Additionally, we compare our method with baseline methods on hyperbolic spaces: ELMC+HNNs and GENKL+HNNs. To the best of our knowledge, EMLC and GENKL have not been developed to the hyperbolic spaces; thus, we reproduce the EMLC and GENKL methods using the HNNs backbone. Moreover, we compared our method with the state-of-the-art methods that use extra

clean data and those that do not. Results are shown in Table 7. Compared to HNNs and C-HNNs, our method achieves superior performance, underscoring its effectiveness in handling noisy data scenarios.

Few-shot learning.

Table 8 presents the accuracy on the mini-Imagenet and tiered-Imagenet for few-shot learning. Our method consistently achieves the best performance compared to both HNNs and C-HNNs, highlighting its ability to improve the generalization of hyperbolic neural networks in few-shot learning tasks.

Table 5 Top-1 Accuracy (%) on CIFAR10-LT and CIFAR100-LT datasets compared with the state-of-the-art methods.

Method	CIFAR10-LT			CIFAR100-LT		
	200	100	50	200	100	50
Rebalanced Classifier	CB-Focal (Cui et al, 2019)	68.89	74.60	79.30	36.23	39.60
	LDAM (Cao et al, 2019)	73.52	77.03	81.03	38.91	42.04
	MiSLAS (Zhong et al, 2021)	77.31	82.06	85.16	42.33	47.50
	BGP (Wang et al, 2022)	-	-	-	41.2	45.2
	GCL (Li et al, 2022a)	79.03	82.68	85.46	44.88	48.71
	CDB-S (Sinha et al, 2022)	-	-	-	37.99	42.59
	AREA (Chen et al, 2023)	74.99	78.88	82.68	43.85	48.83
Contrastive learning	FUR (Ma et al, 2024)	79.80	83.70	86.20	46.20	50.90
	TSC (Li et al, 2022b)	-	79.70	82.90	-	42.80
	KCL (Kang et al, 2020)	-	77.60	81.70	-	42.80
	Paco (Cui et al, 2021)	-	-	-	-	52.0
	SSD (Li et al, 2021)	-	-	-	-	46.0
	GL-Mixture (Du et al, 2023)	81.86	88.5	91.04	44.79	57.97
	SBCL (Hou et al, 2023)	-	-	-	-	44.9
SAM-based	VS-SAM (Rangwani et al, 2022)	-	82.4	-	-	46.6
	CC-SAM (Zhou et al, 2023)	80.94	83.92	86.22	45.66	50.83
Ours		85.07	88.96	91.72	52.33	59.43
						64.11

The best results are shown in bold.

Table 6 Top-1 Accuracy (%) on ImageNet-LT dataset.

Method	Backbone	All	Many	Med	Few
LADE (Hong et al, 2021)	ResNetXt-50	52.3	64.4	47.7	34.3
DisAlign (Zhang et al, 2021a)	ResNetXt-50	53.4	62.7	52.1	31.4
PaCo (Li et al, 2021)	ResNeXt-50	56	64.4	55.7	33.7
SSD (Li et al, 2021)	ResNeXt-50	56	66.8	53.1	35.4
ResLT (Cui et al, 2022)	ResNeXt-50	52.9	63.0	53.3	35.5
GL-Mixture (Du et al, 2023)	ResNeXt-50	56.3	70.1	52.4	30.4
CC-SAM (Zhou et al, 2023)	ResNeXt-50	55.4	63.1	53.4	41.1
Ours	ResNeXt-50	56.8	66.9	55.5	34.3

The best results are shown in bold.

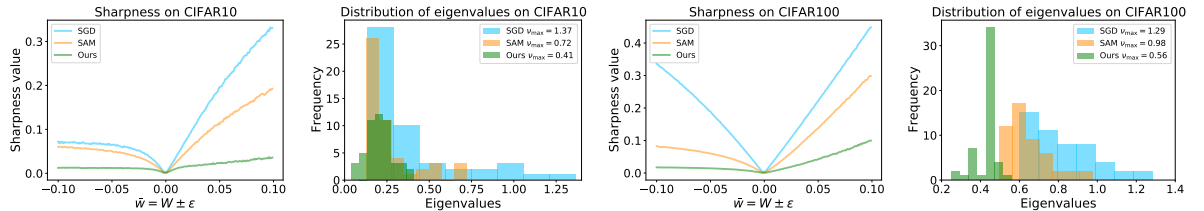


Fig. 2 Sharpness and Eigenvalues on the ResNet18 Backbone

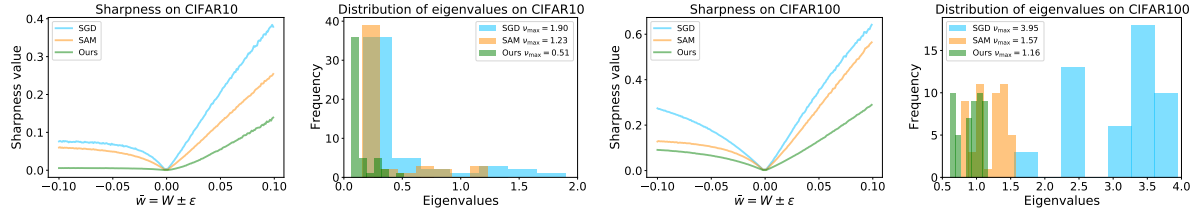


Fig. 3 Sharpness and Eigenvalues on the WideResNet28-2 Backbone

Table 7 Comparison with state-of-the-art methods in test accuracy (%) on Clothing1M.

Method	Extra Data	Acc
Cross-entropy	✗	69.21
Joint-Optim (Tanaka et al, 2018)	✗	72.16
P-correction (Kun and Jianxin, 2019)	✗	73.49
C2D (Zheltonozhskii et al, 2022)	✗	74.30
DivideMix (Li et al, 2020)	✗	74.76
ELR+ (Liu et al, 2020)	✗	74.81
AugDesc (Nishi et al, 2021)	✗	75.11
SANM (Tu et al, 2023)	✗	75.63
Meta Cleaner (Zhang et al, 2019)	✓	72.50
Meta-Learning (Li et al, 2019)	✓	73.47
MW-Net (Shu et al, 2019)	✓	73.72
FaMUS (Xu et al, 2021)	✓	74.4
MLC (Zheng et al, 2021)	✓	75.78
MSLG (Alganc and Ulusoy, 2021)	✓	76.02
Self Learning (Han et al, 2019)	✓	76.44
FasTEN (Kye et al, 2022)	✓	77.83
EMLC (Taraday and Baskin, 2023)	✓	79.35
GENKL (Huang and Chong, 2023)	✓	81.34
EMLC+HNNs	✓	79.40
EMLC+C-HNNs	✓	79.70
EMLC+HNNs+Ours	✓	80.07
EMLC+C-HNNs+Ours	✓	80.38
GENKL+HNNs	✓	81.48
GENKL+C-HNNs	✓	81.56
GENKL+HNNs+Ours	✓	82.04
GENKL+C-HNNs+Ours	✓	82.27

The results of our method are shown in bold. The proposed method not only outperforms the baseline methods, but also achieves the best performance.

7.3 Visualization

In order to further analyze the effectiveness of our method, we conduct smoothness analysis and convergence analysis on the afore-mentioned settings.

7.3.1 Smoothness Analysis

Analysis on classification task. We compare the sharpness of our method to that of the SAM and SGD methods with the fixed curvature $c = 0.01$. To compute the sharpness term $\mathcal{L}_S^{\text{sharp}} = \max \mathcal{L}_S(\mathbf{w} + \epsilon, c) - \mathcal{L}_S(\mathbf{w}, c)$, we approximate $\epsilon_{\|\epsilon\| \leq \rho}$ as $\rho \nabla \mathcal{L}_S(\mathbf{w}, c) / \|\mathcal{L}_S(\mathbf{w}, c)\|$. We set the increasing radii ρ to compute ϵ , and compute perturbed weight as $\bar{\mathbf{w}} = \mathbf{w} \pm \epsilon$. We also visualize the Hessian spectra of HNNs trained with SGD, SAM, and our method for sharpness comparison, where lower Hessian spectra indicate lower sharpness. We use power iteration (Yao et al, 2018) to compute the top eigenvalues of the Hessian and present the histogram of the top-50 eigenvalues for each method. Our experiments are conducted on the CIFAR10 and CIFAR100 datasets using ResNet18 and WideResNet28-2 backbones.

Results on the ResNet18 backbone are shown in Fig. 2. Sharpness values illustrated in Fig. 2 reveal that the proposed method achieves the lowest sharpness value compared to the SGD and SAM methods. Notably, on the CIFAR100 dataset with $\rho = 0.1$, the sharpness of the proposed method is 0.09, significantly lower than 0.29 of the SAM method and 0.45 of C-HNNs. Distributions on eigenvalues presented in Fig. 2 reveal that HNNs trained with the proposed method exhibit the lowest Hessian spectra compared to those trained with SAM and SGD with fixed curvatures. Results on the ResNet18 backbone demonstrate that our method effectively learns

Table 8 Accuracy (%) on the mini-ImageNet and tiered-ImageNet datasets.

Method	Backbone	mini-ImageNet			tiered-ImageNet		
		1-shot	5-way	5-shot	5-way	1-shot	5-way
MAML (Finn et al, 2017)	ResNet12	51.03 \pm 0.50	68.26 \pm 0.47	58.58 \pm 0.49	71.24 \pm 0.43		
L2F (Baik et al, 2020b)	ResNet12	57.48 \pm 0.49	74.68 \pm 0.43	63.94 \pm 0.48	77.61 \pm 0.41		
ALFA (Baik et al, 2020a)	ResNet12	60.06 \pm 0.49	77.42 \pm 0.42	64.43 \pm 0.49	81.77 \pm 0.39		
MetaFun (Xu et al, 2020)	ResNet12	62.12 \pm 0.30	78.20 \pm 0.16	67.72 \pm 0.14	78.20 \pm 0.16		
DSN (Simon et al, 2020)	ResNet12	62.64 \pm 0.66	78.83 \pm 0.45	66.22 \pm 0.75	82.79 \pm 0.48		
Chen <i>et al.</i> (Chen et al, 2021)	ResNet12	63.17 \pm 0.23	79.26 \pm 0.17	68.62 \pm 0.27	83.74 \pm 0.18		
MeTAL (Baik et al, 2021)	ResNet12	59.64 \pm 0.38	76.20 \pm 0.19	63.89 \pm 0.43	80.14 \pm 0.40		
C-HNNs (Guo et al, 2022a)	ResNet12	53.01 \pm 0.22	72.66 \pm 0.15	-	-		
CurAML (Gao et al, 2023a)	ResNet12	63.13 \pm 0.41	81.04 \pm 0.39	68.46 \pm 0.56	83.84 \pm 0.40		
Hyper ProtoNet (Khrulkov et al, 2020a)	ResNet18	59.47 \pm 0.20	76.84 \pm 0.14	62.28 \pm 0.23	74.50 \pm 0.21		
Hyperbolic kernel (Fang et al, 2021a)	ResNet18	61.04 \pm 0.21	77.33 \pm 0.15	61.04 \pm 0.21	77.33 \pm 0.15		
Poincaré radial kernel (Fang et al, 2023)	ResNet18	62.15 \pm 0.20	77.81 \pm 0.15	65.33 \pm 0.21	77.48 \pm 0.20		
Ours+HNNs	ResNet12	64.06 \pm 0.22	81.50 \pm 0.17	70.40 \pm 0.23	84.60 \pm 0.21		
Ours+C-HNNs	ResNet12	65.30 \pm 0.19	82.20 \pm 0.15	72.10 \pm 0.25	86.25 \pm 0.16		

The best results are shown in bold. The experiments are repeated for 5 times, and we report both average accuracy and standard deviation

optimal curvatures, thereby reducing the sharpness and smoothing the loss landscape of the local minima of HNNs.

Similar results are observed on the WideResNet backbone, as shown in Fig. 3. The proposed method consistently achieves the lowest sharpness value compared to the SGD and SAM methods on the CIFAR10 and CIFAR100 datasets. Distributions of eigenvalues show that HNNs trained with the proposed method lead to the lowest Hessian spectra compared to SAM and SGD methods with fixed curvatures. This confirms that our method can effectively smooth the loss landscape of the local minima of HNNs by learning appropriate curvatures, regardless of the backbone used.

Analysis on long-tailed data. We visualize the Hessian spectra of models trained with GL-mixture and the proposed method for sharpness comparison. We use power iteration to compute the top eigenvalues of Hessian and report the histogram of the distribution of top 30 Hessian eigenvalues for each method. We compare models trained with GL-mixture and the proposed method on the CIFAR100-LT with Imbalance Ratio (IR) = 100 and IR = 200. As shown in Fig. 4, models trained with our method lead to the lowest Hessian spectra on both IR = 100 and IR = 200. This again demonstrates that our method

can smooth the loss landscape and further improve the generalization.

For the GL-mixture method, we observe that with IR= 200, the maximum eigenvalues is 8.09×10^2 , while the maximum eigenvalues is 6.94×10^2 with IR = 100. This demonstrates that the local minima obtained by the GL-mixture method converges to sharper regions when IR is set to 200 compared to IR= 100.

Moreover, we observe that the proposed method reduces more sharpness of the loss landscape with IR = 200, compared with IR = 100. To prove this point, we analyze the differences in eigenvalues between GL-mixture and our method. Specifically, we subtract the eigenvalues of the proposed method from the corresponding ranks of the baseline method. We visualize the distributions of differences in eigenvalues, and we plot a line graph of these differences, where the X-axis represents the order of eigenvalues, with '0' denoting the maximum eigenvalue. As shown in Fig. 5, the differences in eigenvalues for IR = 200 are significantly larger than for IR = 00. These results demonstrate that our method can introduce greater improvements with IR= 200 compared to IR= 100, which analyzes the phenomenon in Table 4.

Analysis on noisy data. We conduct visualization analysis on two baselines, ELMC and GenKL

Table 9 Curvature analysis on the tiered-ImageNet dataset.

Curvature	0	1.0×10^{-4}	1.0×10^{-3}	1.0×10^{-2}	1.0×10^{-1}	5.0×10^{-1}	1.0	Ours (Converged Curvature)
1-shot 5-way	56.33	50.97	44.70	38.31	70.25	69.94	69.10	72.10 (1.13×10^{-1})
5-shot 5-way	74.79	74.40	72.40	64.30	85.15	84.75	83.75	86.25 (1.27×10^{-1})

The best results are shown in bold. The contents in ‘()’ represent the learned curvatures.

Table 10 Curvature analysis on the CIFAR10-LT and CIFAR100-LT datasets.

Curvature	0	1.0×10^{-4}	5.0×10^{-4}	1.0×10^{-3}	5.0×10^{-3}	Ours (Converged Curvature)
CIFAR10-LT	82.77	81.77	83.52	80.97	77.49	85.07 (5.36×10^{-4})
CIFAR100-LT	45.92	49.38	48.6	46.48	43.73	52.33 (3.55×10^{-4})

The best results are shown in bold. We adopt the GL-mixture as the baseline. The contents in ‘()’ represent the learned curvatures.

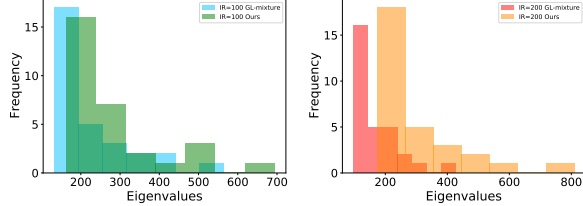


Fig. 4 Distribution of eigenvalues on the CIFAR100-LT dataset

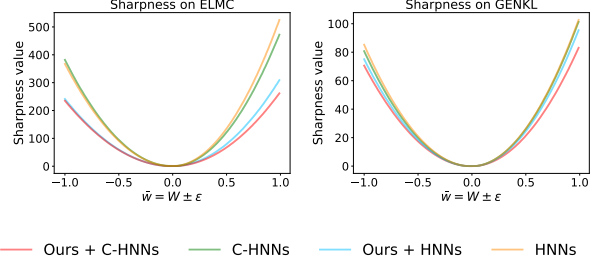


Fig. 6 Sharpness on the learning on noisy data task

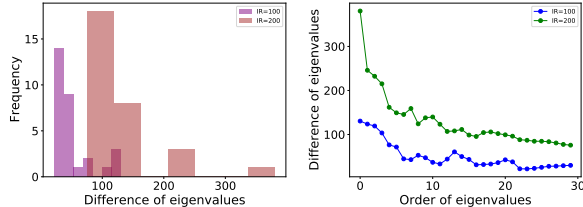


Fig. 5 Analysis of differences in eigenvalues

with HNNs and C-HNNs backbones, which are trained with a fixed curvature 0.1. Sharpness values on the ELMC baseline and GenKL baseline illustrated in Fig. 6 reveal that the proposed method achieves the lowest sharpness value compared to the HNNs and C-HNNs methods. Visualization results demonstrate that our method effectively learns optimal curvatures, thereby reducing the sharpness and smoothing the loss landscape of the local minima of HNNs, improving the generalization performance.

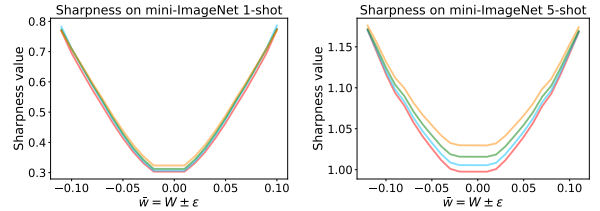


Fig. 7 Sharpness on the few-shot learning task

Analysis on few-shot learning task. We conduct visualization analysis on the mini-imagenet dataset with 1-shot 5-way and 5-shot 5-way two settings. We compare our method with HNNs and C-HNNs two methods, which are trained with a fixed curvature 1. As illustrated in Fig. 7, our method again achieves the lowest sharpness across both settings. These visualization results further

validate that our method effectively learns optimal curvatures, reducing sharpness and smoothing the loss landscape.

Analysis of bi-level framework. We measure the sharpness of models during training to analyze the effect of bi-level optimization framework. We train the curvature and estimate the sharpness $\mathcal{L}_S^{\text{sharp}} = \max_{\epsilon} \mathcal{L}_S(\mathbf{w} + \epsilon, c) - \mathcal{L}_S(\mathbf{w}, c)$, where experiments are conducted by using the ResNet18 as the backbone on CIFAR datasets. We report the evolution of $\max_{\epsilon} \mathcal{L}_S(\mathbf{w} + \epsilon, c) - \mathcal{L}_S(\mathbf{w}, c)$ during training, where $\mathcal{L}_S(\cdot)$ stands for the training loss computed on the current batch. As shown in Fig. 8, as the curvature is trained, the sharpness of HNNs $\max_{\epsilon} \mathcal{L}_S(\mathbf{w} + \epsilon, c) - \mathcal{L}_S(\mathbf{w}, c)$ decreases, indicating that the generalization of HNNs improves.

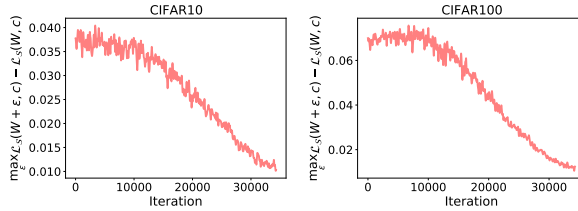


Fig. 8 Evolution of $\max_{\epsilon} \mathcal{L}_S(\mathbf{w} + \epsilon, c) - \mathcal{L}_S(\mathbf{w}, c)$ in curvature training step.

7.3.2 Convergence Analysis

We visualize the loss plots on the test dataset during the training stage. Experiments are conducted on the CIFAR10 and CIFAR100 datasets using ResNet18 and WideResNet28-2 backbones, where results are shown in Fig. 9 and Fig. 10, respectively. Results show that the proposed method outperforms other methods on hyperbolic spaces. From the experimental results, we observe that the proposed method achieves faster convergence speed and obtains the best optima on the unseen data. This further demonstrates that our method can improve the generalization of HNNs.

7.4 Curvature Analysis for the Generalization of HNNs

We set different curvatures to train the HNNs to demonstrate the effects of curvatures for the generalization of HNNs. For the few-shot learning

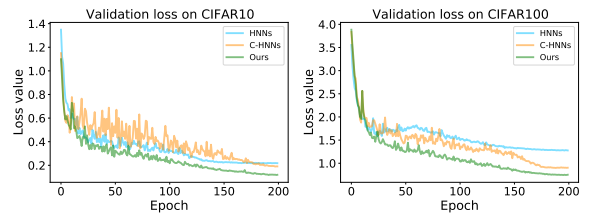


Fig. 9 Loss plots for classification task on the ResNet18 Backbone

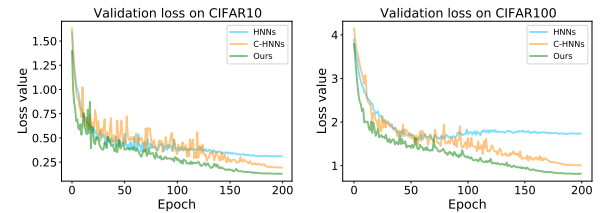


Fig. 10 Loss plots for classification task on the WideResNet28-2 Backbone

task on the tiered-imagenet dataset, we set the curvatures as $\{0, 0.0001, 0.001, 0.01, 0.1, 0.5, 1\}$, where 0 denotes Euclidean spaces. Results are shown in Table 9. For the task of learning from long-tailed data, we set the curvatures as $\{0, 0.0001, 0.0005, 0.001, 0.005\}$ and set the imbalance ratio as 200. The converged curvatures of the few-shot learning task on tiered-imagenet dataset on 1-shot 5-way and 5-shot 5-way settings are 1.13×10^{-1} and 1.27×10^{-1} , respectively. As to the long-tail classification task, the converged curvatures on the CIFAR10-LT and CIFAR100-LT datasets are 5.36×10^{-4} and 3.55×10^{-4} , respectively. Results are shown in Table 10. The experimental results indicate that different curvatures lead to varying generalization performances, highlighting the importance of significance for the generalization of HNNs. Besides, the results demonstrate that the proposed method achieves the best generalization performance, demonstrating its capability to learn optimal curvatures to improve the generalization of HNNs.

Table 11 Test Accuracy (%) on the CIFAR100-LT dataset.

perturbation radius $\hat{\rho}$	0.01	0.02	0.03	0.04	0.05	0.06	0.07	0.08	0.09	0.1
IR = 50	61.62	63.18	62.83	63.53	64.11	62.28	63.55	62.84	61.59	62.07
IR = 100	53.34	57.25	57.00	54.25	59.43	56.76	58.02	57.50	56.84	56.18
IR = 200	52.33	51.30	51.87	51.13	49.49	50.12	49.29	45.94	48.40	46.00

The best results are shown in bold. We adopt the GL-mixture as the baseline.

Table 12 Test Accuracy (%) on the CIFAR100 dataset.

Iterations of inner level T	2	5	10
Resnet18	80.61	80.32	80.38
WideResNet28-2	78.35	77.96	78.16

The best results are shown in bold.

7.5 Analyses of Hyper-Parameters

In this subsection, we analyze the effect of some important hyper-parameters, *i.e.*, the perturbation radius $\hat{\rho}$ and the inner-level iteration T .

7.5.1 Analysis of the Perturbation Radius $\hat{\rho}$

We utilize the perturbation radius $\hat{\rho}$ to update the parameters of HNNs in Eq. (131). We adopt the task of learning from long-tailed data as an example, using the GL-mixture as the baseline. We set $\hat{\rho}$ as $\{0.01, 0.02, 0.03, 0.04, 0.05, 0.06, 0.07, 0.08, 0.09, 0.1\}$. Results are shown in Table 11.

Experimental results show that the overall algorithm is somewhat sensitive to $\hat{\rho}$, which is consistent with the observation in existing works, *i.e.*, the SAM method is also sensitive to the perturbation radius $\hat{\rho}$ (Foret et al, 2020; Wang et al, 2024a; Kwon et al, 2021). The key reason for this sensitivity is the scale-dependency of sharpness, *i.e.*, scaling the model parameters alters the sharpness without affecting the optimal value (Kwon et al, 2021). As a result, small changes in parameter scale may significantly influence optimization, leading to large performance variations when the radius is varied.

In the future, we plan to develop a scale-invariant SAM algorithm by introducing normalization strategies and regularization terms that ensure consistent sharpness behavior under parameter rescaling, improving robustness to the

choice of $\hat{\rho}$. Furthermore, we will explore learning-to-learn strategies to automatically learn the optimal perturbation radius during training, reducing manual hyperparameter tuning and improving the practicality.

We also observe that compared to IR=50 and IR=100, the performances in the setting IR=200 is more sensitive to the perturbation radius $\hat{\rho}$. This is because that the obtained local minima usually converge to the sharper regions with IR set as 200, compared with IR = 100, as discussed in section 7.3.1

7.5.2 Analysis of the Inner-Level Iteration T

In our experimental settings, we set T as 2, meaning that we first update the parameters of HNNs and then update the curvature. Notably, more inner-level iterations do not correspond to more updates of HNNs or more epochs. The iterations for optimizing HNNs remain the same for different values of T , but the iterations for optimizing curvature vary. For example, with $T = 5$, the iterations for optimizing curvature are one-fifth of those with $T = 1$. To analyze the effect of T , we set T as 5 and 10 for the classification task and CIFAR100 dataset. Results are shown in Table 12. We can find that our method is insensitive to the inner-level iterations T . Some works (Wu et al, 2018) argue that more inner-level iterations contribute to better performance theoretically. Our experimental results are contrary to this conclusion. We consider there might be two possible reasons. (1) The implicit differentiation method used to compute the gradients of curvatures is independent of the inner-level iterations. (2) More inner-level optimization iterations result in fewer optimization iterations for curvatures.

Table 13 Training time (seconds) on the classification task.

	BackBone	ResNet18	WideResNet28-2	PyramidNet110
CIFAR10	C-HNNs	1675.732	2509.873	26260.523
	Ours	2032.880	2880.888	29886.101
CIFAR100	C-HNNs	1699.631	2534.344	26338.488
	Ours	2058.302	2908.640	29986.054

Table 14 Training memory (MB) on the classification task.

	BackBone	WideResNet28-2	ResNet18	PyramidNet110
CIFAR10	C-HNNs	1192	1456	13426
	Ours	1411	1816	15592
CIFAR100	C-HNNs	1344	1458	13560
	Ours	1606	1818	15890

7.6 Time and Memory Consumption

We conduct experiments to evaluate the time and memory consumption on the CIFAR datasets using three backbones, *i.e.* WideResNet28-2, ResNet18, and PyramidNet110. C-HNNs are used as the baseline, and we measure the time consumption over 200 epochs. Training time and memory consumption are shown in Table 13 and Table 14, respectively. Results indicate that the proposed method increases 10% – 20% time consumption and memory consumption on the three backbones. Given that our method yields obvious performance improvement over C-HNNs, the additional time and memory costs are acceptable.

8 Conclusion

In this paper, we have presented that curvatures of hyperbolic spaces significantly affect the generalization of HNNs, as evidenced by the derived PAC-Bayesian generalization bound of HNNs. The proposed sharpness-aware curvature learning method can learn optimal curvatures to improve the generalization of HNNs. The introduced implicit differentiation algorithm can efficiently approximate gradients of curvatures. We have presented theoretical analyses, demonstrating that the approximate error in our method is bounded and our algorithm can converge. Experiments on four settings: classification, learning from long-tailed data, learning from noisy data,

and few-shot learning show that our method can learn curvatures to improve the generalization of HNNs.

In this work, we study generalization on a single hyperbolic space with a single curvature. Actually, real-world data with complex hierarchical structures should be represented on product manifolds with multiple curvatures. In the future, we will study generalization for product manifolds.

Acknowledgements. This work was supported by the Natural Science Foundation of China (NSFC) under Grant No.62406009, the Shenzhen Science and Technology Program under Grant No. JCYJ20241202130548062, the Natural Science Foundation of Shenzhen under Grant No. JCYJ20230807142703006, the NSFC under Grant No. 62172041, and the Key Research Platforms and Projects of the Guangdong Provincial Department of Education under Grant No.2023ZDZX1034.

Data Availability. All datasets used in this study are open-access and have been cited in the paper.

References

Abbas M, Xiao Q, Chen L, et al (2022) Sharp-maml: Sharpness-aware model-agnostic meta learning. In: International conference on machine learning, PMLR, pp 10–32

Adcock AB, Sullivan BD, Mahoney MW (2013) Tree-like structure in large social and information networks. In: 2013 IEEE 13th International Conference on Data Mining, pp 1–10, <https://doi.org/10.1109/ICDM.2013.77>

Algan G, Ulusoy I (2021) Meta soft label generation for noisy labels. In: 2020 25th International Conference on Pattern Recognition, IEEE, pp 7142–7148

Atigh MG, Schoep J, Acar E, et al (2022) Hyperbolic image segmentation. In: Proceedings of the IEEE/CVF Conference on Computer Vision and Pattern Recognition, pp 4453–4462

Baik S, Choi M, Choi J, et al (2020a) Meta-learning with adaptive hyperparameters. Advances in Neural Information Processing Systems 33:20755–20765

Baik S, Hong S, Lee KM (2020b) Learning to forget for meta-learning. In: Proceedings of the IEEE/CVF Conference on Computer Vision and Pattern Recognition, pp 2379–2387

Baik S, Choi J, Kim H, et al (2021) Meta-learning with task-adaptive loss function for few-shot learning. In: Proceedings of the IEEE/CVF International Conference on Computer Vision, pp 9465–9474

Baydin AG, Pearlmutter BA, Radul AA, et al (2018) Automatic differentiation in machine learning: a survey. Journal of machine learning research 18

Bdeir A, Landwehr N (2024) Optimizing curvature learning for robust hyperbolic deep learning in computer vision. arXiv preprint arXiv:240513979

Bostock M (2018) Imagenet hierarchy. URL <https://observablehq.com/@mbostock/imagenet-hierarchy>

Cannon JW, Floyd WJ, Kenyon R, et al (1997) Hyperbolic geometry. Flavors of geometry 31(59-115):2

Cao K, Wei C, Gaidon A, et al (2019) Learning imbalanced datasets with label-distribution-aware margin loss. Advances in Neural Information Processing Systems 32

Chami I, Ying Z, Ré C, et al (2019) Hyperbolic graph convolutional neural networks. Advances in Neural Information Processing Systems 32

Chen X, Zhou Y, Wu D, et al (2023) Area: adaptive reweighting via effective area for long-tailed classification. In: Proceedings of the IEEE/CVF International Conference on Computer Vision, pp 19277–19287

Chen Y, Liu Z, Xu H, et al (2021) Meta-baseline: exploring simple meta-learning for few-shot learning. In: Proceedings of the IEEE/CVF International Conference on Computer Vision, pp 9062–9071

Cho S, Lee J, Kim D (2024) Hyperbolic vae via latent gaussian distributions. Advances in Neural Information Processing Systems 36

Cui J, Zhong Z, Liu S, et al (2021) Parametric contrastive learning. In: Proceedings of the IEEE/CVF International Conference on Computer Vision, pp 715–724

Cui J, Liu S, Tian Z, et al (2022) Reslt: Residual learning for long-tailed recognition. IEEE Transactions on Pattern Analysis and Machine Intelligence 45(3):3695–3706. <https://doi.org/10.1109/TPAMI.2022.3174892>

Cui Y, Jia M, Lin TY, et al (2019) Class-balanced loss based on effective number of samples. In: Proceedings of the IEEE/CVF Conference on Computer Vision and Pattern Recognition, pp 9268–9277

Dai J, Wu Y, Gao Z, et al (2021) A hyperbolic-to-hyperbolic graph convolutional network. In: Proceedings of the IEEE/CVF Conference on Computer Vision and Pattern Recognition, pp 154–163

Deng J, Dong W, Socher R, et al (2009) Imagenet: A large-scale hierarchical image database. In: Proceedings of the IEEE/CVF Conference on Computer Vision and Pattern Recognition, Ieee,

pp 248–255

Dinh L, Pascanu R, Bengio S, et al (2017) Sharp minima can generalize for deep nets. In: International Conference on Machine Learning, PMLR, pp 1019–1028

Du F, Yang P, Jia Q, et al (2023) Global and local mixture consistency cumulative learning for long-tailed visual recognitions. In: Proceedings of the IEEE/CVF Conference on Computer Vision and Pattern Recognition, pp 15814–15823

Ermolov A, Mirvakhabova L, Khrulkov V, et al (2022) Hyperbolic vision transformers: Combining improvements in metric learning. In: Proceedings of the IEEE/CVF Conference on Computer Vision and Pattern Recognition (CVPR), pp 7409–7419

Fang P, Harandi M, Petersson L (2021a) Kernel methods in hyperbolic spaces. In: Proceedings of the IEEE/CVF International Conference on Computer Vision, pp 10665–10674

Fang P, Harandi M, Petersson L (2021b) Kernel methods in hyperbolic spaces. In: Proceedings of the IEEE/CVF International Conference on Computer Vision (ICCV), pp 10665–10674

Fang P, Harandi M, Lan Z, et al (2023) Poincaré kernels for hyperbolic representations. International Journal of Computer Vision 131(11):2770–2792. <https://doi.org/10.1007/s11263-023-01834-6>

Finn C, Abbeel P, Levine S (2017) Model-agnostic meta-learning for fast adaptation of deep networks. In: International conference on machine learning, PMLR, pp 1126–1135

Foret P, Kleiner A, Mobahi H, et al (2020) Sharpness-aware minimization for efficiently improving generalization. In: International Conference on Learning Representations

Franceschi L, Frasconi P, Salzo S, et al (2018) Bilevel programming for hyperparameter optimization and meta-learning. In: International Conference on Machine Learning, PMLR, pp 1568–1577

Franco L, Mandica P, Munjal B, et al (2023) Hyperbolic self-paced learning for self-supervised skeleton-based action representations. In: International Conference on Learning Representations

Franco L, Mandica P, Kallidromitis K, et al (2024) Hyperbolic active learning for semantic segmentation under domain shift. In: International Conference on Machine Learning, PMLR

Fu X, Li J, Wu J, et al (2021) Ace-hggn: Adaptive curvature exploration hyperbolic graph neural network. In: 2021 IEEE international conference on data mining (ICDM), IEEE, pp 111–120

Fu X, Wei Y, Sun Q, et al (2023) Hyperbolic geometric graph representation learning for hierarchy-imbalance node classification. In: Proceedings of the ACM Web Conference 2023, pp 460–468

Ganea O, Bécigneul G, Hofmann T (2018) Hyperbolic neural networks. Advances in Neural Information Processing Systems 31

Gao Z, Wu Y, Jia Y, et al (2021) Curvature generation in curved spaces for few-shot learning. In: Proceedings of the IEEE/CVF International Conference on Computer Vision, pp 8691–8700

Gao Z, Wu Y, Harandi M, et al (2023a) Curvature-adaptive meta-learning for fast adaptation to manifold data. IEEE Transactions on Pattern Analysis and Machine Intelligence 45(2):1545–1562. <https://doi.org/10.1109/TPAMI.2022.3164894>

Gao Z, Wu Y, Harandi M, et al (2023b) Curvature-adaptive meta-learning for fast adaptation to manifold data. IEEE Transactions on Pattern Analysis and Machine Intelligence 45(2):1545–1562. <https://doi.org/10.1109/TPAMI.2022.3164894>

Gao Z, Xu C, Li F, et al (2023c) Exploring data geometry for continual learning. In: Proceedings of the IEEE/CVF Conference on Computer Vision and Pattern Recognition, pp 24325–24334

Ge S, Mishra S, Kornblith S, et al (2023) Hyperbolic contrastive learning for visual representations beyond objects. In: Proceedings of the IEEE/CVF Conference on Computer Vision and Pattern Recognition, pp 6840–6849

Gouk H, Frank E, Pfahringer B, et al (2021) Regularisation of neural networks by enforcing lipschitz continuity. *Machine Learning* 110(2):393–416

Griewank A (1993) Some bounds on the complexity of gradients, jacobians, and hessians. In: Complexity in numerical optimization. World Scientific, p 128–162

Griewank A, Walther A (2008) Evaluating derivatives: principles and techniques of algorithmic differentiation. SIAM

Gulcehre C, Denil M, Malinowski M, et al (2019) Hyperbolic attention networks. In: International Conference on Learning Representations

Guo Y, Wang X, Chen Y, et al (2022a) Clipped hyperbolic classifiers are super-hyperbolic classifiers. In: Proceedings of the IEEE/CVF Conference on Computer Vision and Pattern Recognition, pp 11–20

Guo Y, Wang X, Chen Y, et al (2022b) Clipped hyperbolic classifiers are super-hyperbolic classifiers. In: Proceedings of the IEEE/CVF Conference on Computer Vision and Pattern Recognition (CVPR), pp 11–20

Han D, Kim J, Kim J (2017) Deep pyramidal residual networks. In: Proceedings of the IEEE/CVF Conference on Computer Vision and Pattern Recognition, pp 5927–5935

Han J, Luo P, Wang X (2019) Deep self-learning from noisy labels. In: Proceedings of the IEEE/CVF International Conference on Computer Vision, pp 5138–5147

He K, Zhang X, Ren S, et al (2016) Deep residual learning for image recognition. In: Proceedings of the IEEE/CVF Conference on Computer Vision and Pattern Recognition, pp 770–778

Hochreiter S, Schmidhuber J (1994) Simplifying neural nets by discovering flat minima. Advances in Neural Information Processing Systems 7

Hong J, Fang P, Li W, et al (2023a) Curved geometric networks for visual anomaly recognition. *IEEE Transactions on Neural Networks and Learning Systems*

Hong J, Hayder Z, Han J, et al (2023b) Hyperbolic audio-visual zero-shot learning. In: Proceedings of the IEEE/CVF International Conference on Computer Vision, pp 7873–7883

Hong Y, Han S, Choi K, et al (2021) Disentangling label distribution for long-tailed visual recognition. In: Proceedings of the IEEE/CVF Conference on Computer Vision and Pattern Recognition, pp 6626–6636

Hou C, Zhang J, Wang H, et al (2023) Subclass-balancing contrastive learning for long-tailed recognition. In: Proceedings of the IEEE/CVF International Conference on Computer Vision, pp 5395–5407

Hu C, Zhang KY, Yao T, et al (2024a) Rethinking generalizable face anti-spoofing via hierarchical prototype-guided distribution refinement in hyperbolic space. In: Proceedings of the IEEE/CVF Conference on Computer Vision and Pattern Recognition, pp 1032–1041

Hu EJ, Shen Y, Wallis P, et al (2024b) Lora: Low-rank adaptation of large language models. In: The Twelfth International Conference on Learning Representations

Huang X, Chong KFE (2023) Genkl: An iterative framework for resolving label ambiguity and label non-conformity in web images via a new generalized kl divergence. *International Journal of Computer Vision* 131(11):3035–3059. <https://doi.org/10.1007/s11263-023-01815-9>

Jang C, Lee S, Park F, et al (2022) A reparametrization-invariant sharpness measure based on information geometry. *Advances in Neural Information Processing Systems* 35:27893–27905

Ji K, Yang J, Liang Y (2022) Theoretical convergence of multi-step model-agnostic meta-learning. *The Journal of Machine Learning Research* 23(1):1317–1357

Jiang W, Yang H, Zhang Y, et al (2023) An adaptive policy to employ sharpness-aware minimization. In: International Conference on Learning Representations

Kang B, Li Y, Xie S, et al (2020) Exploring balanced feature spaces for representation learning. In: International Conference on Learning Representations

Khrulkov V, Mirvakhoba L, Ustinova E, et al (2020a) Hyperbolic image embeddings. In: Proceedings of the IEEE/CVF Conference on Computer Vision and Pattern Recognition, pp 6418–6428

Khrulkov V, Mirvakhoba L, Ustinova E, et al (2020b) Hyperbolic image embeddings. In: Proceedings of the IEEE/CVF Conference on Computer Vision and Pattern Recognition (CVPR)

Kingma DP, Ba J (2015) Adam: A method for stochastic optimization. In: International Conference on Learning Representations

Krizhevsky A (2009) Learning multiple layers of features from tiny images. URL <https://api.semanticscholar.org/CorpusID:18268744>

Krizhevsky A, Nair V, Hinton G (2009) Cifar-10 and cifar-100 datasets. <https://www.cs.toronto.edu/~kriz/cifar.html>

Kun Y, Jianxin W (2019) Probabilistic End-to-end Noise Correction for Learning with Noisy Labels. In: The IEEE Conference on Computer Vision and Pattern Recognition (CVPR)

Kwon J, Kim J, Park H, et al (2021) Asam: Adaptive sharpness-aware minimization for scale-invariant learning of deep neural networks. In: International Conference on Machine Learning, PMLR, pp 5905–5914

Kye SM, Choi K, Yi J, et al (2022) Learning with noisy labels by efficient transition matrix estimation to combat label miscorrection. In: European Conference on Computer Vision, Springer, pp 717–738

Lee JM (2006) Riemannian manifolds: an introduction to curvature, vol 176. Springer Science & Business Media

Li H, Chen Z, Xu Y, et al (2024) Hyperbolic anomaly detection. In: Proceedings of the IEEE/CVF Conference on Computer Vision and Pattern Recognition, pp 17511–17520

Li J, Wong Y, Zhao Q, et al (2019) Learning to learn from noisy labeled data. In: Proceedings of the IEEE/CVF Conference on Computer Vision and Pattern Recognition, pp 5051–5059

Li J, Socher R, Hoi SC (2020) Dividemix: Learning with noisy labels as semi-supervised learning. In: International Conference on Learning Representations

Li L, Zhang Y, Wang S (2023) The euclidean space is evil: Hyperbolic attribute editing for few-shot image generation. In: Proceedings of the IEEE/CVF International Conference on Computer Vision, pp 22714–22724

Li M, Cheung Ym, Lu Y (2022a) Long-tailed visual recognition via gaussian clouded logit adjustment. In: Proceedings of the IEEE/CVF Conference on Computer Vision and Pattern Recognition, pp 6929–6938

Li T, Wang L, Wu G (2021) Self supervision to distillation for long-tailed visual recognition. In: Proceedings of the IEEE/CVF International Conference on Computer Vision, pp 630–639

Li T, Cao P, Yuan Y, et al (2022b) Targeted supervised contrastive learning for long-tailed recognition. In: Proceedings of the IEEE/CVF Conference on Computer Vision and Pattern Recognition, pp 6918–6928

Liang T, Poggio T, Rakhlin A, et al (2019) Fisher-rao metric, geometry, and complexity of neural networks. In: The 22nd international conference on artificial intelligence and statistics, PMLR,

pp 888–896

Lin F, Bai B, Guo Y, et al (2023) Mhcnn: A hyperbolic neural network model for multi-view hierarchical clustering. In: Proceedings of the IEEE/CVF International Conference on Computer Vision, pp 16525–16535

Liu S, Niles-Weed J, Razavian N, et al (2020) Early-learning regularization prevents memorization of noisy labels. Advances in Neural Information Processing Systems 33

Long T, Mettes P, Shen HT, et al (2020) Searching for actions on the hyperbole. In: Proceedings of the IEEE/CVF Conference on Computer Vision and Pattern Recognition, pp 1141–1150

Lorraine J, Vicol P, Duvenaud D (2020) Optimizing millions of hyperparameters by implicit differentiation. In: International Conference on Artificial Intelligence and Statistics, PMLR, pp 1540–1552

Ma Y, Jiao L, Liu F, et al (2024) Geometric prior guided feature representation learning for long-tailed classification. International Journal of Computer Vision pp 1–18. <https://doi.org/10.1007/s11263-024-01983-2>

Mettes P, Ghadimi Atigh M, Keller-Ressel M, et al (2024) Hyperbolic deep learning in computer vision: A survey. International Journal of Computer Vision pp 1–25. <https://doi.org/10.1007/s11263-024-02043-5>

Nickel M, Kiela D (2017) Poincaré embeddings for learning hierarchical representations. In: Guyon I, Luxburg UV, Bengio S, et al (eds) Advances in Neural Information Processing Systems, vol 30. Curran Associates, Inc., URL <https://proceedings.neurips.cc/paper/files/paper/2017/file/59dfa2df42d9e3d41f5b02bfc32229dd-Paper.pdf>

Nishi K, Ding Y, Rich A, et al (2021) Augmentation strategies for learning with noisy labels. In: Proceedings of the IEEE/CVF Conference on Computer Vision and Pattern Recognition, pp 8022–8031

Peng W, Varanka T, Mostafa A, et al (2021) Hyperbolic deep neural networks: A survey. IEEE Transactions on Pattern Analysis and Machine Intelligence 44(12):10023–10044. <https://doi.org/10.1109/TPAMI.2021.3136921>

Petzka H, Kamp M, Adilova L, et al (2021) Relative flatness and generalization. Advances in Neural Information Processing Systems 34:18420–18432

Qu Z, Li X, Duan R, et al (2022) Generalized federated learning via sharpness aware minimization. In: International conference on machine learning, PMLR, pp 18250–18280

Rajeswaran A, Finn C, Kakade SM, et al (2019) Meta-learning with implicit gradients. Advances in Neural Information Processing Systems 32

Rangwani H, Aithal SK, Mishra M, et al (2022) Escaping saddle points for effective generalization on class-imbalanced data. Advances in Neural Information Processing Systems 35:22791–22805

Reddi SJ, Kale S, Kumar S (2018) On the convergence of adam and beyond. In: International Conference on Learning Representations

Ren M, Triantafillou E, Ravi S, et al (2018) Meta-learning for semi-supervised few-shot classification. In: International Conference on Learning Representations

Shimizu R, Mukuta Y, Harada T (2021) Hyperbolic neural networks++. In: International Conference on Learning Representations

Shu J, Xie Q, Yi L, et al (2019) Meta-weight-net: Learning an explicit mapping for sample weighting. Advances in Neural Information Processing Systems 32

Simon C, Koniusz P, Nock R, et al (2020) Adaptive subspaces for few-shot learning. In: Proceedings of the IEEE/CVF Conference on Computer Vision and Pattern Recognition, pp 4136–4145

Sinha S, Ohashi H, Nakamura K (2022) Class-difficulty based methods for long-tailed visual recognition. *International Journal of Computer Vision* 130(10):2517–2531. <https://doi.org/10.1007/s11263-022-01643-3>

Skopek O, Ganea OE, Bécigneul G (2020) Mixed-curvature variational autoencoders. In: *International Conference on Learning Representations*

Tanaka D, Ikami D, Yamasaki T, et al (2018) Joint optimization framework for learning with noisy labels. In: *Proceedings of the IEEE/CVF Conference on Computer Vision and Pattern Recognition*, pp 5552–5560

Taraday MK, Baskin C (2023) Enhanced meta-label correction for coping with label corruption. In: *Proceedings of the IEEE/CVF International Conference on Computer Vision*, pp 16295–16304

Tu Y, Zhang B, Li Y, et al (2023) Learning with noisy labels via self-supervised adversarial noisy masking. In: *Proceedings of the IEEE/CVF Conference on Computer Vision and Pattern Recognition*, pp 16186–16195

Ungar AA (2001) Hyperbolic trigonometry and its application in the poincaré ball model of hyperbolic geometry. *Computers & Mathematics with Applications* 41(1-2):135–147

Ungar AA (2008) Analytic hyperbolic geometry and Albert Einstein’s special theory of relativity. World Scientific

Vinyals O, Blundell C, Lillicrap T, et al (2016) Matching networks for one shot learning. *Advances in Neural Information Processing Systems* 29

Wang D, Liu Y, Fang L, et al (2022) Balanced gradient penalty improves deep long-tailed learning. In: *Proceedings of the 30th ACM International Conference on Multimedia*, pp 5093–5101

Wang X, Jiang W, Fu S, et al (2024a) Enhancing sharpness-aware minimization by learning perturbation radius. In: *Joint European Conference on Machine Learning and Knowledge Discovery in Databases*, Springer, pp 375–391

Wang Y, Li Y, Wang S (2024b) $G^3\text{-lq}$: Marrying hyperbolic alignment with explicit semantic-geometric modeling for 3d visual grounding. In: *Proceedings of the IEEE/CVF Conference on Computer Vision and Pattern Recognition*, pp 13917–13926

Wu Y, Ren M, Liao R, et al (2018) Understanding short-horizon bias in stochastic meta-optimization. In: *International Conference on Learning Representations*

Xiao T, Xia T, Yang Y, et al (2015) Learning from massive noisy labeled data for image classification. In: *Proceedings of the IEEE/CVF Conference on Computer Vision and Pattern Recognition*, pp 2691–2699

Xie S, Girshick R, Dollár P, et al (2017) Aggregated residual transformations for deep neural networks. In: *Proceedings of the IEEE/CVF Conference on Computer Vision and Pattern Recognition*, pp 1492–1500

Xu J, Ton JF, Kim H, et al (2020) Metafun: Meta-learning with iterative functional updates. In: *International Conference on Machine Learning*, PMLR, pp 10617–10627

Xu Y, Zhu L, Jiang L, et al (2021) Faster meta-update strategy for noise-robust deep learning. In: *Proceedings of the IEEE/CVF Conference on Computer Vision and Pattern Recognition*, pp 144–153

Yan J, Luo L, Deng C, et al (2021a) Unsupervised hyperbolic metric learning. In: *Proceedings of the IEEE/CVF Conference on Computer Vision and Pattern Recognition*, pp 12465–12474

Yan J, Luo L, Deng C, et al (2021b) Unsupervised hyperbolic metric learning. In: *Proceedings of the IEEE/CVF Conference on Computer Vision and Pattern Recognition (CVPR)*, pp 12465–12474

Yang E, Shen L, Wang Z, et al (2023a) Data augmented flatness-aware gradient projection for continual learning. In: *Proceedings of the IEEE/CVF International Conference on Computer Vision*, pp 5630–5639

Yang L, Jiang H, Song Q, et al (2022) A survey on long-tailed visual recognition. *International Journal of Computer Vision* 130(7):1837–1872. <https://doi.org/10.1007/s11263-022-01622-8>

Yang M, Zhou M, Pan L, et al (2023b) κ hgcn: Tree-likeness modeling via continuous and discrete curvature learning. In: *Proceedings of the 29th ACM SIGKDD Conference on Knowledge Discovery and Data Mining*, pp 2965–2977

Yao Z, Gholami A, Lei Q, et al (2018) Hessian-based analysis of large batch training and robustness to adversaries. *Advances in Neural Information Processing Systems* 31

Yu Z, Nguyen T, Gal Y, et al (2022) Skin lesion recognition with class-hierarchy regularized hyperbolic embeddings. In: *International Conference on Medical Image Computing and Computer-Assisted Intervention*, Springer, pp 594–603

Zagoruyko S, Komodakis N (2016) Wide residual networks. In: *British Machine Vision Conference 2016*, British Machine Vision Association

Zeng Y, Lee K (2024) The expressive power of low-rank adaptation. In: *The Twelfth International Conference on Learning Representations*

Zhang S, Li Z, Yan S, et al (2021a) Distribution alignment: A unified framework for long-tail visual recognition. In: *Proceedings of the IEEE/CVF Conference on Computer Vision and Pattern Recognition*, pp 2361–2370

Zhang W, Wang Y, Qiao Y (2019) Metacleaner: Learning to hallucinate clean representations for noisy-labeled visual recognition. In: *Proceedings of the IEEE/CVF Conference on Computer Vision and Pattern Recognition*, pp 7373–7382

Zhang Y, Wang X, Shi C, et al (2021b) Lorentzian graph convolutional networks. In: *Proceedings of the Web Conference 2021*. Association for Computing Machinery, New York, NY, USA, WWW '21, p 1249–1261, <https://doi.org/10.1145/3442381.3449872>, URL <https://doi.org/10.1145/3442381.3449872>

Zheltonozhskii E, Baskin C, Mendelson A, et al (2022) Contrast to divide: Self-supervised pre-training for learning with noisy labels. In: *Proceedings of the IEEE/CVF Winter Conference on Applications of Computer Vision*, pp 1657–1667

Zheng G, Awadallah AH, Dumais S (2021) Meta label correction for noisy label learning. In: *Proceedings of the AAAI Conference on Artificial Intelligence*, pp 11053–11061

Zhong Z, Cui J, Liu S, et al (2021) Improving calibration for long-tailed recognition. In: *Proceedings of the IEEE/CVF Conference on Computer Vision and Pattern Recognition*, pp 16489–16498

Zhou Z, Li L, Zhao P, et al (2023) Class-conditional sharpness-aware minimization for deep long-tailed recognition. In: *Proceedings of the IEEE/CVF Conference on Computer Vision and Pattern Recognition*, pp 3499–3509

Zhuang J, Gong B, Yuan L, et al (2022) Surrogate gap minimization improves sharpness-aware training. In: *International Conference on Learning Representations*